

DOTTORATO DI RICERCA
in
MATEMATICA APPLICATA E INFORMATICA
CICLO VII

Consorzio tra Università di Catania, Università di Napoli Federico II,
Università di Palermo, Università di Salerno

SEDE AMMINISTRATIVA: UNIVERSITÀ DI NAPOLI FEDERICO II

**ON GAUSSIAN PROCESSES AND NEURONAL MODELING:
COMPUTATIONAL AND SIMULATION APPROACHES**

Enrica Pirozzi

TESI DI DOTTORATO DI RICERCA

IL COORDINATORE
Prof. Luigi M. Ricciardi

Contents

Introduction	1
1 Gaussian processes: first passage time problems and neuronal models	3
1.1 Essentials on the first passage time (FPT)	3
1.2 Gaussian Processes	5
1.2.1 Definitions	5
1.2.2 Some properties	7
1.3 Introduction to neuronal modeling	11
1.3.1 Neuronal firing and the first passage time problem	12
1.3.2 Gaussian neuronal models	15
1.3.3 Gauss-Markov (GM) processes	15
1.3.4 Non-Markov processes	18
2 Closed form solutions and computational results	19
2.1 Closed form results for GM processes	19
2.1.1 A preliminary closed-form result	19
2.1.2 A generalization of Daniels boundary	21
2.2 A Computational method for GM processes	24
2.3 Approximations for neuronal models by GM processes	29
2.3.1 The Ornstein-Uhlenbeck process as a GM process	32
2.3.2 An inverse problem	34
2.3.3 Leaky Integrate-and-Fire (LIF) neuronal model	35
2.3.4 LIF model with constant stimulus	35
2.3.5 LIF model with periodic stimulus	37
2.3.6 Some approximations	38
3 Simulation algorithms and comparing analysis	49
3.1 A simulation procedure	49
3.2 Covariance function with damped oscillations	56
3.2.1 About simulations	61
3.2.2 First passage time estimations	62
3.3 Parallel simulations for upcrossing FPT problem	67
3.3.1 Using the diffusive approximation	67
3.3.2 Markov versus non-Markov models	68
3.3.3 Asymptotic results for Gaussian processes	72
3.4 Upcrossing FPT problem and the correlation time	77

3.4.1	Asymptotic results for large correlation times	79
3.4.2	Simulation results	81
4	Auxiliary results	85
4.1	An algorithm for data samples representation	85
4.1.1	Description of the Random Algorithm	86
4.1.2	Statistical tests to verify the RANDOM rule	87
4.1.3	Modified RANDOM rule	93
4.1.4	Comparing histograms	94
4.2	A quadrature technique	105
4.2.1	The moments method	105
4.2.2	A recursive relation for moments	107
4.2.3	Examples	112
4.2.4	Application to a contact problem	117

Introduction

This thesis is focused on problems concerning the modeling of the activity of single neurons in which stochastic processes of various nature are involved to mimic neuron's spiking activity. A central role is played by Gaussian processes and the related first-passage-time (FPT) problem that, within the present framework, is representative of the neuronal firing times. The Gaussian processes use of which is made are of a two-fold type: Markov and non Markov. For both an abridged outline of the main features is provided, and analytic, computation and simulation methods developed to obtain information on the FPT probabilistic and statistical features are discussed. For Gaussian processes of Markov type a purely computational approach based on numerical quadratures for integral equations is presented, which is suitable for FPT probability densities determination. The major problem of modeling neuronal activity by means of Leaky-Integrate-and Fire (LIF) models in the presence of both constant and periodic stimuli is then approached. Here, essential role is played by previously obtained results on the Ornstein-Uhlenbeck process and on Markov-Gaussian processes in the presence of asymptotically constant or asymptotically periodic boundaries (henceforth also called "thresholds"). A totally different approach to the understanding of the statistical features of FPT probability densities for non Markov Gaussian processes has been adopted. This consists of direct simulation of the process' sample paths. The implemented simulation techniques, long considered by us, are then described, and the analysis of the corresponding performances and accuracies is performed. Motivated by the need of enhanced flexibility of the mathematical models in relation to certain phenomenological features of neuronal activity, the possibility of varying initial state according to pre-assigned distributions or of differently specified correlation times and asymptotic behaviors are introduced as well. The representation of the simulated data has finally been considered by resorting to the construction of histograms whose detailed specification is provided jointly with various other auxiliary results. These include an algorithm for numerical evaluation of integrals via the construction of certain families of orthogonal polynomials.

Chapter 1

Gaussian processes: first passage time problems and neuronal models

1.1 Essentials on the first passage time (FPT)

Let $\{X(t); t \in [t_0, \infty), t_0 \in \mathbb{R}\}$ be a stochastic process in \mathbb{R} and let $P\{X(t_0) = x_0\} = 1, x_0 \in \mathbb{R}$. Let us define the following functions:

$$F(x, t | x_0, t_0) = P\{X(t) \leq x | X(t_0) = x_0\} \quad (1.1.1)$$

and

$$f(x, t | x_0, t_0) = \frac{\partial}{\partial x} F(x, t | x_0, t_0). \quad (1.1.2)$$

The former is the distribution function of $X(t)$ conditioned by the initial state $x_0 = X(t_0)$ at the initial time t_0 ; the latter is the conditioned probability density function (pdf) of $X(t)$. If $X(t)$ is Markov, f identifies with the transition pdf. We now define the random variable

$$\mathcal{T} = \inf_{t \geq t_0} \{t : X(t) > S(t) | X(t_0) = x_0\}, \quad (1.1.3)$$

representing the first passage time (FPT) of $X(t)$ through the time-dependent boundary (or barrier or “threshold”), $S(t)$ for $x_0 = X(t_0) < S(t_0)$. Let us denote by

$$g[S(t), t | x_0, t_0] = \frac{\partial}{\partial t} P\{\mathcal{T} \leq t\} \quad (1.1.4)$$

the FPT pdf of $X(t)$ through $S(t)$. Finally, let us define the conditional pdf of $X(t)$ in the presence of an absorbing barrier $S(t)$. To this purpose one has to construct the conditional pdf of the sample paths originating at x_0 at time t_0 that up to time t did not cross $S(t)$. Denoting such pdf by $\alpha^{S(t)}(x, t | x_0, t_0)$, it is easy to convince oneself that the following identity holds:

$$\int_{-\infty}^{S(t)} \alpha^{S(t)}(x, t | x_0, t_0) dx = 1 - \int_{t_0}^t g[S(\tau), \tau | x_0, t_0] d\tau. \quad (1.1.5)$$

Hence,

$$g[S(t), t | x_0, t_0] = -\frac{\partial}{\partial t} \int_{-\infty}^{S(t)} \alpha^{S(t)}(x, t | x_0, t_0) dx. \quad (1.1.6)$$

One thus understands that the problem of determining the FPT pdf for a stochastic process offers the same degree of difficulties as the determination of the conditional pdf in the presence of an absorbing boundary. In the few instances in which the latter can be determined, via equation (1.1.6) one immediately obtains the function g .

The above definitions can be immediately extended to the case when $x_0 = X(t_0) > S(t_0)$. Then, one refers to the FPT through a “lower” barrier or threshold. In the sequel we shall exclusively refer to the case $x_0 < S(t_0)$, i.e. to FPT problems through “higher” boundaries.

It is finally possible to take into account FPT problems through a pair of boundaries. Indeed, let $S_1(t)$ and $S_2(t)$ be continuous functions such that $S_1(t_0) < x_0 < S_2(t_0)$. One can then define the random variable \mathcal{T}^+ representing the FPT through the higher boundary $S_2(t)$ with the condition that $S_1(t)$ has not been previously crossed. Similarly, one can define a random variable \mathcal{T}^- denoting the FPT through the lower barrier $S_1(t)$ with the condition that $S_2(t)$ has not been crossed before. The FPT pdf's g^+ and g^- are correspondingly defined. Their sum, $g = g^+ + g^-$, finally provides the FPT pdf of $X(t)$ through any of the two boundaries, namely the pdf of the time when first the process $X(t)$, conditioned by $X(t_0) = x_0$, leaves the region $\{x \in \mathbb{R} : S_1(t) < x < S_2(t)\}$, $\forall t \geq t_0$. A rigorous definition of such random variable and of its corresponding pdf's can be found in [4].

FPT problems have been extensively studied for continuous Markov processes, i.e. for diffusion processes. The transition pdf $f(x, t | x_0, t_0)$ is then solution of Kolmogorov equation

$$\frac{\partial f}{\partial t_0} + A_1(x_0, t_0) \frac{\partial f}{\partial x_0} + \frac{1}{2} A_2(x_0, t_0) \frac{\partial^2 f}{\partial x_0^2} = 0, \quad (1.1.7)$$

with the initial condition

$$\lim_{t \downarrow t_0} f(x, t | x_0, t_0) = \delta(x - x_0), \quad (1.1.8)$$

where the coefficients are the drift and infinitesimal variance of $X(t)$, respectively:

$$A_k(x_0, t_0) = \lim_{\Delta t \downarrow 0} \frac{1}{\Delta t} \int_{-\infty}^{\infty} (y - x_0)^k f(y, t_0 + \Delta t | x_0, t_0) dy, \quad (k = 1, 2). \quad (1.1.9)$$

The Markov nature of diffusion processes allows one to write down some Volterra-kind integral equations in the unknown FPT pdf. Here we limit ourselves to recalling Fortet equation

$$f(x, t | x_0, t_0) = \int_{t_0}^t g[S(\tau), \tau | x_0, t_0] f[x, t | S(\tau), \tau] d\tau, \quad (1.1.10)$$

where a single boundary $S(t)$, such that $S(t_0) > x_0$, has been considered and where $x > S(t)$ is an otherwise arbitrary real. As proved in Fortet [32], equation (2.10) remains valid in the limit as $x \downarrow S(t)$:

$$f[S(t), t | x_0, t_0] = \int_{t_0}^t g[S(\tau), \tau | x_0, t_0] f[S(t), t | S(\tau), \tau] d\tau. \quad (1.1.11)$$

This is a Volterra first kind integral equation whose kernel and left-hand-side term are specified once the transition pdf has been determined. The main difficulty one faces when looking for the solution of equation (1.1.11) is due to the singular nature of the kernel for $\tau = t$. This circumstance has suggested the search for alternative equations possessing continuous kernels. In previous papers ([3], [5], [40]), it has been proved that this task can indeed be achieved, and algorithms to obtain numerical solutions in a sufficient rapid fashion have been provided.

Totally different is the situation when $X(t)$ is a non-Markov process. Indeed, even though \mathcal{T} , the FPT through a boundary $S(t)$, and the random variables \mathcal{T}^+ and \mathcal{T}^- can be similarly defined, it does not appear that equations can be obtained in which the corresponding FPT pdf's appear as the unknown functions.

Before coming to the problem of evaluating FPT densities for normal processes, we shall recall the main definitions and the essential properties of the normal processes in a form that suits our needs.

1.2 Gaussian Processes

1.2.1 Definitions

We start with an outline (see, for instance, [89]) of the essential properties of normal random variables in \mathbb{R} and \mathbb{R}^n ($n > 1$).

Definition 1.1 A random variable defined in a probability space (Ω, \mathcal{F}, P) is said to be Gaussian, or normally distributed, with mean m and variance σ^2 if its pdf $f_1(x)$ is given by

$$f_1(x) \equiv f(x; m, \sigma^2) = \frac{\exp\left\{-\frac{1}{2}Q_1(x; m, \sigma^2)\right\}}{\sqrt{2\pi\sigma^2}}, \quad (x \in \mathbb{R}) \quad (1.2.1)$$

where

$$Q_1(x; m, \sigma^2) = \frac{(x - m)^2}{\sigma^2} \equiv (x - m)(\sigma^2)^{-1}(x - m), \quad (1.2.2)$$

with $m \in \mathbb{R}$ and $\sigma \in \mathbb{R}^+$.

Definition 1.2 The random vector $\mathbf{X} = (X_1, X_2)^T$ is said to be normally distributed if the one-dimensional random variables X_1 and X_2 are defined in the same probability space and if their joint pdf $f_2(x_1, x_2)$ is

$$f_2(x_1, x_2) \equiv f(\mathbf{x}; \mathbf{m}, \Lambda) = \frac{\exp\left\{-\frac{1}{2}Q_2(\mathbf{x}; \mathbf{m}, \Lambda)\right\}}{2\pi\sqrt{|\Lambda|}}, \quad (\mathbf{x} \in \mathbb{R}^2) \quad (1.2.3)$$

where

$$Q_2(\mathbf{x}; \mathbf{m}, \Lambda) = (\mathbf{x} - \mathbf{m})^T \Lambda^{-1} (\mathbf{x} - \mathbf{m}) \quad (1.2.4)$$

with

$$\mathbf{m} = [E(X_1), E(X_2)]^T = (m_1, m_2)^T \quad (1.2.5)$$

and

$$\Lambda = E[(\mathbf{X} - \mathbf{m})(\mathbf{X} - \mathbf{m})^T] = \begin{pmatrix} \sigma_1^2 & \sigma_{12} \\ \sigma_{12} & \sigma_2^2 \end{pmatrix} \quad (1.2.6)$$

in which, for $j = 1, 2$, $\sigma_j = \text{var}(X_j) > 0$, $\sigma_{12} = \text{cov}(X_1, X_2)$. Finally, $|\Lambda| \equiv \det \Lambda = \sigma_1^2 \sigma_2^2 - \sigma_{12}^2 > 0$. Denoting by $\rho = \sigma_{12} / \sigma_1 \sigma_2$ ($|\rho| < 1$) the correlation coefficient of X_1 and X_2 , one has:

$$|\Lambda| = \sigma_1^2 \sigma_2^2 (1 - \rho^2). \quad (1.2.7)$$

Furthermore, since $|\Lambda| > 0$ the matrix Λ^{-1} exists and is given by

$$\Lambda^{-1} = \frac{1}{|\Lambda|} \begin{pmatrix} \sigma_2^2 & -\sigma_1 \sigma_2 \rho \\ -\sigma_1 \sigma_2 \rho & \sigma_1^2 \end{pmatrix}. \quad (1.2.8)$$

Making use of (1.2.4)–(1.2.8), the pdf (1.2.3) of \mathbf{X} takes the form:

$$f_2(\mathbf{x}; \mathbf{m}, \Lambda) = \frac{1}{2\pi\sigma_1\sigma_2\sqrt{1-\rho^2}} \exp \left\{ -\frac{1}{2(1-\rho^2)} \left[\left(\frac{x_1-m_1}{\sigma_1} \right)^2 + \right. \right. \\ \left. \left. -2\rho \left(\frac{x_1-m_1}{\sigma_1} \right) \left(\frac{x_2-m_2}{\sigma_2} \right) + \left(\frac{x_2-m_2}{\sigma_2} \right)^2 \right] \right\}. \quad (1.2.9)$$

Hence, the characteristic function of \mathbf{X} is

$$\varphi_{\mathbf{X}}(u_1, u_2) \equiv E \left[\exp \{ i (u_1 X_1 + u_2 X_2) \} \right] \\ = \exp \left\{ i (m_1 u_1 + m_2 u_2) - \frac{1}{2} P_2(\mathbf{u}; \Lambda) \right\} \quad (1.2.10)$$

where

$$P_2(\mathbf{u}; \Lambda) = \mathbf{u}^T \Lambda \mathbf{u} = \sigma_1^2 u_1^2 + 2\sigma_{12} u_1 u_2 + \sigma_2^2 u_2^2. \quad (1.2.11)$$

Remark 1.1 Definition 1.2 is meaningful as far as Λ is non singular. If $|\Lambda| = 0$ the definition of a normal two-dimensional random variable cannot be given by means of (1.2.3).

Definition 1.3 If $|\Lambda| = 0$ the random variables X_1 and X_2 are said to be jointly normal if their characteristic function is given by (1.2.10). The normal distribution is then said to be singular.

Definition 1.4 A random vector $\mathbf{X} = (X_1, X_2, \dots, X_n)^T$ whose components are defined on the same probability space is normal, or Gaussian, if its characteristic function has the form

$$\varphi_{\mathbf{X}}(u_1, u_2, \dots, u_n) \equiv E \left[\exp \{ i (u_1 X_1 + u_2 X_2 + \dots + u_n X_n) \} \right] \\ = \exp \left\{ i \sum_{r=1}^n m_r u_r - \frac{1}{2} P_n(\mathbf{u}; \Lambda) \right\} \quad (1.2.12)$$

where $m_j \in \mathbb{R}$ ($j = 1, 2, \dots, n$), Λ is a $n \times n$ non-negative definite symmetric matrix and $P_n(\mathbf{u}; \Lambda)$ is the quadratic form associated to Λ :

$$P_n(\mathbf{u}; \Lambda) = \mathbf{u}^T \Lambda \mathbf{u} = \sum_{r,k=1}^n u_r u_k \lambda_{rk}. \quad (1.2.13)$$

The constants m_r in (1.2.12) are the mean values of X_r ($r = 1, 2, \dots, n$):

$$\mathbf{m} = (m_1, m_2, \dots, m_n)^T = [E(X_1), E(X_2), \dots, E(X_n)]^T. \quad (1.2.14)$$

Finally, Λ is the covariance matrix whose elements λ_{jk} are defined as follows:

$$\lambda_{jk} = E[(X_j - m_j)(X_k - m_k)], \quad (j, k = 1, 2, \dots, n). \quad (1.2.15)$$

Remark 1.2 If $|\Lambda| > 0$, from (1.2.12) one obtains the n -dimensional joint pdf $f_n(\mathbf{x})$:

$$f_n(\mathbf{x}) \equiv f(\mathbf{x}; \mathbf{m}, \Lambda) = \frac{\exp \left\{ -\frac{1}{2} Q_n(\mathbf{x}; \mathbf{m}, \Lambda) \right\}}{(2\pi)^{n/2} \sqrt{|\Lambda|}}, \quad (1.2.16)$$

where

$$Q_n(\mathbf{x}; \mathbf{m}, \Lambda) = (\mathbf{x} - \mathbf{m})^T \Lambda^{-1} (\mathbf{x} - \mathbf{m}) = \sum_{j,k=1}^n l_{jk} (x_j - m_j)(x_k - m_k), \quad (1.2.17)$$

with l_{jk} ($j, k = 1, 2, \dots, n$) denoting the (j, k) element in Λ^{-1} .

In view of the forthcoming considerations, let us write down explicitly the conditional pdf of $n + 1$ jointly distributed Gaussian random variables X_r ($r = 0, 1, \dots, n$), assuming that such distribution is non-singular and that $E(X_r) = 0$ ($r = 0, 1, \dots, n$). From (1.2.1), (1.2.16) and (1.2.18) one obtains:

$$\begin{aligned} f_n(x_1, \dots, x_n | x_0) &\equiv \frac{f_{n+1}(x_0, x_1, \dots, x_n)}{f_1(x_0)} \\ &= \frac{\exp\left\{-\frac{1}{2}\left(\sum_{j,k=0}^n l_{j+1,k+1} x_j x_k - \frac{x_0^2}{\sigma_0^2}\right)\right\}}{\sqrt{(2\pi)^n |\Lambda|}} \end{aligned} \quad (1.2.18)$$

where, now, the covariance matrix refers to variables X_0, X_1, \dots, X_n and $\sigma_0^2 = \lambda_{11}$.

Definition 1.5 Let $T \subseteq \mathbb{R}$. A continuous-parameter stochastic process $\{X(t), t \in T\}$ is normal if the random variables $X(t_1), X(t_2), \dots, X(t_n)$ are jointly normal for all $n \in \mathbf{N}$ and for all n -tuples t_1, t_2, \dots, t_n ($t_r \in T; r = 1, 2, \dots, n$).

1.2.2 Some properties

Definition 1.6 A random process $\{X(t), t \in T\}$, where T is a linear set (i.e. if $t, \tau \in T$ then $t + \tau \in T$) is said to be strictly stationary (or, for short, stationary) if its probability law coincides with that of $\{X(t + \tau), t \in T\}$ for any $\tau \in T$.

In other words, for a strictly stationary process one has

$$f_n(X(t_1), \dots, X(t_n)) = f_n(X(t_1 + \tau), \dots, X(t_n + \tau)) \quad (1.2.19)$$

for all $n \in \mathbf{N}$, for all n -tuples ($t_1 < \dots < t_n$) and for all $\tau \in T$.

Remark 1.3 For $n = 1$ and $n = 2$, (1.2.19) yields

$$\begin{aligned} \forall t_1 \in T, \quad f_1(X(t_1)) &\equiv f_1(x_1, t_1) = f_1(x_1), \\ \forall t_1 < t_2 \in T, \quad f_2(X(t_1), X(t_2)) &\equiv f_2(x_1, t_1; x_2, t_2) = f_2(x_1, x_2, t_2 - t_1), \end{aligned}$$

respectively.

From Remark 1.3 one sees that, if existing, mean and variance of such a process are time independent:

$$E[X(t)] = \mu, \quad E\{[X(t) - \mu]^2\} = \sigma^2. \quad (1.2.20)$$

Similarly, if existing, the correlation function $\gamma(t_1, t_2)$, for $t_2 > t_1$, depends only on the difference $t_2 - t_1$ and not on t_1 and t_2 , separately. Hence, for all $t_1, t_2 \in T$ one has:

$$\gamma(t_1, t_2) = E[X(t_1)X(t_2)] = E[X(t_2)X(t_1)] = \gamma(|t_2 - t_1|) \quad (1.2.21)$$

implying

$$\gamma(-t) = \gamma(t). \quad (1.2.22)$$

Furthermore,

$$E[X^2(t)] = \gamma(0). \quad (1.2.23)$$

Since $\gamma(t)$ is an even function, in the sequel we shall limit ourselves to specifying the positive branch alone.

By virtue of relations (1.2.20) and (1.2.21) the covariance function

$$\begin{aligned} c(t_1, t_2) &\equiv E\left\{\{X(t_1) - E[X(t_1)]\}\{X(t_2) - E[X(t_2)]\}\right\} \\ &= \gamma(|t_2 - t_1|) - E[X(t_1)]E[X(t_2)] = \gamma(|t_2 - t_1|) - \mu^2. \end{aligned} \quad (1.2.24)$$

Definition 1.7 A random process $\{X(t), t \in T\}$, is weakly stationary (or wide sense stationary, or covariance stationary) if it possesses finite second order moments ($|E\{X^2(t)\}| < \infty, \forall t \in T$), constant mean and correlation function $E[X(t)X(s)]$ depending on t and s only through their difference $|t - s|$.

Remark 1.4 A strictly stationary random process possessing finite second order moments is wide sense stationary. The converse does not generally hold; the reason is that weak stationarity only involves first and second order moments.

Note that if $X(t)$ is Gaussian then weak stationarity implies strict stationarity. Indeed its probability law is completely specified by first and second order moments.

Remark 1.5 It is worth remarking explicitly that if $X(t)$ has finite second order moments then $m(t) = E[X(t)]$ and the correlation function $\gamma(t, \tau) = E[X(t)X(\tau)]$ exists for all $t, \tau \in T$. Furthermore, the covariance function $c(t, \tau)$ also exists for all $t, \tau \in T$ since

$$c(t, \tau) = \gamma(t, \tau) - m(t)m(\tau).$$

Definition 1.8 Let $\{X(t), t \in T\}$ be a continuous parameter stochastic process and let $E\{|X(t)|^2\} < \infty$ for all $t \in T$. $X(t)$ is said to be mean square (m.s.) continuous for $t \in T$ if one has

$$\lim_{\tau \rightarrow 0} E\{[X(t + \tau) - X(t)]^2\} = 0.$$

Such limit is often denoted as

$$\text{l.i.m.}_{\tau \rightarrow 0} X(t + \tau) = X(t).$$

From

$$E\{[X(t + \tau) - X(t)]^2\} = \gamma(t + \tau, t + \tau) - \gamma(t + \tau, t) - \gamma(t, t + \tau) + \gamma(t, t) \quad (1.2.25)$$

and since

$$\lim_{\tau, \tau' \rightarrow 0} E[X(t + \tau)X(t + \tau')] = \lim_{\tau, \tau' \rightarrow 0} \gamma(t + \tau, t + \tau'),$$

one can easily prove (cfr., for instance, [49]) the following results.

Theorem 1.1 The process $\{X(t), t \in T\}$ is mean square continuous for $t \in T$ iff the correlation function $\gamma(t, \tau)$ is continuous at (t, t) .

Corollary 1.1 If $\gamma(t, \tau)$ is continuous in each point of the diagonal $t = \tau$ it is also continuous in each point (t, τ) .

Note that if $X(t)$ is stationary from (1.2.25) one obtains

$$E\{[X(t + \tau) - X(t)]^2\} = 2[\gamma(0) - \gamma(\tau)].$$

Therefore, the following theorem holds.

Theorem 1.2 A stationary process $\{X(t), t \in T\}$ is m.s. continuous iff its correlation function $\gamma(t)$ is continuous at $t = 0$.

Definition 1.9 A stochastic process $\{X(t), t \in T\}$ admits m.s. derivative at $t \in T$ if the limit

$$\text{l.i.m.}_{\tau \rightarrow 0} \frac{X(t + \tau) - X(t)}{\tau} = \dot{X}(t)$$

exists. In such a case one writes

$$\dot{X}(t) = \frac{dX(t)}{dt}.$$

The following theorems hold (see, for instance, [49]).

Theorem 1.3 If $\{X(t), t \in T\}$ admits m.s. derivative at $t \in T$, then it is there m.s. continuous.

Theorem 1.4 The stochastic process $\{X(t), t \in T\}$ admits m.s. derivative at $t \in T$ iff $\partial^2\gamma(t, \tau)/\partial t\partial\tau$ exists at (t, t) .

Corollary 1.2 If $\partial^2\gamma(t, \tau)/\partial t\partial\tau$ exists in each diagonal point (t, t) , then it exists in each point (t, τ) .

Theorem 1.5 If $\{X(t), t \in T\}$ is stationary, it admits m.s. derivative iff $\partial^2\gamma(t, t)/\partial t^2$ exists at $t = 0$.

Theorem 1.6 Let $\{X(t), t \in T\}$ be a stochastic process possessing m.s. derivative in T . Then,

$$\begin{aligned} m_{\dot{X}}(t) &\equiv E[\dot{X}(t)] = \frac{d}{dt}E[X(t)] \equiv \dot{m}_X(t), \\ \gamma_{\dot{X}X}(t, \tau) &\equiv E[\dot{X}(t)X(\tau)] = \frac{d}{dt}E[X(t)X(\tau)] \equiv \frac{\partial\gamma_{XX}(t, \tau)}{\partial t}, \\ \gamma_{\dot{X}\dot{X}}(t, \tau) &\equiv E[\dot{X}(t)\dot{X}(\tau)] = \frac{d}{dt}\frac{d}{d\tau}E[X(t)X(\tau)] \equiv \frac{\partial^2\gamma_{XX}(t, \tau)}{\partial t\partial\tau}. \end{aligned}$$

Let us now assume that $X(t)$ is a zero-mean stationary normal process. For all $t \in T$ the random variable $X(t)$ is then Gaussian with zero mean and variance $\gamma(0)$, i.e. its pdf is

$$f_1(x) = \frac{1}{\sqrt{2\pi\gamma(0)}} \exp\left\{-\frac{1}{2}\frac{x^2}{\gamma(0)}\right\}, \quad (x \in \mathbb{R}).$$

Proposition 1.1 Let $X(t)$ is a zero-mean stationary normal process having $\gamma(\tau)$ as correlation function and possessing m.s. derivative. Let $\Lambda_{2n+1} = \|\lambda_{j,k}\|$ be the covariance matrix of

$$X(t_0), X(t_1), \dots, X(t_n), \dot{X}(t_1), \dots, \dot{X}(t_n)$$

with $t_0 < t_1 < \dots < t_n$. Then, Λ_{2n+1} is a symmetric matrix whose elements are specified as follows:

$$\lambda_{j+1, k+1} = E[X(t_j)X(t_k)] = \gamma(t_j - t_k) \quad (j, k = 0, 1, \dots, n), \quad (1.2.26)$$

$$\lambda_{n+j+1, n+k+1} = E[\dot{X}(t_j)\dot{X}(t_k)] = -\dot{\gamma}(t_j - t_k) \quad (j, k = 1, 2, \dots, n), \quad (1.2.27)$$

$$\lambda_{j+1, n+k+1} = E[X(t_j)\dot{X}(t_k)] = -\dot{\gamma}(t_j - t_k) \quad (j = 0, 1, \dots, n; k = 1, 2, \dots, n). \quad (1.2.28)$$

Proof By definition of covariance for a zero-mean process and from the stationarity of $X(t)$ relation (1.2.26) follows. Similarly one has

$$\lambda_{n+j+1, n+k+1} = E[\dot{X}(t_j)\dot{X}(t_k)] \quad (j, k = 1, 2, \dots, n).$$

From Theorem 1.6 and (1.2.22) one then easily obtains (1.2.27). Making again use of Theorem 1.6 and of (1.2.22), relation (1.2.28) finally follows. \diamond

Let us now calculate the conditional pdf $p_{2n}(x_1, \dots, x_n; \dot{x}_1, \dots, \dot{x}_n | x_0)$ of

$$X(t_1), \dots, X(t_n), \dot{X}(t_1), \dots, \dot{X}(t_n)$$

conditional upon $X(t_0) = x_0$, when $\gamma(0) = 1$ and $\dot{\gamma}(0) \equiv \{d^2\gamma(t)/dt^2\}_{t=0}$ exists and is finite.

By virtue of (1.2.18) one can then write

$$\begin{aligned} p_{2n}(x_1, \dots, x_n; \dot{x}_1, \dots, \dot{x}_n | x_0) &= \frac{p_{2n+1}(x_0, x_1, \dots, \dot{x}_n)}{p_1(x_0)} \\ &= \frac{\exp\left\{-\frac{1}{2}\left(\sum_{i,j=0}^{2n} l_{i+1,j+1} x_i x_j - x_0^2\right)\right\}}{(2\pi)^n |\Lambda_{2n+1}|^{1/2}}, \end{aligned} \quad (1.2.29)$$

where for $i = 1, \dots, n$ we have set

$$x_{n+i} = \dot{x}_i, \quad \gamma(t_{n+i}) = \dot{\gamma}(t_i).$$

(Recall that any linear operation, such as differentiation or integration, on a normal process yields a normal process.)

One can see that the following equalities hold:

$$\sum_{i=0}^{2n} \lambda_{i+1,j+1} l_{i+1,k+1} = \sum_{i=0}^{2n} \lambda_{j+1,i+1} l_{i+1,k+1} = \begin{cases} 1, & j = k \\ 0, & j \neq k, \end{cases} \quad (1.2.30)$$

$$\sum_{j=0}^{2n} \lambda_{i+1,j+1} l_{k+1,j+1} = \sum_{j=0}^{2n} \lambda_{j+1,i+1} l_{k+1,j+1} = \begin{cases} 1, & i = k \\ 0, & i \neq k. \end{cases} \quad (1.2.31)$$

Hence,

$$\sum_{i=0}^{2n} l_{i+1,j+1} \gamma(t_i) = \sum_{i=0}^{2n} l_{i+1,j+1} \lambda_{i+1,1} = \begin{cases} 1, & j = 0 \\ 0, & j \neq 0, \end{cases} \quad (1.2.32)$$

$$\sum_{j=0}^{2n} l_{i+1,j+1} \gamma(t_j) = \sum_{j=0}^{2n} l_{i+1,j+1} \lambda_{1,j+1} = \begin{cases} 1, & i = 0 \\ 0, & i \neq 0. \end{cases} \quad (1.2.33)$$

Making use of (1.2.30)-(1.2.33) one has:

$$\begin{aligned}
\sum_{i,j=0}^{2n} l_{i+1,j+1} x_i x_j - x_0^2 &= \sum_{i,j=0}^{2n} l_{i+1,j+1} x_i x_j - x_0^2 - x_0^2 + x_0^2 \\
&= \sum_{i,j=0}^{2n} l_{i+1,j+1} x_i x_j - x_0 \sum_{j=0}^{2n} x_j \sum_{i=0}^{2n} l_{i+1,j+1} \gamma(t_i) \\
&\quad - x_0 \sum_{i=0}^{2n} x_i \sum_{j=0}^{2n} l_{i+1,j+1} \gamma(t_j) + x_0^2 \sum_{i=0}^{2n} \gamma(t_i) \sum_{j=0}^{2n} l_{i+1,j+1} \gamma(t_j) \\
&= \sum_{i,j=0}^{2n} l_{i+1,j+1} x_i x_j - \sum_{i,j=0}^{2n} l_{i+1,j+1} \gamma(t_i) x_0 x_j \\
&\quad - \sum_{i,j=0}^{2n} l_{i+1,j+1} \gamma(t_j) x_0 x_i + \sum_{i,j=0}^{2n} l_{i+1,j+1} \gamma(t_i) \gamma(t_j) x_0^2 \\
&= \sum_{i,j=0}^{2n} l_{i+1,j+1} [x_i x_j - \gamma(t_i) x_0 x_j - \gamma(t_j) x_0 x_i + \gamma(t_i) \gamma(t_j) x_0^2] \\
&= \sum_{i,j=0}^{2n} l_{i+1,j+1} [x_i - x_0 \gamma(t_i)] [x_j - x_0 \gamma(t_j)].
\end{aligned}$$

The function p_{2n} given by (1.2.29) thus takes the following form:

$$\begin{aligned}
p_{2n} &= (x_1, \dots, x_n, \dot{x}_1, \dots, \dot{x}_n | x_0) \\
&= \frac{1}{(2\pi)^n |\Lambda_{2n+1}|^{1/2}} \exp \left\{ -\frac{1}{2} \sum_{i,j=1}^{2n} l_{i+1,j+1} [x_i - x_0 \gamma(t_i)] [x_j - x_0 \gamma(t_j)] \right\}.
\end{aligned}$$

Hereafter t will be identified with the time variable and hence we shall take $t \in [t_0, +\infty)$, with $t_0 \geq 0$. In the case of stationary processes, no loss of generality arises by taking $t_0 = 0$, which will be consistently done in the sequel.

1.3 Introduction to neuronal modeling

The phenomenology of single neurons electrical activity and the understanding of the ultimate mechanisms responsible for it have been the object of numerous investigations by neurophysiologists, physicists and mathematicians during the last four decades. Despite the availability of some mathematical interesting models based on various assumptions on the type of input to which the neuron is subject and on possible generation mechanisms of the corresponding output, a “universal model” to which refer in general instances is still lacking. In addition, the existing mathematical tools appear to be hardly effective due to the high degree of nonlinearity exhibited by the neuron input-output behavior. Hence, to focus on the description of neuronal behaviors corresponding to well-specified input classes should, in our view, deserve higher priority with respect to searching for general methods for describing processing and transmission of information in neuronal systems.

The present thesis shall refer to evolution models of neuronal membrane potentials that fall within the class of Gaussian processes. The cases of Markov and of non-Markov Gaussian processes are then separately considered. The aim is to make available a summary of analytic, computational and simulation methods whose implementations appear to be effective for the mathematical description of neuronal activities, at least in several cases of interest. Hereafter we shall deal with

- (i) analytic methods resting on transformations of Gauss-Markov processes to simpler well-known processes;
- (ii) a study of the role played by the correlation time in determining the probability densities of neuronal outputs;
- (iii) the determination of asymptotic behaviors of the probability densities in (ii) for large thresholds and/or for large times.

The obtained analytic and numerical results are then systematically compared with the results of simulations for a twofold purpose: on the one hand to evaluate the goodness of the simulations, and on the other hand to gather hints, from inspection of simulation results, on theoretical properties to be explored, proved or rejected.

Despite the massive efforts along the above research directions, it is fair to claim that there is presently a great need to construct some kinds of “new” mathematics, specifically suited to quantitatively describe the realm of neural biological processes. Hopefully, such an ambitious, though very necessary, enterprise will increasingly attract the interests of anyone who aims at a deep understanding of single neurons activity and of neural networks dynamics.

1.3.1 Neuronal firing and the first passage time problem

In this Section we deal with an outline of procedures and methods for the description of the dynamics of neuronal firing along a line first discussed in [72].

In a variety of modeling approaches, it is customary to assume that a neuron is subject to input pulses occurring randomly in time (see, for instance, [37], [76], [90], [91], and references therein). As a consequence of the received stimulations, the neuron reacts by producing a response that usually consists of a spike train. The reproduction of the statistical features of such spike trains has been the goal of many researches that have focused the attention on analysis of the interspike intervals. Indeed, the relevance of interspike intervals is due to the generally accepted hypothesis that the information transferred within the nervous system is encoded by the timing of occurrence of neuronal spikes.

To describe the dynamics of the neuronal firing, we consider a one-dimensional non-singular stochastic process $X(t)$ representing the change in the neuron membrane potential between two consecutive spikes. In this context, the threshold voltage is viewed as a deterministic function $S(t)$, and the instant when the membrane potential attains it (i.e. when a spike occurs) as a first passage time (FPT) random variable (rv). It is customary to assume that the stochastic process $X(t)$ originates at a preassigned under-threshold state x_0 at the initial time t_0 . Hereafter, we shall also consider the FPT upcrossing model in order to include more physiologically significant features – such as a finite decay constant of the membrane potential, the presence of reversal potentials, time-dependent firing thresholds – and also in order to refer to wider classes of inputs as responsible for the observed sequences of output signals. The upcrossing model is viewed as

a FPT problem to threshold $S(t)$ for the subset of sample paths of the process originating at a random state X_0 .

It is worth recalling that the year 1964 marks the beginning of the history of neuronal models based on continuous time - continuous space stochastic processes. Indeed, in a much celebrated article [36] invoked a random walk type process as responsible for the fluctuations of the membrane potential, under the assumption of numerous simultaneously and independently acting input processes. These authors were able to show that, by suitably choosing the parameters of the model, the experimentally recorded interspike interval histograms of numerous units could be fitted to an excellent degree of approximations by means of the FPT probability density function (pdf) of a Wiener process. Despite the excellent fitting of a variety of data, this model has been the target of severe criticism on the base of its extreme idealization in contrast with some electrophysiological evidence: for example, this model does not take into account the spontaneous exponential decay of the neuron membrane potential. An improved version is the Ornstein-Uhlenbeck (OU) model ([7], [91]), which includes the presence of the exponential decay of the neuron's membrane potential occurring between successive post-synaptic pulses, at the price, however, of a great increase of analytical complexity. Indeed, the OU model does not allow to obtain any closed form expression for the FPT pdf, except for some particular cases of no interest within the context of neuronal modeling. Rather cumbersome computations are thus required to obtain evaluations of the statistics of the FPT.

Ever since, alternative stochastic models have been proposed in the literature, aiming at refinements and embodiments of other neurophysiological features. The literature on this subject is too vast to be recalled here. We limit ourselves to mentioning that a review of most significant neuronal models can be found in [75], [76], and in the references therein. In particular, in [75], an outline is offered of mathematical techniques by which to approach the FPT problem by means of diffusion processes in the neuronal context. In particular for diffusion processes [3, 17] and for Gauss-Markov (GM) processes [23] it has been proven that the firing pdf is the solution of a second kind Volterra integral equation. For generally regular thresholds a fast and accurate numerical procedure for solving such integral equation has been designed, and successfully implemented, and the obtained approximations have been compared with those stemming out of standard numerical methods. Furthermore, by adopting a symmetry-based approach, the exact firing pdf for thresholds of a suitable analytical form has been determined.

Diffusion neuronal models rest on the strong Markov assumption. However, if one deals with problems involving processes characterized by memory effects, or evolving on a time scale comparable with that of measurements, such a property does not hold; hence, to face FPT problems for non-Markov processes becomes unavoidable.

While mathematical models based on non-Markov stochastic processes better describe the correlated firing activity, their analytic treatment is quite complicated and only rare and fragmentary results appear to be available in literature.

Here, by analogy with GM and OU-models, we shall focus on neuronal models rooted on Gaussian processes. Indeed, we are motivated by the generally accepted hypothesis that the neuronal firing can often be thought of as being caused by the superposition of a very large number of synaptic inputs, which is suggestive of the generation of Gaussian distributions by analogy with central limit theorems. The selection of one of the various methods that are available to compute the firing pdfs depends on the assumptions made on the membrane potential $X(t)$. Kostyukov in [54] suggested to approach single neuron modeling by referring to Gaussian stationary processes and to the construction of upcrossing FPT pdf. The interesting new idea

was to resort to Stratonovich notion of correlation time as a global characteristic of the process, so that processes with the same correlation time would have the same upcrossing FPT.

If the Gaussian stochastic process is stationary and mean-square differentiable, in general one ends up with a very cumbersome series expansion of the FPT pdf, hardly manageable for any practical purpose [74]. We shall review the terminology and the necessary definitions to characterize FPT pdf when $X(t)$ is either a Markov or a non Markov Gaussian process. We shall also briefly review Kostyukov model (henceforth denoted as the K-model) for the purpose of evaluating the approximations performed therein with respect to other available methods.

A totally different approach has been recently undertaken in order to obtain information on the behavior of the FPT densities for a class of stationary Gaussian processes with rational spectral densities in the presence of various types of thresholds. This consists of a simulation procedure [25] implemented to generate sample paths and to estimate the corresponding FPT densities. Such simulation procedure originates from Franklin algorithm [33]. In Chapter 3 we give a thorough description of the simulation algorithm and we refer to [20] and [22] for particular implementations.

In the present context, the goal of the simulation procedure is to sample N values of the FPT by a suitable construction of N time-discrete sample paths of the process and then to record the instants when such sample paths first cross the threshold. In such a way, one is led to obtain estimates of the firing pdf and of its statistics that can be of use for data fitting.

Within our approaches, the role of the simulation procedure is threefold:

- (i) to suggest the theoretical exploration of the behavior of the firing densities in a variety of different conditions by inspection of qualitative features of the simulation results;
- (ii) to permit quantitative evaluation of reliability and precision of the results obtained via numerical and analytic approximations;
- (iii) to offer a viable alternative whenever analytic and computational methods fail.

For instance, when the stochastic process is Gaussian, stationary and mean-square differentiable, a numerically reliable evaluation of the first term of the afore-mentioned series expansion of the FPT pdf can be obtained. By comparison with the simulated firing densities, one can conclude that for small times this first term is a good approximation of firing pdf [26]. Moreover, by comparing the results obtained by computer simulation of sample paths of non-Markov stationary Gaussian processes characterized by correlation times identical to those of the K-model, one can show that the approximations suggested therein ultimately amount to removing the non-Markov character of the model [21].

We wish to stress that our endeavors strive to improve simulation techniques, within the context of stationary Gaussian processes, that are particularly relevant within the neuronal modeling context. The aim is to design efficient algorithms to simulate Gaussian processes of a more general type.

Finally, special attention is paid to the asymptotic behavior of FPT pdf, which turns out to be appropriate for the description of neuronal activities even for small times. This is reasonable whenever the intrinsic time scale of the microscopic events involved during the neuron's evolution is much smaller than the macroscopic observation time scale, or when the asymptotic regime is exhibited also in the case of firing thresholds not too distant from the resting potential.

The study of the asymptotic behavior of the FPT pdf for Gaussian processes as thresholds or time grow larger originated in [24], [26] and [27]. By computational methods as well

as by analytic tools we show that the FPT pdf admits an excellent non-homogeneous exponential approximation for large thresholds, and in some cases even when such thresholds are not very distant from the initial state of the process. Our analysis is a natural extension of some investigations performed for the OU model [68] and successively extended to the class of one-dimensional diffusion processes admitting steady state densities in the presence of single asymptotically constant thresholds or of single asymptotically periodic thresholds [67, 41].

1.3.2 Gaussian neuronal models

Let us consider a real one-dimensional non-singular Gaussian stochastic process $\{X(t), t \geq t_0\}$ and a threshold $S(t) \in C^1[t_0, +\infty)$. We assume $P\{X(t_0) = x_0\} = 1$, with $x_0 < S(t_0)$, i.e. we focus our attention on the subset of sample paths of $X(t)$ that originate at a preassigned state x_0 at the initial time t_0 . Then,

$$T_{x_0} = \inf_{t \geq t_0} \{t : X(t) > S(t)\}, \quad x_0 < S(t_0)$$

is the FPT of $X(t)$ through $S(t)$ with pdf

$$g(t | x_0, t_0) = \frac{\partial}{\partial t} P(T_{x_0} < t). \quad (1.3.1)$$

Henceforth, $g(t | x_0, t_0)$ will be identified with the firing pdf of a neuron whose membrane potential is modeled by $X(t)$ and whose firing threshold is $S(t)$.

Now, consider a subset of sample paths of $X(t)$ that originate at the random state $X_0 = X(t_0)$ having pdf

$$\gamma_\varepsilon(x_0, t_0) := \begin{cases} \frac{f(x_0)}{P\{X(t_0) < S(t_0) - \varepsilon\}}, & x_0 < S(t_0) - \varepsilon \\ 0, & x_0 \geq S(t_0) - \varepsilon. \end{cases} \quad (1.3.2)$$

Here, $\varepsilon > 0$ is a fixed real number and $f(x_0)$ denotes the Gaussian pdf of $X(t_0)$. Then,

$$T_{X_0}^{(\varepsilon)} = \inf_{t \geq t_0} \{t : X(t) > S(t)\},$$

is the ε -upcrossing FPT of $X(t)$ through $S(t)$ and the related pdf is given by

$$g_u^{(\varepsilon)}(t | t_0) = \frac{\partial}{\partial t} P(T_{X_0}^{(\varepsilon)} < t) = \int_{-\infty}^{S(t_0) - \varepsilon} g(t | x_0, t_0) \gamma_\varepsilon(x_0, t_0) dx_0 \quad (t \geq t_0),$$

where $g(t | x_0, t_0)$ is defined in (1.3.1). Without loss of generality, we set $t_0 = 0$ and $x_0 = 0$, and for this case we write $g(t) := g(t | 0, 0)$ and $g_u^{(\varepsilon)}(t) := g_u^{(\varepsilon)}(t | 0)$, for fixed values of ε .

1.3.3 Gauss-Markov (GM) processes

Let the random process $\{X(t), t \geq 0\}$ have the following properties:

- (i) the mean $m(t) := E[X(t)]$ is continuous in $[0, +\infty)$;
- (ii) the covariance $c(s, t) := E\{[X(s) - m(s)][X(t) - m(t)]\}$ is continuous in $[0, +\infty) \times [0, +\infty)$;

(iii) $X(t)$ is non-singular, except possibly at the end points of $[0, +\infty)$ where it could be equal to $m(t)$ with probability one.

A Gaussian process is Markov if and only if its covariance satisfies (cf., for instance, [58])

$$c(s, u) = \frac{c(s, t) c(t, u)}{c(t, t)} \quad 0 \leq s \leq t \leq u. \quad (1.3.3)$$

Well-behaved solutions of (1.3.3) are of the form

$$c(s, t) = h_1(s) h_2(t), \quad s \leq t, \quad (1.3.4)$$

where

$$r(t) := \frac{h_1(t)}{h_2(t)} \quad (1.3.5)$$

is a monotonically increasing function by virtue of the Cauchy-Schwarz inequality, and $h_1(t) \cdot h_2(t) > 0$ because of the assumed non-singularity of the process. The conditional pdf $f(x, t | y, \tau)$ of $X(t)$, with $\tau < t$, is a normal density characterized respectively by conditional mean and variance

$$\mathbb{E}[X(t) | y, \tau] = m(t) + \frac{h_2(t)}{h_2(\tau)} [y - m(\tau)] \quad (1.3.6)$$

$$\text{Var}[X(t) | y, \tau] = h_2(t) \left[h_1(t) - \frac{h_2(t)}{h_2(\tau)} h_1(\tau) \right], \quad (1.3.7)$$

with $t > \tau \geq 0$. It satisfies the Fokker-Planck equation and the associated initial condition

$$\frac{\partial f(x, t | y, \tau)}{\partial t} = - \frac{\partial}{\partial x} [A_1(x, t) f(x, t | y, \tau)] + \frac{1}{2} \frac{\partial^2}{\partial x^2} [A_2(t) f(x, t | y, \tau)], \quad (1.3.8)$$

$$\lim_{\tau \uparrow t} f(x, t | y, \tau) = \delta(x - y),$$

with $A_1(x, t)$ and $A_2(t)$ given by

$$A_1(x, t) = m'(t) + [x - m(t)] \frac{h_2'(t)}{h_2(t)}, \quad A_2(t) = h_2^2(t) r'(t),$$

the prime denoting derivative with respect to the argument.

The class of Gauss-Markov processes, such that $f(x, t | y, \tau) \equiv f(x, t - \tau | y)$, includes the Wiener process and the OU process. In particular, any Gaussian process with covariance as in (1.3.4) can be represented in terms of the standard Wiener process $\{W(t), t \geq 0\}$ as

$$X(t) = m(t) + h_2(t) W[r(t)], \quad (1.3.9)$$

and is therefore Markov. This last equation suggests the way to construct the FPT pdf of a Gauss-Markov process $X(t)$ in terms of the FPT pdf of the standard Wiener process $W(t)$. Indeed, the following relation is valid

$$g[S(t), t | x_0, t_0] = \frac{dr(t)}{dt} g_W \{S^*[r(t)], r(t) | x_0^*, r(t_0)\} \quad (1.3.10)$$

where $r(t)$ is defined in (1.3.5) and $g_W[S^*(\vartheta), \vartheta | x_0^*, \vartheta_0]$ is the FPT pdf of $W(\vartheta)$ from x_0^* at time ϑ_0 to the continuous boundary $S^*(\vartheta)$, with

$$x_0^* = \frac{x_0 - m[r^{-1}(\vartheta_0)]}{h_2[r^{-1}(\vartheta_0)]}, \quad S^*(\vartheta) = \frac{S[r^{-1}(\vartheta)] - m[r^{-1}(\vartheta)]}{h_2[r^{-1}(\vartheta)]}. \quad (1.3.11)$$

Hence results on the FPT pdf for the standard Wiener process can thus be used via (1.3.10) to obtain the FPT pdf of any continuous Gauss-Markov process. For instance, if $S^*(\vartheta)$ is linear in ϑ , $g_W[S^*(\vartheta), \vartheta | x_0^*, \vartheta_0]$ is known and $g[S(t), t | x_0, t_0]$ can be obtained via (1.3.10). Instead, if $g_W[S^*(\vartheta), \vartheta | x_0^*, \vartheta_0]$ is not known, a numerical algorithm or a simulation procedure should be used for the standard Wiener process, and after that one can obtain $g[S(t), t | x_0, t_0]$ via the indicated transformation. However, such a procedure often exhibits the serious drawback of ensuing unacceptable time dilations [23]. (As is well-known, exponentially large times are involved when transforming the Ornstein-Uhlenbeck process to the Wiener process.)

It is desirable to dispose of a direct and efficient computational method to obtain evaluation of the FPT pdf. Partly inspired by previous papers dealing exclusively with diffusion processes (see [3] and references therein), along such direction, one can prove ([23]) that the conditioned FPT pdf of a Gauss-Markov process can be obtained by solving the non-singular Volterra second kind integral equation (identifying $g[S(t), t | x_0, t_0]$ with $g(t)$)

$$g(t) = -2\psi[S(t), t | x_0, t_0] + 2 \int_{t_0}^t g(\tau) \psi[S(t), t | S(\tau), \tau] d\tau \quad (1.3.12)$$

with $S(t_0) > x_0$, $S(t), m(t), h_1(t), h_2(t) \in C^1[0, +\infty)$ and

$$\begin{aligned} \psi[S(t), t | y, \tau] = & \left\{ \frac{S'(t) - m'(t)}{2} - \frac{S(t) - m(t)}{2} \frac{h_1'(t)h_2(\tau) - h_2'(t)h_1(\tau)}{h_1(t)h_2(\tau) - h_2(t)h_1(\tau)} \right. \\ & \left. - \frac{y - m(\tau)}{2} \frac{h_2'(t)h_1(t) - h_2(t)h_1'(t)}{h_1(t)h_2(\tau) - h_2(t)h_1(\tau)} \right\} f[S(t), t | y, \tau], \end{aligned} \quad (1.3.13)$$

where $f(x, t | y, \tau)$ is the transition pdf of $X(t)$.

We give some closed form solutions of (1.3.12) in the next Chapter for various families of thresholds.

Alternatively, $g(t)$ can be numerically obtained by using a fast and accurate computational method, mainly centered on the repeated Simpson rule, extensively described in the Chapter 2 of this thesis. In all our computations this has yielded by far the most accurate results with respect to all other methods. The iteration procedure allows one to compute $\tilde{g}(kp)$, for $k = 2, 3, \dots$, with time discretization step p in terms of computed values at the previous times $p, 2p, \dots, (k-1)p$. The noteworthy feature of this algorithm is its being implementable after simply specifying the functions $m(t), h_1(t), h_2(t)$ that characterize the process, the threshold $S(t)$ and the discretization step p . Furthermore, it does not involve any heavy computation, neither it requires use of any library subroutines, Monte Carlo methods or other special software packages to calculate high dimension multiple integrals.

Referring to the upcrossing FPT problem, note that for a non singular Gauss-Markov process the pdf (1.3.2) can be immediately evaluated, (setting $t_0 = 0$) since $f(x_0)$ is normal with mean $m(0)$ and variance $h_1(0)h_2(0)$ and

$$P\{X(0) < S(0) - \varepsilon\} = \frac{1}{2} \left\{ 1 + \text{Erf} \left[\frac{S(0) - \varepsilon - m(0)}{\sqrt{2h_1(0)h_2(0)}} \right] \right\}.$$

Furthermore, the ε -upcrossing FPT pdf is the unique solution of the second kind Volterra integral equation:

$$g_u^{(\varepsilon)}(t) = -2\psi_u^{(\varepsilon)}[S(t), t] + 2 \int_0^t \psi[S(t), t | S(\tau), \tau] g_u^{(\varepsilon)}(\tau) d\tau \quad (1.3.14)$$

where

$$\psi_u^{(\varepsilon)}[S(t), t] = \int_{-\infty}^{S(0)-\varepsilon} \psi[S(t), t | x_0] \gamma_\varepsilon(x_0) dx_0$$

and $\psi[x, t | y, \tau]$ is given in (1.3.13). A glance at (1.3.12) and (1.3.14), that possess identical kernels, immediately suggests to solve integral equation (1.3.14) by the same numerical iterative procedure pointed out for (1.3.12). If $\lim_{t \downarrow 0} S(t) = +\infty$, then $P\{X(0) < S(0) - \varepsilon\} = 1$ for all $\varepsilon > 0$, and X_0 becomes a random variable with pdf $\gamma(x_0) \equiv f(x_0)$, that is independent of ε .

1.3.4 Non-Markov processes

Let $X(t)$ be a stationary Gaussian process with mean $m(t) = 0$ and covariance $E[X(t)X(\tau)] = c(t, \tau) = c(t - \tau)$ such that $c(0) = 1$, $\dot{c}(0) = 0$ and $\ddot{c}(0) < 0$ (this last assumptions being equivalent to the mean square differentiable property). The following series expansion for the conditioned FPT pdf was derived in [74]:

$$g(t) = W_1(t) + \sum_{i=1}^{+\infty} (-1)^i \int_0^t dt_1 \int_{t_1}^t dt_2 \cdots \int_{t_{i-1}}^t dt_i W_{i+1}(t_1, \dots, t_i, t), \quad (1.3.15)$$

where $W_n(t_1, \dots, t_n) dt_1 \cdots dt_n$, $\forall n \in \mathbb{N}$ and $0 < t_1 < \cdots < t_n$, denotes the joint probability that $X(t)$ crosses $S(t)$ from below in the time intervals $(t_1, t_1 + dt_1), \dots, (t_n, t_n + dt_n)$ given that $X(0) = 0$. By using a straightforward variant of the method proposed by [74], the following series expansion for the upcrossing FPT pdf is obtained [26]:

$$g_u^{(\varepsilon)}(t) = W_1^{(\varepsilon)}(t) + \sum_{i=1}^{+\infty} (-1)^i \int_0^t dt_1 \int_{t_1}^t dt_2 \cdots \int_{t_{i-1}}^t dt_i W_{i+1}^{(\varepsilon)}(t_1, \dots, t_i, t) \quad (1.3.16)$$

with

$$W_{i+1}^{(\varepsilon)}(t_1, \dots, t_i, t) = \frac{\int_{-\infty}^{S(0)-\varepsilon} W_{i+1}(t_1, \dots, t_i, t | x_0) f(x_0) dx_0}{\int_{-\infty}^{S(0)-\varepsilon} f(z) dz}.$$

Due to the complexity of the involved multiple integrals, expressions (1.3.15) and (1.3.16) do not appear to be manageable for practical uses. Nevertheless, the first terms allow to obtain some interesting asymptotic results, as outlined in the follows. Since (1.3.15) and (1.3.16) are Leibnitz series for each fixed $t > 0$, estimates of the FPT pdf can in principle be obtained as its partial sum of order n provides a lower or an upper bound depending on whether n is even or odd. However, also the evaluation of such partial sums is extremely cumbersome.

In conclusion no effective analytical methods, nor viable numerical algorithms are presently available to evaluate the FPT pdf for this class of Gaussian processes. A simulation procedure seems to be the only possible resort (see Chapter 3).

Chapter 2

Closed form solutions and computational results

2.1 Closed form results for GM processes

2.1.1 A preliminary closed-form result

Let us consider a real one-dimensional non-singular Gauss-Markov stochastic process $\{X(t), t \in T\}$ with T is a continuous parameter set. Its pdf $g[S(t), t|x_0, t_0]$ satisfies the equation (1.3.12) with $\Psi[S(t), t|y, \tau]$ as in (1.3.13). The following theorem provides us with the necessary preliminary result.

Theorem 2.1.1 *Let $S(t), m(t), h_1(t), h_2(t)$ be $C^1(T)$ functions. One has*

$$\Psi[S(t), t|S(\tau), \tau] = 0 \quad \forall \tau, t \in T \text{ with } \tau \leq t$$

iff

$$S(t) = m(t) + d_1 h_1(t) + d_2 h_2(t) \quad \forall t \in T, \quad d_1, d_2 \in \mathbf{R}. \quad (2.1.1)$$

Proof 2.1.1 *We have*

$$\Psi_W \left[S^*[r(t)], r(t) | S^*[r(\tau)], r(\tau) \right] = \left[\frac{dr(t)}{dt} \right]^{-1} \Psi[S(t), t|S(\tau), \tau] \quad (2.1.2)$$

where W refers to the standard Wiener process. It follows that $\Psi[S(t), t|S(\tau), \tau] = 0 \quad \forall \tau, t \in T$ with $\tau \leq t$, iff

$$\Psi_W \left[S^*[r(t)], r(t) | S^*[r(\tau)], r(\tau) \right] = 0, \quad \forall \tau, t \in T, \quad \tau \leq t$$

i.e., recalling that

$$\Psi_W[S^*(\vartheta), \vartheta|y, \xi] = \frac{1}{2} \left[\frac{dS^*(\vartheta)}{d\vartheta} - \frac{S^*(\vartheta) - y}{\vartheta - \xi} \right] f_W[S^*(\vartheta), \vartheta|y, \xi] \quad (2.1.3)$$

with $f_W[x, \vartheta|y, \xi]$ denotes the transition pdf for the standard Wiener process, iff

$$S^*[r(t)] = d_1 r(t) + d_2 \quad \forall t \in T, \quad d_1, d_2 \in \mathbf{R}. \quad (2.1.4)$$

By virtue of the second of (1.3.11), relation (2.1.4) becomes

$$\frac{S(t) - m(t)}{h_2(t)} = d_1 r(t) + d_2 \quad \forall t \in T, \quad d_1, d_2 \in \mathbf{R}, \quad (2.1.5)$$

from which (2.1.1) follows. This completes the proof.

It should be stressed that in the present context the valuable part of Theorem 2.1.1 is that the kernel of equation (1.3.12) vanishes identically for boundaries (2.1.1), and only for those, rather than (2.1.5) that also follows immediately from (1.3.9).

The following statement expresses the FPT pdf through the boundary $S(t)$ in terms of the free transition pdf.

Corollary 2.1.1 *Under the assumptions of Theorem 2.1.1, if (2.1.1) holds the FPT pdf is given by*

$$g[S(t), t|x_0, t_0] = \frac{S(t_0) - x_0}{r(t) - r(t_0)} \frac{h_2(t)}{h_2(t_0)} \frac{dr(t)}{dt} f[S(t), t|x_0, t_0] \quad (x_0 < S(t_0)). \quad (2.1.6)$$

Furthermore, if $T = [a, b]$ and $\lim_{t \rightarrow b} r(t) = +\infty$, then

$$\int_{t_0}^b g[S(t), t|x_0, t_0] dt = \begin{cases} 1, & d_1/h_2(t_0) \leq 0 \\ \exp \left\{ -\frac{2 d_1 [S(t_0) - x_0]}{h_2(t_0)} \right\}, & d_1/h_2(t_0) > 0. \end{cases} \quad (2.1.7)$$

Proof 2.1.2 *Making use of Theorem 2.1.1, from (1.3.12) one obtains*

$$g[S(t), t|x_0, t_0] = -2 \Psi[S(t), t|x_0, t_0] \quad (2.1.8)$$

where Ψ is defined in (1.3.13). Relation (2.1.6) follows from (2.1.8) by substituting (2.1.1) in (1.3.13). Moreover, if $T = [a, b]$, then

$$\begin{aligned} \int_{t_0}^b g[S(t), t|x_0, t_0] dt &= \frac{[S(t_0) - x_0]}{h_2(t_0)} \int_{t_0}^b \frac{h_2(t)}{r(t) - r(t_0)} \frac{dr(t)}{dt} f[S(t), t|x_0, t_0] dt \\ &= \frac{[S(t_0) - x_0]}{\sqrt{2\pi|h_2(t_0)|}} \exp \left\{ -\frac{d_1[S(t_0) - x_0]}{h_2(t_0)} \right\} \\ &\quad \times \int_0^{r(b)-r(t_0)} y^{-3/2} \exp \left\{ -\frac{d_1^2}{2} y - \frac{[S(t_0) - x_0]^2}{2h_2^2(t_0) y} \right\} dy, \end{aligned} \quad (2.1.9)$$

where the last equality follows by setting $r(t) - r(t_0) = y$. In particular, if $\lim_{t \rightarrow b} r(t) = +\infty$, equation (2.1.7) follows from (2.1.9) by using

$$\int_0^\infty \exp \left\{ -py - \frac{\alpha}{4y} \right\} y^{-3/2} dy = 2 \sqrt{\frac{\pi}{\alpha}} \exp(-\sqrt{\alpha p}) \quad (Re \alpha > 0, Re p \geq 0).$$

This completes the proof.

It should be stressed that the closed-form result (2.1.6) cannot be employed to test the accuracy of numerical methods to solve equation (1.3.12) because its kernel is identically zero for boundaries (2.1.1). Hence, the need to discover another suitable boundary family starting from (2.1.1), which is being accomplished in the next Section.

In the following we shall make use of transformation (1.3.10) to obtain a family of boundaries (the so called "symmetry curves") whose role will be to lead us to a second family of boundaries for which the FPT pdf is obtained in closed-form in the case of Gauss-Markov processes. These boundaries will be seen to represent a generalization of the boundary

$$S(t) = \frac{\alpha}{2} - \frac{t}{\alpha} \ln \left(\frac{c_1 + \sqrt{c_1^2 + 4c_2 e^{-\alpha^2/t}}}{2} \right), \quad (2.1.10)$$

ingeniously determined by Daniels [12], via the method of images, for the standard Wiener process originated at time $t_0 = 0$ in the state $x_0 = 0$.

The boundaries thus obtained by us will play an essential role to provide a secure test for the accuracy of the forthcoming numerical computations.

2.1.2 A generalization of Daniels boundary

The closed-form expression of FPT pdf that we shall now determine will allow us to dispose of a quantitative test of the goodness of the computational procedure that will be provided to solve equation (1.3.12).

We start remarking that the transition pdf of a Gauss-Markov process characterized by conditional mean (1.3.6) and variance (1.3.7), possesses the following symmetry properties:

$$f(x, t|x_0, t_0) = \frac{\phi(x, t)}{\phi(x_0, t_0)} f[\psi(x, t), t|\psi(x_0, t_0), t_0] \quad (2.1.11)$$

and

$$\phi(x, t) f[\psi(x, t), t|x_0, t_0] = f(x, t|x_0, t_0) \exp \left\{ - \frac{2 [x - z(t)] [x_0 - z(t_0)]}{h_1(t)h_2(t_0) - h_1(t_0)h_2(t)} \right\}, \quad (2.1.12)$$

where

$$\begin{aligned} \psi(x, t) &= 2z(t) - x \\ \phi(x, t) &= \exp \left\{ - \frac{2d_1 [x - z(t)]}{h_2(t)} \right\} \\ z(t) &= m(t) + d_1 h_1(t) + d_2 h_2(t), \end{aligned} \quad (2.1.13)$$

with $d_1, d_2 \in \mathbf{R}$. As in a previous work [16], we shall call $z(t)$ a "symmetry curve" with respect to the symmetry function $\psi(x, t)$. Let now

$$\begin{aligned} y(t) &= m(t) + d_1 h_1(t) + d_2 h_2(t) \\ u(t) &= m(t) + d_1^* h_1(t) + d_2^* h_2(t) \\ v(t) &= 2u(t) - y(t) \end{aligned} \quad (2.1.14)$$

be symmetry curves such that $y(t) < u(t) < v(t)$ for all $t \geq t_0$, $t, t_0 \in T$ and t_0 fixed with $d_1, d_2, d_1^*, d_2^* \in \mathbf{R}$. We denote by $\psi_1(x, t)$ and $\phi_1(x, t)$ the symmetry functions corresponding to $u(t)$ and by $\psi_2(x, t)$ and $\phi_2(x, t)$ the symmetry functions corresponding to $v(t)$. Being $v(t) = \psi_1[y(t), t]$, the symmetry curve $v(t)$ is the "image" of the symmetry curve $y(t)$ in the "mirror" $u(t)$ via the symmetry function ψ_1 . If, for instance, one has $y(t) < u(t) < v(t)$ for all $t \geq t_0$, conditions $y(t) < x < u(t)$ amount to requiring $\psi_1[y(t), t] > \psi_1(x, t) > \psi_1[u(t), t]$, i.e. $u(t) < \psi_1(x, t) < v(t)$.

Theorem 2.1.2 *Let*

$$S(t; t_0) = u(t) - \frac{h_1(t)h_2(t_0) - h_1(t_0)h_2(t)}{2[u(t_0) - y(t_0)]} \ln \left[\frac{c_1 + \sqrt{\Delta(t; t_0)}}{2} \right] \quad (2.1.15)$$

$$\left(c_1 > 0, c_2 \in \mathbf{R}, \lim_{t \rightarrow \sup T} \Delta(t; t_0) > 0 \right)$$

with

$$\Delta(t; t_0) = c_1^2 + 4c_2 \exp \left\{ -\frac{4[u(t) - y(t)][u(t_0) - y(t_0)]}{h_1(t)h_2(t_0) - h_1(t_0)h_2(t)} \right\}. \quad (2.1.16)$$

The transition pdf of $X(t)$ in the presence of the absorbing boundary (2.1.15) is then

$$\alpha[x, t|y(t_0), t_0] = f[x, t|y(t_0), t_0] - c_1 \phi_1(x, t) f[\psi_1(x, t), t|y(t_0), t_0] \\ - c_2 \phi_2(x, t) f[\psi_2(x, t), t|y(t_0), t_0] \quad (x < S(t; t_0), y(t_0) < u(t_0)). \quad (2.1.17)$$

Proof 2.1.3 *Let $\tilde{\alpha}[x, t|y(t_0), t_0]$ denote the right-hand-side of (2.1.17). Since (2.1.11) holds, one has*

$$\tilde{\alpha}[x, t|y(t_0), t_0] = f[x, t|y(t_0), t_0] - c_1 \phi_1[2u(t_0) - y(t_0), t_0] f[x, t|2u(t_0) - y(t_0), t_0] \\ - c_2 \phi_2[2v(t_0) - y(t_0), t_0] f[x, t|4u(t_0) - 3y(t_0), t_0], \quad (2.1.18)$$

where

$$\phi_1[2u(t_0) - y(t_0), t_0] = \exp \left\{ -\frac{2d_1^*[u(t_0) - y(t_0)]}{h_2(t_0)} \right\},$$

$$\phi_2[2v(t_0) - y(t_0), t_0] = \exp \left\{ -\frac{4[2d_1^* - d_1][u(t_0) - y(t_0)]}{h_2(t_0)} \right\}.$$

Hence, $\tilde{\alpha}[x, t|y(t_0), t_0]$ satisfies Fokker-Planck equation (1.3.8). Furthermore, by virtue of (2.1.12), $\tilde{\alpha}[x, t|y(t_0), t_0]$ can also be written as

$$\tilde{\alpha}[x, t|y(t_0), t_0] = -c_2 f[x, t|y(t_0), t_0] \exp \left\{ -\frac{4[y(t) - u(t)][y(t_0) - u(t_0)]}{h_1(t)h_2(t_0) - h_1(t_0)h_2(t)} \right\} \\ \times \left[\exp \left\{ -\frac{2[x - u(t)][y(t_0) - u(t_0)]}{h_1(t)h_2(t_0) - h_1(t_0)h_2(t)} \right\} - \frac{2}{c_1 + \sqrt{\Delta(t; t_0)}} \right] \\ \times \left[\exp \left\{ -\frac{2[x - u(t)][y(t_0) - u(t_0)]}{h_1(t)h_2(t_0) - h_1(t_0)h_2(t)} \right\} - \frac{2}{c_1 - \sqrt{\Delta(t; t_0)}} \right]. \quad (2.1.19)$$

In order for $\tilde{\alpha}[x, t|y(t_0), t_0]$ to be a transition pdf in the presence of the absorbing boundary $S(t; t_0)$, the right-hand-side of (2.1.19) must be zero at $x = S(t; t_0)$, non negative for all $x < S(t; t_0)$ and $y(t_0) < \lim_{t \downarrow t_0} S(t; t_0) = u(t_0)$; finally, it must satisfy the initial delta-condition. It is easy to prove that all these conditions hold iff $S(t; t_0)$ is as in (2.1.15) with $c_1 > 0, c_2 \in \mathbf{R}$ and $\lim_{t \rightarrow \sup T} \Delta(t; t_0) > 0$. Hence, $\tilde{\alpha}$ equals to the pdf α . This completes the proof.

It should not pass unnoticed that (2.1.15) is a generalization of Daniels' boundary (2.1.10). Indeed, if Theorem 2.1.2 is applied to the zero-mean Gauss-Markov process with $c(s, t) = s$ ($0 \leq s \leq t < +\infty$), the boundary (2.1.15) generalizes Daniels' boundary in that the latter

requires the choice $t_0 = 0$, $y(t) \equiv 0$, $u(t) \equiv \alpha/2$ with $\alpha \neq 0$, whereas the former holds for all $t_0 \geq 0$, $t > t_0$, $y(t) = d_1 t + d_2$, $u(t) = d_1^* t + d_2^*$, with $d_1, d_2, d_1^*, d_2^* \in \mathbf{R}$ and such that $y(t) < u(t)$.

The following theorem shows the existence of a closed-form relation of the FPT pdf through the boundary $S(t; t_0)$ in terms of the free transition pdf.

Theorem 2.1.3 *Under the assumptions of Theorem 2.1.2, for the boundary (2.1.15) one has:*

$$g[S(t; t_0), t|y(t_0), t_0] = \frac{u(t_0) - y(t_0)}{r(t) - r(t_0)} \frac{h_2(t)}{h_2(t_0)} \frac{dr(t)}{dt} \frac{2\sqrt{\Delta(t; t_0)}}{c_1 + \sqrt{\Delta(t; t_0)}} \\ \times f[S(t; t_0), t|y(t_0), t_0] \quad (y(t_0) < u(t_0)). \quad (2.1.20)$$

Furthermore, if $T = [a, b]$ then

$$\int_{t_0}^b g[S(t; t_0), t|y(t_0), t_0] dt = 1 - \lim_{t \rightarrow b} F[S(t; t_0), t|y(t_0), t_0] \\ + c_1 \exp \left\{ -\frac{2d_1^*[u(t_0) - y(t_0)]}{h_2(t_0)} \right\} \lim_{t \rightarrow b} F[S(t; t_0), t|2u(t_0) - y(t_0), t_0] \\ + c_2 \exp \left\{ -\frac{4[2d_1^* - d_1][u(t_0) - y(t_0)]}{h_2(t_0)} \right\} \lim_{t \rightarrow b} F[S(t; t_0), t|4u(t_0) - 3y(t_0), t_0], \quad (2.1.21)$$

where F is the distribution function of a normal process with conditional mean (1.3.6) and variance (1.3.7).

Proof 2.1.4 *By integration of both sides of (2.1.18) with respect to x between $-\infty$ and $S(t; t_0)$ one obtains*

$$\int_{-\infty}^{S(t; t_0)} \alpha[x, t|y(t_0), t_0] dx = F[S(t; t_0), t|y(t_0), t_0] \\ - c_1 \exp \left\{ -\frac{2d_1^*[u(t_0) - y(t_0)]}{h_2(t_0)} \right\} F[S(t; t_0), t|2u(t_0) - y(t_0), t_0] \\ - c_2 \exp \left\{ -\frac{4[2d_1^* - d_1][u(t_0) - y(t_0)]}{h_2(t_0)} \right\} F[S(t; t_0), t|4u(t_0) - 3y(t_0), t_0]. \quad (2.1.22)$$

Since

$$\int_{-\infty}^{S(t)} \alpha(x, t|y, \tau) dx = 1 - \int_{\tau}^t g[S(\vartheta), \vartheta|y, \tau] d\vartheta, \quad y < S(\tau) \quad (2.1.23)$$

implies

$$g[S(t; t_0), t|y(t_0), t_0] = -\frac{\partial}{\partial t} \int_{-\infty}^{S(t; t_0)} \alpha[x, t|y(t_0), t_0] dx.$$

Furthermore we note that

$$\lim_{\tau \uparrow t} \Psi[S(t), t|S(\tau), \tau] = \frac{dr(t)}{dt} \lim_{\tau \uparrow t} \Psi_W \left[S^*[r(t)], r(t) | S^*[r(\tau)], r(\tau) \right] \\ = \frac{dr(t)}{dt} \lim_{\xi \uparrow \vartheta} \Psi_W \left[S^*(\vartheta), \vartheta | S^*(\xi), \xi \right] = 0, \quad (2.1.24)$$

$r(t)$ being a monotonically increasing function in the parameter set T , which also proves the non-singularity of equation (1.3.12). The relation (2.1.20) immediately follows by making use of (2.1.24) and (2.1.22). Finally, (2.1.21) follows by taking the limit of (2.1.23) as t goes to b . This completes the proof.

We wish to emphasize that for boundaries of family (2.1.15) the FPT pdf's are provided in closed-form by (2.1.20) while the kernel of equation (1.3.12) is in general non identically vanishing on accounts of Theorem 2.1.1. Hence, (2.1.20) provides an exact reference to test the accuracy of numerical solutions of (1.3.12). With such a goal, we now consider the following special case.

Example 2.1.1 (*Brownian Bridge*) Let $\{X(t), t \in [0, 1]\}$ be the zero-mean Gauss-Markov process with covariance $c(s, t) = s(1-t)$ ($0 \leq s \leq t \leq 1$), so that $h_1(t) = t$ and $h_2(t) = 1-t$. Hence, the transition pdf $f(x, t|y, \tau)$ is normal with mean and variance respectively given by

$$E[X(t)|X(\tau) = y] = \frac{1-t}{1-\tau} y \quad \text{Var}[X(t)|X(\tau) = y] = \frac{1-t}{1-\tau} (t-\tau).$$

The functions $y(t) = (d_1 - d_2)t + d_2$ and $u(t) = (d_1^* - d_2^*)t + d_2^*$, with $d_1, d_2, d_1^*, d_2^* \in \mathbb{R}$ and such that $y(t) < u(t) \forall t \in [0, 1]$, are symmetry curves in the above specified sense. Hence, from Theorem 2.1.3 it follows that the FPT pdf through the boundary

$$S(t; t_0) = u(t) - \frac{t-t_0}{2[u(t_0) - y(t_0)]} \ln \left\{ \frac{c_1 + \sqrt{\Delta(t; t_0)}}{2} \right\}, \quad (2.1.25)$$

with

$$\Delta(t; t_0) = c_1^2 + 4 c_2 \exp \left\{ -\frac{4[u(t) - y(t)][u(t_0) - y(t_0)]}{t-t_0} \right\},$$

is given by

$$g[S(t; t_0), t|y(t_0), t_0] = \frac{2[u(t_0) - y(t_0)] \sqrt{\Delta(t; t_0)}}{(t-t_0)[c_1 + \sqrt{\Delta(t; t_0)}]} f[S(t; t_0), t|y(t_0), t_0]. \quad (2.1.26)$$

Furthermore, from (2.1.21) it follows

$$\int_{t_0}^1 g[S(t; t_0), t|y(t_0), t_0] dt = c_1 \exp \left\{ -\frac{2 d_1^* [u(t_0) - y(t_0)]}{1-t_0} \right\} + c_2 \exp \left\{ -\frac{4[2d_1^* - d_1][u(t_0) - y(t_0)]}{1-t_0} \right\} \quad (2.1.27)$$

if $\lim_{t \rightarrow 1} S(t; t_0) > 0$, while the left-hand-side is unity if $\lim_{t \rightarrow 1} S(t; t_0) < 0$.

2.2 A Computational method for GM processes

The present Section is focussed on two main items: (i) to address directly the question of numerical solutions by constructing effective computational procedures to evaluate FPT pdf's for Gauss-Markov processes without resorting to the transformation methods, and (ii) to test accuracy and reliability of our computational results, by comparison with the corresponding exact results and with some examples drawn from the literature. Other computational matters will be considered with reference to "upcrossing problems", hitherto ignored by other authors. We shall describe into some details the procedure to compute g and estimate the related computational errors by solving Equation (1.3.12) via an algorithm based, for convenience, on the repeated Simpson rule (cf. [15]), that in all our computations has yielded by far the most accurate results with respect to various other methods tested by us.

For the sake of conciseness, in the sequel the following short-hand notation will be employed:

$$\begin{aligned}
g(t) &:= g[S(t), t|x_0, t_0], & t, t_0 \in T, t_0 < t \\
\Psi(t) &:= \Psi[S(t), t|x_0, t_0], & t, t_0 \in T, t_0 < t \\
\Psi(t|\tau) &:= \Psi[S(t), t|S(\tau), \tau], & t, \tau \in T, t_0 < \tau \leq t,
\end{aligned} \tag{2.2.1}$$

so that Equation (1.3.12) reads

$$g(t) = -2\Psi(t) + 2 \int_{t_0}^t g(\tau) \Psi(t|\tau) d\tau \quad (x_0 < S(t_0)). \tag{2.2.2}$$

A discretization via step $p > 0$, after setting $t = t_0 + kp$ ($k = 1, 2, \dots$), yields:

$$\begin{aligned}
g(t_0 + kp) &= -2\Psi(t_0 + kp) + 2 \int_{t_0}^{t_0+kp} g(\tau) \Psi(t_0 + kp|\tau) d\tau \\
&\quad (x_0 < S(t_0), k = 1, 2, \dots).
\end{aligned} \tag{2.2.3}$$

To compute $g(t_0 + kp)$ ($k = 1, 2, \dots$) we proceed as follows. Let n be a positive integer. Then,

(i) If $k = 2n$, the function $g(\tau) \Psi(t_0 + kp|\tau)$ under the integral sign in (2.2.3) is evaluated by a three-point formula with weights $1/3, 4/3, 1/3$, respectively, at $t_0 + jp, t_0 + (j+1)p, t_0 + (j+2)p$, with $j = 0, 1, \dots, 2n-2$;

(ii) If $k = 2n+1$, in (2.2.3) we set:

$$\begin{aligned}
\int_{t_0}^{t_0+(2n+1)p} g(\tau) \Psi(t_0 + kp|\tau) d\tau &= \int_{t_0}^{t_0+(2n-2)p} g(\tau) \Psi(t_0 + kp|\tau) d\tau \\
&\quad + \int_{t_0+(2n-2)p}^{t_0+(2n+1)p} g(\tau) \Psi(t_0 + kp|\tau) d\tau.
\end{aligned}$$

The first integral on the right-hand-side is calculated as in (i), whereas to the second integral Simpson's $3/8$ rule with weights $3/8, 9/8, 9/8, 3/8$ is applied. (It may be useful to recall that thus doing the truncation errors of the above numerical evaluations are all alike, namely $O(p^5)$).

Denoting by $\tilde{g}(t_0 + kp)$ the numerical evaluation of $g(t_0 + kp)$ ($k = 1, 2, \dots$), we are led to the following iterative algorithm:

$$\tilde{g}(t_0 + p) = -2\Psi(t_0 + p) \tag{2.2.4}$$

$$\begin{aligned}
\tilde{g}(t_0 + kp) &= -2\Psi(t_0 + kp) + 2p \sum_{j=1}^{k-1} w_{k,j} \tilde{g}(t_0 + jp) \Psi(t_0 + kp|t_0 + jp) \\
&\quad (k = 2, 3, \dots)
\end{aligned}$$

where the weights $w_{k,j}$ are specified as follows:

$$\begin{aligned}
w_{2n,2j-1} &= \frac{4}{3} \quad (j = 1, 2, \dots, n; n = 1, 2, \dots) \\
w_{2n,2j} &= \frac{2}{3} \quad (j = 1, 2, \dots, n-1; n = 2, 3, \dots) \\
w_{2n+1,2j-1} &= \frac{4}{3} \quad (j = 1, 2, \dots, n-1; n = 2, 3, \dots) \\
w_{2n+1,2j} &= \frac{2}{3} \quad (j = 1, 2, \dots, n-2; n = 3, 4, \dots) \\
w_{2n+1,2(n-1)} &= \frac{17}{24} \quad (n = 2, 3, \dots) \\
w_{2n+1,2n-1} &= w_{2n+1,2n} = \frac{9}{8} \quad (n = 1, 2, \dots).
\end{aligned} \tag{2.2.5}$$

We emphasize that the above outlined algorithm has been conceived with the specific aim of disposing of an iterative procedure to evaluate g . Indeed, the numerical evaluation of $\tilde{g}(t_0 + kp)$ follows from (2.2.4) in terms of the computed values at the previous times $t_0 + p, t_0 + 2p, \dots, t_0 + (k-1)p$, a computationally valuable feature that is not always shared by existing alternative procedures.

The convergence of the above computational method is expressed by the following theorem.

Theorem 2.2.1 *Let p be the discretization step, $t_m = t_0 + Np$ with $N \in \mathbf{N}_0$, and set*

$$\Delta_{kp} := g(t_0 + kp) - \tilde{g}(t_0 + kp) \quad (k = 1, 2, \dots, N). \tag{2.2.6}$$

Then,

$$\lim_{p \rightarrow 0} |\Delta_{kp}| = 0 \quad (k = 1, 2, \dots, N) \tag{2.2.7}$$

for all fixed kp .

Proof 2.2.1 *The proof, extensively given in Appendix 2 of [23], is based on a suitable adaptation of some arguments typical of the numerical analysis realm. It consists of showing that the absolute error $|\Delta_{kp}|$ is bounded from above as follows:*

$$|\Delta_{kp}| \leq 2Np e^{8Mkp/3} \omega[(\Psi g)_{Kp}, 2p/3], \tag{2.2.8}$$

where

$$M = \max_{t_0 \leq \tau \leq t_m} |\Psi(t|\tau)| \tag{2.2.9}$$

and

$$\omega[(\Psi g)_{Kp}, 2p/3] \equiv \sup_{\substack{\tau_1, \tau_2 \in [t_0, t_0 + kp] \\ |\tau_1 - \tau_2| < 2p/3}} \left| g(\tau_1)\Psi(t_0 + kp|\tau_1) - g(\tau_2)\Psi(t_0 + kp|\tau_2) \right| \tag{2.2.10}$$

is the modulus of continuity of $(\Psi g)_{Kp}$ in $[t_0, t_0 + kp]$. Since this continuity modulus tends to 0 as $p \rightarrow 0$, (2.2.7) follows, being thus insured the convergence of the devised computational procedure.

A noteworthy feature of the above algorithm is its being implementable after simply specifying the initial data t_0, x_0 , the functions $m(t), h_1(t), h_2(t)$ that characterize the process, the boundary $S(t)$ and the discretization step p . Furthermore, it does not involve any heavy computation, neither requires use of any library subroutines, Monte Carlo methods or other special software packages to calculate high dimension multiple integrals, as for instance required in [73], [74], [31] and [79].

The following examples are instrumental to indicate the efficacy of our computational procedures, as well as the extremely high achieved precision.

Example 2.2.1 (*Brownian bridge*) Let $\{X(t), t \in [0, 1]\}$ be the zero-mean Gauss-Markov process with covariance $c(s, t) = s(1 - t)$ ($0 \leq s \leq t < 1$). For the \cap -convex boundary

$$S(t) = 1 - \frac{t}{2} \ln \left\{ \frac{1 + \sqrt{1 + 8e^{-4/t}}}{4} \right\} \quad (t \geq 0), \quad (2.2.11)$$

obtained by setting $t_0 = 0, d_1^* = d_2^* = 1, d_1 = d_2 = 0, c_1 = c_2 = 1/2$ in (2.1.25) we have evaluated $g(t) \equiv g[S(t), t|0, 0]$ via (2.2.4). Tables 2.1 and 2.2 show, for some choices of times, the computed density $\tilde{g}(t)$, the cumulative distribution $\tilde{P}(t)$, the absolute error $\varrho_a(t) = g(t) - \tilde{g}(t)$ and the relative error $\varrho_r(t) = [g(t) - \tilde{g}(t)]/g(t)$, the exact values of $g(t)$ having been obtained from (2.1.26). The integration step has been taken as 10^{-3} in Table 2.1, and as 10^{-4} in Table 2.2. We note that from (2.1.27) applied to boundary (2.2.11), one has:

$$P(1) = \int_0^1 g[S(t), t|0, 0] dt = \frac{1}{2} (e^{-2} + e^{-8}) = 0.0678353730 \quad (2.2.12)$$

within the precision range used for our computations. Evidently, this value is very close to $\tilde{P}(0.99)$ in the case of Table 2.1, while coinciding with $\tilde{P}(0.99)$ in the case of Table 2.2.

Table 2.1: Brownian bridge and boundary (2.2.11). For the integration step 10^{-3} , the computed FPT pdf $\tilde{g}(t)$, absolute error $\varrho_a(t)$, relative error $\varrho_r(t)$ and cumulative distribution $\tilde{P}(t)$ are listed for various values of t .

t	$\tilde{g}(t)$	$\varrho_a(t)$	$\varrho_r(t)$	$\tilde{P}(t)$
0.10	0.347459967E-01	-0.124900090E-15	-0.359466132E-14	0.644856704E-03
0.20	0.139954064E+00	-0.297650793E-12	-0.212677492E-11	0.100014935E-01
0.30	0.159385079E+00	-0.785003729E-10	-0.492520212E-09	0.255324243E-01
0.40	0.136708217E+00	-0.794865340E-09	-0.581432019E-08	0.405185953E-01
0.50	0.101835978E+00	-0.223092766E-08	-0.219070681E-07	0.524874424E-01
0.60	0.653465678E-01	-0.310597582E-08	-0.475308203E-07	0.608373477E-01
0.70	0.321204479E-01	-0.243059077E-08	-0.756711414E-07	0.656640738E-01
0.80	0.804695990E-02	-0.799463207E-09	-0.993497291E-07	0.675618836E-01
0.90	0.123300790E-03	-0.141406632E-10	-0.114684300E-06	0.678341757E-01
0.99	0.105579170E-37	-0.127528519E-44	-0.120789484E-06	0.678353740E-01

Table 2.2: Same as in Table 2.1 but with the integration step 10^{-4} .

t	$\tilde{g}(t)$	$\varrho_a(t)$	$\varrho_r(t)$	$\tilde{P}(t)$
0.10	0.347459967E-01	-0.124900090E-15	-0.359466132E-14	0.644757990E-03
0.20	0.139954064E+00	-0.106026299E-13	-0.757579280E-13	0.100014449E-01
0.30	0.159385079E+00	-0.247568632E-11	-0.155327358E-10	0.255324319E-01
0.40	0.136708216E+00	-0.251180465E-10	-0.183734726E-09	0.405186213E-01
0.50	0.101835976E+00	-0.705221853E-10	-0.692507579E-09	0.524874724E-01
0.60	0.653465648E-01	-0.982059017E-10	-0.150284720E-08	0.608373766E-01
0.70	0.321204455E-01	-0.768602890E-10	-0.239287743E-08	0.656640977E-01
0.80	0.804695913E-02	-0.252824341E-10	-0.314186189E-08	0.675618963E-01
0.90	0.123300777E-03	-0.447208432E-12	-0.362697175E-08	0.678341755E-01
0.99	0.105579158E-37	-0.403327099E-46	-0.382013940E-08	0.678353730E-01

Example 2.2.2 We consider the Brownian bridge of Example 2.2.1 and the \cap -convex boundaries

$$S(t; t_0) = d - \frac{t - t_0}{2d} \ln \left\{ \frac{1 + \sqrt{1 + 8e^{-4d^2/(t-t_0)}}}{4} \right\} \quad (t \geq t_0, d \in \mathbf{R}). \quad (2.2.13)$$

Note that these boundaries identify with those of (2.1.25) after setting in it $d_1^* = d_2^* = d$, $d_1 = d_2 = 0$, $c_1 = c_2 = 1/2$. The cumulative distribution $\tilde{P}(t)$ at $t = 1$, obtained for various values of d and t_0 via (2.2.4), is shown in Table 2.3. Absolute and relative errors, $\xi_a(1) = P(1) - \tilde{P}(1)$ and $\xi_r(1) = [P(1) - \tilde{P}(1)]/P(1)$, are also shown. They have been calculated by making use of the exact value

$$P(1) = \int_{t_0}^1 g[S(t; t_0), t|0, t_0] dt = \frac{1}{2} \left[\exp\left(-\frac{2d^2}{1-t_0}\right) + \exp\left(-\frac{8d^2}{1-t_0}\right) \right], \quad (2.2.14)$$

It should be pointed out that $d = 0.50$ and $t_0 = 0$ yields the same problem earlier considered by Durbin [31]. In Table 1 of [31] the values of the crossing probabilities, obtained by means of successive approximations, are listed. The most accurate results shown in Durbin [31] were obtained by truncating the series expansion of the first crossing pdf to the fourth term. The related absolute error is $-2 \cdot 10^{-8}$. A better result is obtained via our simple numerical method. Indeed, the one-order better absolute error $\xi_a(1) = -5 \cdot 10^{-9}$ is obtained via (2.2.4) with integration step 10^{-4} .

Example 2.2.3 Let $\{X(t), t \in [0, \infty)\}$ be the standard Brownian motion. As a further example of implementation of our numerical procedure, we have evaluated via (2.2.4) the FPT density and cumulative distribution through boundaries $S(t) = 0.5\sqrt{t+1}$ and $S(t) = \sqrt{t+1}$ (see Tables 2.4 and 2.5). This has allowed us to compare our computations with those listed in Table 1 of Ref. [13], that were ingeniously obtained by Daniels via a transformation from an Ornstein-Uhlenbeck process with a constant boundary, followed by a numerical differentiation of its cumulative FTP distribution ([51]), in order to circumvent the heavy computations required by Durbin's method [31]. Our results clearly support Daniels conjecture that his g_1 -approximation globally yields better results than those obtained via his g_2 -approximation or by the tangent approximation method [13].

Table 2.3: Brownian bridge and boundaries (2.2.13). For integration step 10^{-4} , the computed cumulative distribution $\tilde{P}(1)$, absolute error $\xi_a(1)$ and relative error $\xi_r(1)$ are listed for various values of d and t_0 .

	d	$\tilde{P}(1)$	$\xi_a(1)$	$\xi_r(1)$
$t_0 = 0.0$	0.25	0.744513827E+00	-0.454947562E-07	-0.611066676E-07
	0.50	0.370932977E+00	-0.518469667E-08	-0.139774489E-07
	0.75	0.167880733E+00	-0.647733311E-09	-0.385829454E-08
	1.00	0.678353730E-01	-0.331178696E-10	-0.488209442E-09
	1.25	0.219703301E-01	-0.594121974E-12	-0.270420139E-10
	1.50	0.555450588E-02	-0.377562565E-14	-0.679741047E-12
	1.75	0.109374557E-02	-0.954097912E-17	-0.872321623E-14
	2.00	0.167731314E-03	0.433680869E-18	0.258556890E-14
$t_0 = 0.2$	0.25	0.695303424E+00	-0.456968964E-07	-0.657222413E-07
	0.50	0.308673218E+00	-0.465904054E-08	-0.150937637E-07
	0.75	0.124333552E+00	-0.355789273E-09	-0.286157091E-08
	1.00	0.410651993E-01	-0.789675964E-11	-0.192298096E-09
	1.25	0.100579789E-01	-0.474585649E-13	-0.471849915E-11
	1.50	0.180328165E-02	-0.724247051E-16	-0.401627250E-13
	1.75	0.236539066E-03	-0.116551734E-17	-0.492737777E-14
	2.00	0.226999649E-04	0.101643954E-18	0.447771414E-14
$t_0 = 0.4$	0.25	0.623267323E+00	-0.458354389E-07	-0.735405829E-07
	0.50	0.235136105E+00	-0.360244176E-08	-0.153206664E-07
	0.75	0.769540257E-01	-0.110181100E-09	-0.143177825E-08
	1.00	0.178378065E-01	-0.598483069E-12	-0.335513825E-10
	1.25	0.273539248E-02	-0.581566045E-15	-0.212607898E-12
	1.50	0.276542185E-03	-0.216840434E-18	-0.784113405E-15
	1.75	0.184309265E-04	-0.880914265E-19	-0.477954412E-14
	2.00	0.809798396E-06	0.370576914E-20	0.457616261E-14

2.3 Approximations for neuronal models by GM processes

Motivated by some unsolved problems of biological interest, such as the description of firing probability densities for Leaky Integrate-and-Fire (LIF) neuronal models, we consider the first-passage-time problem for Gauss-Markov diffusion processes along the line of [58]. This is essentially based on a space-time transformation, originally due to [30], by which any Gauss-Markov process can be expressed in terms of the standard Wiener process. Starting with an analysis that pinpoints certain properties of mean and autocovariance of a Gauss-Markov process, we are led to the formulation of some numerical and time-asymptotically analytical methods for evaluating first-passage-time probability density functions for Gauss-diffusion processes. Implementations for neuronal models under various parameter choices of biological significance confirm the expected excellent accuracy of our methods.

Using more than one GM process and devoting a special care to the dimensional analysis of the involved quantities, we slightly change the notation; for this reason, some definitions and certain properties of Gauss-Markov processes are recalled hereafter. Let t be a parameter, that in the sequel will be identified with the time, varying in a continuous set T . Let $\mathbb{E}(X)$ and

Table 2.4: Brownian motion and boundary $S(t) = 0.5 \sqrt{t+1}$. Integration step is 10^{-3} .

t	$\tilde{g}(t)$	$\tilde{P}(t)$
0.05	0.129274898E+01	0.223748238E-01
0.10	0.159630708E+01	0.100516304E+00
0.15	0.131926269E+01	0.173736012E+00
0.20	0.105653448E+01	0.232866032E+00
0.25	0.857737843E+00	0.280474807E+00
0.30	0.710190790E+00	0.319493408E+00
0.35	0.599029027E+00	0.352097912E+00
0.40	0.513479093E+00	0.379821327E+00
0.45	0.446245784E+00	0.403749874E+00
0.50	0.392394149E+00	0.424668141E+00
0.60	0.312271725E+00	0.459647598E+00
0.70	0.256190490E+00	0.487915717E+00
0.80	0.215186409E+00	0.511384269E+00
0.90	0.184153285E+00	0.531283251E+00
1.00	0.160002793E+00	0.548443159E+00
1.20	0.125164473E+00	0.576717999E+00
1.40	0.101517303E+00	0.599245664E+00
1.60	0.845937282E-01	0.617768940E+00
1.80	0.719835620E-01	0.633368612E+00
2.00	0.622844596E-01	0.646755302E+00
2.20	0.546308564E-01	0.658418112E+00
2.40	0.484625650E-01	0.668706273E+00

$\mathbb{P}(E)$ denote mean of random variable X and probability of the event E , respectively. Let us consider the Gauss-Markov process $\{G(t), t \in T\}$ with mean $m_G(t) := \mathbb{E}[G(t)]$ and covariance $c_G(\tau, t) := \mathbb{E}\{[G(\tau) - m_G(\tau)][G(t) - m_G(t)]\}$ such that $c_G(\tau, t) = u_G(\tau)v_G(t)$ where $u_G(t)$ and $v_G(t)$ are continuous functions in T .

Claim 2.3.1 *Let x, y be admissible states of $G(t)$ and $\tau < t$, with $t \in T^0$. Then, the transition probability density function $f_G(x, t|y, \tau)$ of $G(t)$ is normal with mean*

$$M_G(t|y, \tau) = m_G(t) + \frac{v_G(t)}{v_G(\tau)} [y - m_G(\tau)] \quad (2.3.1)$$

and variance

$$D_G^2(t|\tau) = \frac{v_G(t)}{v_G(\tau)} [u_G(t)v_G(\tau) - u_G(\tau)v_G(t)]. \quad (2.3.2)$$

From $f_G(x, t|y, \tau)$ the infinitesimal moments of $G(t)$ follow:

$$A_G^{(n)}(x, t) := \lim_{\Delta t \rightarrow 0} \frac{\mathbb{E}\{[G(t + \Delta t) - G(t)]^n | G(t) = x\}}{\Delta t}, \quad \forall n \geq 1.$$

Claim 2.3.2 *If $m_G(t)$, $u_G(t)$ and $v_G(t)$ are $C^1(T)$ class functions, the fourth order infinitesimal moment $A_G^{(4)}(x, t)$ vanishes. Hence, $G(t)$ is a diffusion process whose transition pdf is a solution*

Table 2.5: Same as Table 2.3 with boundary $S(t) = \sqrt{t+1}$.

t	$\tilde{g}(t)$	$\tilde{P}(t)$
0.2	0.222873116E+00	0.154108859E-01
0.3	0.280144236E+00	0.413536801E-01
0.4	0.277181917E+00	0.694873306E-01
0.5	0.255860533E+00	0.962062728E-01
0.6	0.231087153E+00	0.120554235E+00
0.7	0.207638450E+00	0.142471240E+00
0.8	0.186811581E+00	0.162170469E+00
0.9	0.168723835E+00	0.179925222E+00
1.0	0.153118413E+00	0.195998061E+00
1.2	0.127988932E+00	0.223988389E+00
1.4	0.108964682E+00	0.247599006E+00
1.6	0.942514658E-01	0.267860386E+00
1.8	0.826304147E-01	0.285504883E+00
2.0	0.732751189E-01	0.301063046E+00
2.5	0.564636052E-01	0.333179476E+00
3.0	0.454174648E-01	0.358473402E+00
3.5	0.376907849E-01	0.379144148E+00
4.0	0.320260184E-01	0.396504971E+00
4.5	0.277190389E-01	0.411394978E+00
5.0	0.243482807E-01	0.424379222E+00
5.5	0.216474620E-01	0.435854431E+00
6.0	0.194408787E-01	0.446108758E+00

of Fokker-Planck equation with drift and infinitesimal variance given by

$$A_G^{(1)}(x, t) = \dot{m}_G(t) + [x - m_G(t)] \frac{\dot{v}_G(t)}{v_G(t)}, \quad (2.3.3)$$

$$A_G^{(2)}(x, t) = v_G^2(t) \dot{r}_G(t) \equiv A_G^{(2)}(t), \quad (2.3.4)$$

where the dot over the letter denotes time derivative and $r_G(t) = \frac{u_G(t)}{v_G(t)}$.

Remark 2.3.1 Equations (2.3.3) and (2.3.4) show that for Gauss-diffusion processes the drift is in general time-dependent and dependent on x at most linearly. The infinitesimal variance depends at most on t .

Remark 2.3.2 Note that the non-uniqueness of the product form of the covariance of GM processes is absent for $M_G(t|y, \tau)$, $D_G^2(t|\tau)$, $A_G^{(1)}(x, t)$ and $A_G^{(2)}(x, t)$. Moreover, since $r_G(t)$ represents time and the product $u_G(t)v_G(t)$ has dimension of the variance of $G(t)$, there follows that $v_G(t)$ has dimension of the square root of the infinitesimal variance.

Table 2.6 lists the functions of the interest for two well-known GM processes, namely the standard Wiener $\{W(t), t \geq 0\}$ and Ornstein-Uhlenbeck $\{U(t), t \geq 0\}$ processes, henceforth denoted by $W(t)$ and $U(t)$, respectively. Note that the dimensions of $\varsigma > 0$ and $\vartheta > 0$ are square root of infinitesimal variance and time, respectively. For these processes they are both unity.

Table 2.6: Notation and some properties of standard Wiener and Ornstein-Uhlenbeck processes. Here it is assumed $\tau \leq t$, κ is a dimensionless arbitrary positive parameter, and ς and ϑ are both unity but with different dimensions, which will play a role in the sequel.

Wiener: $W(t)$	Ornstein-Uhlenbeck: $U(t)$
$T_W = [0, +\infty[$	$T_U = [0, +\infty[$
$m_W(t) = 0$	$m_U(t) = 0$
$c_W(\tau, t) = \varsigma^2 \tau$	$c_U(\tau, t) = (e^{\tau/\vartheta} - e^{-\tau/\vartheta})e^{-t/\vartheta} \varsigma^2 \vartheta / 2$
$u_W(t) = \sqrt{\kappa} \varsigma t$	$u_U(t) = (e^{t/\vartheta} - e^{-t/\vartheta}) \sqrt{\kappa} \varsigma \vartheta / 2$
$v_W(t) = \varsigma / \sqrt{\kappa}$	$v_U(t) = e^{-t/\vartheta} \varsigma / \sqrt{\kappa}$
$M_W(t y, \tau) = y$	$M_U(t y, \tau) = ye^{-(t-\tau)/\vartheta}$
$D_W^2(t \tau) = \varsigma^2(t - \tau)$	$D_U^2(t \tau) = [1 - e^{-2(t-\tau)/\vartheta}] \varsigma^2 \vartheta / 2$
$A_W^{(1)}(x) = 0$	$A_U^{(1)}(x) = -x/\vartheta$
$A_W^{(2)}(t) = \varsigma^2$	$A_U^{(2)}(t) = \varsigma^2$

However, for dimensional considerations they will be denoted by these symbols in all formulas concerning $W(t)$ and $U(t)$. Note that since $c_W(0, 0) = c_U(0, 0) = 0$, both $W(t)$ and $U(t)$ are singular at $t = 0$ where they vanish with probability 1 (w.p.1).

2.3.1 The Ornstein-Uhlenbeck process as a GM process

We shall now turn to the FPT problem in connection with the Ornstein-Uhlenbeck process. We start by re-writing the relation (1.3.9).

Claim 2.3.3 *The GM process $\{G(t), t \in [t_0, +\infty[$, having mean $m_G(t)$ and autocovariance $c_G(\tau, t) = u_G(\tau)v_G(t)$ for $\tau \leq t$, such that $G(t_0) = m_G(t_0)$ w.p.1, admits the following representation:*

$$G(t) = m_G(t) + \varphi_{G,W}(t) W[\rho_{G,W}(t)], \quad t \in [t_0, +\infty[\quad (2.3.5)$$

where $W(t)$ is the standard Wiener process, and

$$\varphi_{G,W}(t) = \frac{v_G(t)}{\sqrt{\kappa} \varsigma}, \quad (2.3.6)$$

$$\rho_{G,W}(t) = \kappa r_G(t) \quad (2.3.7)$$

with $\kappa > 0$ an arbitrary constant.

The central rule will be instead played by the following more suitable and general form of the above relation involving the Ornstein-Uhlenbeck process.

Proposition 2.3.1 *Let $\{G(t), t \in [t_0, +\infty[$ be a GM process with mean $m_G(t)$, $G(t_0) = m_G(t_0)$ w.p.1 and autocovariance $c_G(\tau, t) = u_G(\tau)v_G(t)$ ($\tau \leq t$). Then,*

$$G(t) = m_G(t) + \varphi_{G,U}(t) U[\rho_{G,U}(t)], \quad t \in [t_0, +\infty[\quad (2.3.8)$$

where $U(t)$ denotes the Ornstein-Uhlenbeck process of Table 2.6, and

$$\varphi_{G,U}(t) = \frac{v_G(t)}{\sqrt{\kappa\varsigma}} \sqrt{1 + \frac{2\kappa}{\vartheta} r_G(t)}, \quad (2.3.9)$$

$$\rho_{G,U}(t) = \frac{\vartheta}{2} \ln \left[1 + \frac{2\kappa}{\vartheta} r_G(t) \right] \quad (2.3.10)$$

with $\kappa > 0$ an arbitrary constant.

Since $m_0 = m_G(t_0) < S_G(t_0)$ and $v_G(t_0) > 0$, $[S_G(t_0) - m_0]/\varphi_{G,U}(t_0) > 0$, for the FPT pdf of the GM process $G(t)$ originating at m_0 at time t_0 through the threshold $S_G(t)$, one has

$$g_G[S_G(t), t] = \dot{\rho}_{G,U}(t) g_U \left[\frac{S_G(t) - m_G(t)}{\varphi_{G,U}(t)}, \rho_{G,U}(t) \right] \quad (2.3.11)$$

where on the right hand side appears the FPT pdf of the Ornstein-Uhlenbeck process $U(t)$ originating at 0 at time 0 through transformed threshold $S_U[\rho_{G,U}(t)] = [S_G(t) - m_G(t)]/\varphi_{G,U}(t)$ at the transformed time $\rho_{G,U}(t)$.

Following [41], Eq. (2.3.11) can be seen to be of particular interest in the case of asymptotically constant and asymptotically periodic thresholds $S_U[\rho_{G,U}(t)]$, due to certain features of the transition pdf as will be seen hereafter. In order to obtain our results in a form that will be directly implemented by us in the sequel, we shall restrain from a mathematically more rigorously formulation and rely on the evident intuitive meaning of our formulas.

Claim 2.3.4 ([41]) *Let $S_U(t)$ be an asymptotically constant threshold:*

$$\lim_{t \rightarrow +\infty} S_U(t) = S_U,$$

and let θ_s be a constant representing the “relaxation” time of $S_U(t)$ on S_U . Setting

$$h_U := -\vartheta \lim_{t \rightarrow +\infty} \psi_U[S_U(t), t|y, \tau] = \frac{S_U}{\sqrt{\pi\varsigma^2\vartheta}} e^{-\frac{S_U^2}{\varsigma^2\vartheta}}, \quad (2.3.12)$$

for $t \gg \max\{\theta_s, \vartheta\}$ and for $S_U > 2\sqrt{\varsigma^2\vartheta}$ one has

$$g_U[S_U(t), t] \simeq \frac{h_U}{\vartheta} e^{-h_U t/\vartheta}. \quad (2.3.13)$$

Claim 2.3.5 ([41]) *Let $S_U(t)$ be an asymptotically P -periodic threshold:*

$$\lim_{n \rightarrow \infty} S_U(nP + t) = s_U(t)$$

with

$$s_U(nP + t) = s_U(t), \quad n = 0, 1, \dots$$

Then, setting

$$h_U(t) := -\vartheta \lim_{n \rightarrow \infty} \psi_U[S_U(t + nP), t + nP|y, \tau] = [s_U(t) - \vartheta \dot{s}_U(t)] \frac{1}{\sqrt{\pi\varsigma^2\vartheta}} e^{-\frac{s_U^2(t)}{\varsigma^2\vartheta}}, \quad (2.3.14)$$

$$S_U = \int_0^P s_U(t) dt, \quad \Delta s_U = \max_{0 \leq t \leq P} s_U(t) - \min_{0 \leq t \leq P} s_U(t),$$

and defining θ_s in analogy with θ_s of Claim 2.3.4, for $t \gg \max\{\theta_s, \vartheta\}$ and for $S_U - \Delta s_U/2 > 2\sqrt{\zeta^2 \vartheta}$ one has:

$$g_U[S_U(t), t] \simeq \frac{h_U(t)}{\vartheta} e^{-\int_0^t h_U(\tau) d\tau / \vartheta}. \quad (2.3.15)$$

In conclusion, whenever the transformed threshold $S_U[\rho_{G,U}(t)]$ approaches a constant or a periodic function as the transformed time $\rho_{G,U}(t)$ diverges, Claim 2.3.4 or Claim 2.3.5 can be used, as appropriate.

2.3.2 An inverse problem

In a variety of applied fields, as a result of suitable hypothesis, one is led to models based on stochastic differential equations such as

$$dX = f(X, t)dt + \frac{1}{\zeta} \sqrt{g(X, t)} dW \quad (2.3.16)$$

whose coefficients are defined in a domain $I \times T$ of plain x, t and where $W(t)$ is the standard Wiener process. The associated initial condition is customarily $X(t_0) = x_0$ w.p. 1, $t_0 \in T$. Then, under suitable regularity conditions, the solution $\{X(t), t \in T\}$ of (2.3.16) is a diffusion process that, within Ito's theory of stochastic integrals, has drift $f(x, t)$ and infinitesimal variance $g(x, t)$. If $X(t)$ has to be a diffusion Gaussian process, the coefficients of Eq. (2.3.16) must be such that

$$f(x, t) = x b_1(t) + b_2(t), \quad (2.3.17)$$

$$g(x, t) = b_3(t), \quad (2.3.18)$$

with functions $b_1(t)$, $b_2(t)$ and $b_3(t)$ to be specified accordingly. As outlined in the foregoing, the mean $m_X(t)$ and the autocovariance $c_X(\tau, t)$ of $\{X(t), t \in T\}$ play an essential role within the FPT problem. In the following Proposition we can specify the GM diffusion process that is solution of equation (2.3.16).

Proposition 2.3.2 *Let $b_i(t)$, $i = 1, 2, 3$, be defined in $[t_0, +\infty[$ such that functions*

$$B_1(t) = \int_{t_0}^t b_1(\tau) d\tau, \quad \int_{t_0}^t b_2(\tau) e^{-B_1(\tau)} d\tau, \quad \int_{t_0}^t b_3(\tau) e^{-2B_1(\tau)} d\tau$$

exist in $[t_0, +\infty[$. Then, the solution of equation

$$dX = [X b_1(t) + b_2(t)] dt + \frac{1}{\zeta} \sqrt{b_3(t)} dW \quad (2.3.19)$$

with condition $X(t_0) = x_0$ w.p. 1 is the GM process $\{X(t), t \in [t_0, +\infty[$ having mean

$$m_X(t) = \left[x_0 + \int_{t_0}^t b_2(\tau) e^{-B_1(\tau)} d\tau \right] e^{B_1(t)}, \quad t_0 \leq t < +\infty \quad (2.3.20)$$

and autocovariance

$$c_X(\tau, t) = e^{B_1(t)} e^{B_1(\tau)} \int_{t_0}^{\tau} b_3(\xi) e^{-2B_1(\xi)} d\xi, \quad t_0 \leq \tau \leq t < +\infty. \quad (2.3.21)$$

Proof 2.3.1 *Recalling (2.3.3) and (2.3.4), we require that*

$$\begin{aligned} A_x^{(1)}(x, t) &= xb_1(t) + b_2(t), \\ A_x^{(2)}(t) &= b_3(t), \end{aligned}$$

namely

$$\begin{cases} \dot{v}_x(t)/v_x(t) &= b_1(t) \\ \dot{m}_x(t) - m_x(t)\dot{v}_x(t)/v_x(t) &= b_2(t) \\ v_x^2(t)\dot{r}_x(t) &= b_3(t). \end{cases} \quad (2.3.22)$$

System (2.3.22) in the unknown $m_x(t)$, $v_x(t)$ and $r_x(t)$ must be solved under initial conditions $r_x(t_0) = 0$ (and hence $u_x(0) = 0$), and $m_x(t_0) = m_0$.

Taking $v(t_0)$ as a positive real number, the first of Eqs. (2.3.22) immediately yields $v_x(t) = v(t_0)e^{B_1(t)}$. After setting it in the third equation one then obtains

$$r_x(t) = \frac{1}{v^2(t_0)} \int_{t_0}^t b_3(\tau) e^{-2B_1(\tau)} d\tau.$$

The autocovariance is thus expressed as $r_x(\tau)v_x(\tau)v_x(t)$. Finally, substituting $b_1(t)$ in place of $\dot{v}_x(t)/v_x(t)$ in the second equation, one is led to a first order linear differential equation with right hand side $b_2(t)$ and initial condition $m_x(t_0) = m_0$, whose solution is readily seen to be given by (2.3.20). ■

2.3.3 Leaky Integrate-and-Fire (LIF) neuronal model

In the sequel, the implications of Proposition 2.3.2 and of Claims 2.3.4 will be used to shed light on a much discussed but still poorly understood features of the LIF neuronal model for the release of action potentials of neurophysiological relevance. For brevity, we shall refer to [76] for the relevant electrophysiological background and for some of the customary notation.

2.3.4 LIF model with constant stimulus

Let $V(t) = \Delta V(t) - \rho$, where $\Delta V(t)$ denotes the electric potential difference (inside minus outside) across the neuronal membrane, and ρ the resting potential to which in the absence of stimulations $\Delta V(t)$ exponentially tends with a time constant θ . Therefore, in the absence of stimulations, $V(t)$ exponentially tends to zero with the same time constant θ . Further, let v_0 denote the constant value that we assume to be instantaneously achieved by $V(t)$ after each firing, namely after the release of each action potential. Hereafter, we shall refer to $V(t)$ simply as to the membrane potential, and to v_0 as to the reset potential. In view of the very large number of excitatory and inhibitory synapses that are activated as a result of endogenous and exogenous signals impinging on neurons, it is often legitimate to assume that $V(t)$ undergoes some kind of random changes after starting at v_0 . Since the much celebrated paper [36] in which the evolution of $V(t)$ was viewed as a random walk leading to the neuronal firing whenever it reaches a preassigned threshold value, numerous paper have appeared to achieve a higher degree of adherence of the mathematical models to the physiological reality. Some of these stem out of phenomenological equations of type (2.3.19), as discussed for instance in [76] and in the references indicated therein. In summary, the neuron's firing is assumed to occur whenever $V(t)$

attains the so-called firing threshold,¹ which is instantaneously followed by the reset of $V(t)$ to v_0 . Here the neuron's refractoriness arising after each firing is not taken into account. This is an approximation that should be acceptable whenever the firing frequency is not very high. Within such a framework, the neuron's firing pdf is modeled by the FPT pdf of the random process modeling $V(t)$ through the neuron's threshold. Without loss of generality, in the sequel we shall denote by $t_0 = 0$ the instant when a firing is released and the membrane potential resets at the initial value $V(0) = v_0$.

Let θ and σ positive parameters with dimension of time and square root of infinitesimal variance, respectively, and let μ denote a real parameter having dimension of drift. The LIF model with constant stimulus is obtained from (2.3.16) by setting

$$f(v, t) = -\frac{v}{\theta} + \mu, \quad g(v, t) = \sigma^2 \quad (2.3.23)$$

or, in the form (2.3.19), by setting

$$b_1(t) = -1/\theta, \quad b_2(t) = \mu, \quad b_3(t) = \sigma^2. \quad (2.3.24)$$

Note that the functions in (2.3.24) denote, respectively, the inverse of the time constant of the spontaneous decay of $V(t)$ to the resting potential in the absence of stimuli, a constant stimulus (or endogenous or exogenous origin) and the intensity of the random perturbation originating from the overall action of excitatory and inhibitory potentials. By virtue of Proposition 2.3.2, $\{V(t), t \in [0, \infty[\}$ is a GM process having mean

$$m_V(t) = v_0 e^{-t/\theta} + \mu\theta(1 - e^{-t/\theta}), \quad 0 \leq t < +\infty \quad (2.3.25)$$

and autocovariance

$$c_V(\tau, t) = \frac{\sigma\theta}{2} \left(e^{\tau/\theta} - e^{-\tau/\theta} \right) \cdot \sigma e^{-t/\theta}, \quad 0 \leq \tau \leq t < +\infty$$

which implies

$$u_V(t) = \frac{\sigma\theta}{2} \left(e^{t/\theta} - e^{-t/\theta} \right) \quad \text{and} \quad v_V(t) = \sigma e^{-t/\theta}.$$

After setting $\kappa = \vartheta/\theta$, from (2.3.9) and (2.3.10) one obtains²:

$$\varphi_{V,U} := \varphi_{V,U}(t) = \frac{\sqrt{\sigma^2\theta}}{\sqrt{\zeta^2\vartheta}}, \quad t' := \rho_{V,U}(t) = \frac{\vartheta}{\theta}t. \quad (2.3.26)$$

Let now $S_V(t) \equiv S_V$ be the firing threshold that we assume to be time-independent and

$$S_U(t') = \frac{\sqrt{\zeta^2\vartheta}}{\sqrt{\sigma^2\theta}} \left[S_V - v_0 e^{-t'/\vartheta} - \mu\theta \left(1 - e^{-t'/\vartheta} \right) \right]$$

the transformed threshold obtained via (2.3.8), (2.3.25) and (2.3.26). By means of Eq. (2.3.11) we are thus led to:

$$g_V(S_V, t) = \frac{\vartheta}{\theta} g_U[S_U(t'), t']. \quad (2.3.27)$$

¹In the present notation, the firing threshold considered hereafter is the difference between the neurophysiologically defined neuronal threshold and the resting potential.

²Note the necessity of introducing the parameters ϑ and ζ^2 to make all quantities dimensionally correct.

Since

$$\lim_{t' \rightarrow +\infty} S_U(t') = \frac{\sqrt{\zeta^2 \vartheta}}{\sqrt{\sigma^2 \theta}} (S_V - \mu \theta)$$

by virtue of the Claim 2.3.4, the right hand side of (2.3.27) admits the approximation (2.3.13) as far as

$$\frac{\sqrt{\zeta^2 \vartheta}}{\sqrt{\sigma^2 \theta}} (S_V - \mu \theta) > 2\sqrt{\zeta^2 \vartheta} \Leftrightarrow (S_V - \mu \theta) > 2\sqrt{\sigma^2 \theta} \quad (2.3.28)$$

holds. From (2.3.27) we finally obtain:

$$g_V(S_V, t) \simeq \frac{\vartheta}{\theta} \frac{h_U}{\vartheta} e^{-h_U t'/\vartheta} = \frac{h_V}{\theta} e^{-h_V t/\theta} \quad (2.3.29)$$

for $t' \gg \vartheta \Leftrightarrow t \gg \theta$, where we have set

$$h_V := -\theta \lim_{t \rightarrow +\infty} \psi_V[S_V, t|y, \tau] = \frac{S_V - \mu \theta}{\sqrt{\pi \sigma^2 \theta}} e^{-\frac{(S_V - \mu \theta)^2}{\sigma^2 \theta}} = h_U. \quad (2.3.30)$$

2.3.5 LIF model with periodic stimulus

Recently (see [81, 82]) the problem of determining the pdf of the interspike intervals (ISI), namely of the time intervals elapsing between pairs of successive firings, has been again raised. This is of interest in order to ultimately arise to the information carried by the neuron's spike trains. While referring to [6] for some more detailed considerations and for a discussion concerning the differences between ISI and FPT pdf's, here we limit ourselves to pointing out that the determination of the FPT pdf is the first unavoidable step towards the characterization of ISI pdf³. In [82] the LIF model is considered under the assumption that the neuron is subject to a deterministic periodic sinusoidal stimulus as well. See also [57] and reference therein. Hence, a substantial difference now emerges with respect to the case of the LIF model with a constant stimulus, in that in (2.3.24) one must take $b_2(t) = \mu \cos(\omega t + \varphi)$, with μ assumed hereafter to be a positive quantity. As a consequence, by virtue of Proposition 2.3.2, for all $0 \leq t < +\infty$ the GM process modeling the time course of the membrane potential has mean

$$m_V(t) = v_0 e^{-t/\theta} + \frac{\mu \theta [\cos(\omega t + \varphi) + \omega \theta \sin(\omega t + \varphi) - (\cos \varphi + \omega \theta \sin \varphi) e^{-t/\theta}]}{1 + \omega^2 \theta^2}. \quad (2.3.31)$$

With analogous meanings of $c_V(\tau, t)$, $u_V(t)$, $v_V(t)$, $\varphi_{V,U}(t)$, $\rho_{V,U}(t) \equiv t'$ and S_V as in Sect. 2.3.4, Eq. (2.3.11) yields

$$g_V(S_V, t) = \frac{\vartheta}{\theta} g_U[S_U(t'), t']$$

where

$$S_U(t') = \frac{\sqrt{\zeta^2 \vartheta}}{\sqrt{\sigma^2 \theta}} \left\{ S_V - v_0 e^{-t'/\vartheta} - \frac{\mu \theta}{1 + (\omega' \vartheta)^2} \left[\cos(\omega' t' + \varphi) + \omega' \vartheta \sin(\omega' t' + \varphi) - (\cos \varphi + \omega' \vartheta \sin \varphi) e^{-t'/\vartheta} \right] \right\}$$

with $\omega' = \omega \theta / \vartheta$.

³Note that in the case of constant stimuli, the FPT pdf and the ISI pdf coincide.

Let now $P' = 2\pi/\omega'$. Then,

$$s_U(t') := \lim_{n \rightarrow \infty} S_U(t' + nP') = \frac{\sqrt{\zeta^2 \vartheta}}{\sqrt{\sigma^2 \theta}} \left\{ S_V - \frac{\mu \theta}{1 + (\omega' \vartheta)^2} \left[\cos(\omega' t' + \varphi) + \omega' \vartheta \sin(\omega' t' + \varphi) \right] \right\}.$$

Hence, whatever frequency of the stimulus, use of Claim 2.3.5 can be made, provided

$$\begin{aligned} \inf_{\omega' > 0} \min_{t' > 0} s_U(t') > 2\sqrt{\zeta^2 \vartheta} &\Leftrightarrow \frac{\sqrt{\zeta^2 \vartheta}}{\sqrt{\sigma^2 \theta}} (S_V - \mu \theta) > 2\sqrt{\zeta^2 \vartheta} \\ &\Leftrightarrow (S_V - \mu \theta) > 2\sqrt{\sigma^2 \theta}. \end{aligned} \quad (2.3.32)$$

Let us now note that from (2.3.14) in this case one has:

$$\begin{aligned} h_U(t') &= \left\{ S_V - \frac{\mu \theta}{1 + (\omega' \vartheta)^2} \left[(1 - (\omega' \vartheta)^2) \cos(\omega' t' + \varphi) + 2\omega' \vartheta \sin(\omega' t' + \varphi) \right] \right\} \\ &\quad \times \frac{1}{\sqrt{\pi \sigma^2 \theta}} e^{-\frac{\left\{ S_V - \frac{\mu \theta}{1 + (\omega' \vartheta)^2} [\cos(\omega' t' + \varphi) + \omega' \vartheta \sin(\omega' t' + \varphi)] \right\}^2}{\sigma^2 \theta}} \\ &= \left\{ S_V - \frac{\mu \theta}{1 + \omega^2 \theta^2} \left[(1 - \omega^2 \theta^2) \cos(\omega t + \varphi) + 2\omega \theta \sin(\omega t + \varphi) \right] \right\} \\ &\quad \times \frac{1}{\sqrt{\pi \sigma^2 \theta}} e^{-\frac{\left\{ S_V - \frac{\mu \theta}{1 + \omega^2 \theta^2} [\cos(\omega t + \varphi) + \omega \theta \sin(\omega t + \varphi)] \right\}^2}{\sigma^2 \theta}} \\ &= -\theta \lim_{n \rightarrow \infty} \psi_V[S_V(t + nP), t + nP | y, \tau] =: h_V(t). \end{aligned} \quad (2.3.33)$$

Hence, for $t' \gg \vartheta \Leftrightarrow t \gg \theta$, if (2.3.32) holds, one obtains:

$$g_V(S_V, t) \simeq \frac{\vartheta h_U(t')}{\theta} e^{-\int_0^{t'} h_U(\tau') d\tau' / \vartheta} = \frac{h_V(t)}{\theta} e^{-\int_0^t h_V(\tau) d\tau / \theta}. \quad (2.3.34)$$

2.3.6 Some approximations

In particular now we shall obtain some numerical and analytical approximations to the FPT pdf. We shall also test the validity ranges of the approximations of the FPT pdf for the LIF model based on Eq. (2.3.29). As pointed out, these are valid for $t \gg \theta$ and $\gamma \geq 1$, where we have now set

$$\gamma := \frac{S_V - \mu \theta}{2\sqrt{\sigma^2 \theta}}. \quad (2.3.35)$$

Note, that the condition $\gamma \geq 1$ is equivalent to $(S_V - \mu \theta) > 2\sqrt{\sigma^2 \theta}$ required in (2.3.28). We shall finally design a correction procedure that for $\gamma \geq 1$ yields a new approximation to the FPT pdf valid for $t \in [0, +\infty[$.

We note that Eq. (1.3.12), valid for the FPT pdf of the GM process, can be thrown in the form

$$g(t) = -\psi_0(t) + \int_{t_0}^t \psi(t, \tau)g(\tau)d\tau \quad (2.3.36)$$

with

$$\psi_0(t) = \psi_G[S_G(t), t|m_0, t_0], \quad \psi(t, \tau) = \psi_G[S_G(t), t|S_G(\tau), \tau], \quad g(t) = g_G[S_G(t), t].$$

We set

$$t_i = t_0 + i\Delta t, \quad i = 0, 1, \dots \quad (2.3.37)$$

with Δt a suitable small positive real number, and denote by $g_0(t)$ the approximation to $g(t)$ obtained by solving Eq. (2.3.36) by the numerical method of [3]:

$$g_0(t_i) = \begin{cases} 0, & i = 0; \\ -\psi_0(t_i) + \Delta t \sum_{j=0}^{i-1} \psi(t_i, t_j)g_0(t_j), & i \geq 1. \end{cases} \quad (2.3.38)$$

Approximation $g_0(t)$ will be used as a reference to evaluate the goodness of the new approximations that will be discussed within the context of the LIF models.

Approximation for LIF model with constant stimulus

In the case of the LIF model with constant stimulus, the only characteristic time to be considered is the decay constant θ of membrane potential $V(t)$. Hence, we shall set $\Delta t = \theta/M$, with M a suitable integer number. The validity of the approximation $g_0(t)$ to the FPT pdf $g(t)$ is manifested by the data of Table 2.7. These have been obtained by two methods: (i) by numerical integration via (2.3.38) and (ii) by simulations of the sample paths of the membrane potential via Eqs. (2.3.16) and (2.3.23) after discretizing it by Euler method. Further details are given in the caption of Table 2.7.

We shall now proceed by sketching various approximations to $g(t)$.

Let $g_1(t)$ be the approximation to $g(t)$ provided by (2.3.29) for $\gamma \geq 1$ and $t \geq t_m \gg \theta$, where m denotes a suitably chosen integer number. Setting

$$a := \frac{h_V}{\theta}, \quad (2.3.39)$$

at the times t_i of (2.3.37), Eq. (2.3.29) yields:

$$g_1(t_i) = a e^{-at_i}, \quad i \geq 0. \quad (2.3.40)$$

Parameter a can be expressed in terms of γ . Indeed, from (2.3.30), (2.3.35) and (2.3.39) there follows:

$$a = \frac{2\gamma}{\theta\sqrt{\pi}}e^{-4\gamma^2}. \quad (2.3.41)$$

We shall now obtain an extension of the approximation $g_1(t)$ for small times and to improve the approximation level as well. To this purpose, we make use of the circumstance that in the present model the kernel $\psi(t, \tau)$ of Eq. (2.3.36), due to (2.3.30), is such that:

$$\lim_{t \rightarrow +\infty} \psi(t, \tau) = -a \quad (2.3.42)$$

Table 2.7: Percent relative differences of mean (A), standard deviation (B), coefficient of variation (C) and skewness (D) of FPT for LIF model with constant stimulus. The indicated values have been obtained by evaluating these quantities via the numerical method (2.3.38) and via the results of 10^5 sample path simulations. Parameters have been chosen as follows: $S = 10$ mV, $v_0 = 2$ mV, $\theta = 5$ ms, $\gamma = 0.5$ (this choice having been suggested in order not to make the simulation time exceedingly large), σ^2 as in the first column and μ as indicated in the second column and calculated via Eq. (2.3.35). The numerical approximation has been performed by setting $\Delta t = \theta/100$ in the interval $[0, 50\theta]$. The sample path simulations have been computed via Eqs. (2.3.16) and (2.3.23) with $dt = \theta \cdot 10^{-4}$.

σ^2	μ	A	B	C	D
2.000	1.368	1.09%	1.18%	0.09%	2.56%
4.000	1.106	1.27%	1.07%	0.19%	2.16%
6.000	0.905	1.35%	0.90%	0.44%	1.01%
8.000	0.735	1.36%	0.93%	0.42%	0.83%
10.000	0.586	1.47%	1.06%	0.41%	0.96%
12.000	0.451	1.51%	1.07%	0.44%	1.02%
14.000	0.327	1.47%	1.03%	0.43%	1.10%
16.000	0.211	1.56%	1.11%	0.44%	1.08%

1. Denote by $l < m$ an integer number such that the function $-\psi_0(t)$ is an approximation to $g(t)$ in $[0, t_l]$ with a requested precision, and set:

$$\bar{g}(t) := \begin{cases} 0, & 0 \leq t < t_l; \\ \hat{g}(t) = ae^{-(t-t_l)a}, & t \geq t_l; \end{cases}$$

$$\bar{\psi}(t, \tau) := \begin{cases} \psi(t, \tau), & 0 \leq t - \tau < t_m; \\ \hat{\psi}(t, \tau) = -a, & t - \tau \geq t_m. \end{cases}$$

2. We partition the time axis as follows:

$$0 \leq t < t_l, \quad t_l \leq t < t_{l+m}, \quad t \geq t_{l+m}. \quad (2.3.43)$$

3. For each t , the numerical algorithm is based on the following substitutions on the right-hand-side of Eq. (2.3.36):

$$\bar{g}(t) \longrightarrow g(t), \quad \bar{\psi}(t, \tau) \longrightarrow \psi(t, \tau). \quad (2.3.44)$$

For the sake of brevity, we shall outline this procedure only for the (most cumbersome) case, namely for $t \geq t_{l+m}$. Similarly, one proceeds in the other two cases specified in (2.3.43).

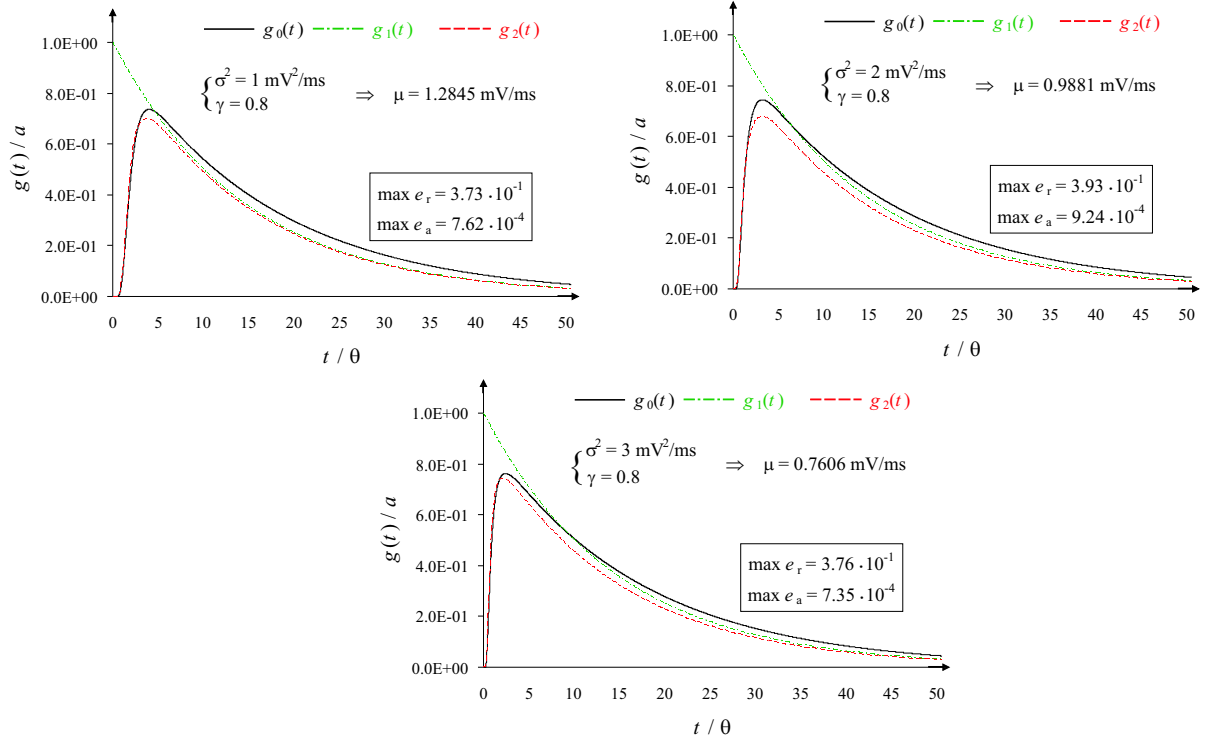


Figure 2.1: For the LIF model with constant stimulus, approximations $g_0(t)$, $g_1(t)$ and $g_2(t)$ to the FPT pdf $g(t)$ normalized to a — namely to the inverse of the mean FPT of the asymptotic exponential approximation (2.3.29) — are plotted for the following choice of parameters: $S = 10 \text{ mV}$, $v_0 = 2 \text{ mV}$ and $\theta = 5 \text{ ms}$. The values of σ^2 and μ are indicated for each plot. Times are expressed in units of θ . Having chosen $\gamma = 0.8$, μ is obtained via (2.3.35) and parameter a of $g_1(t)$, due to (2.3.41), takes the value 0.01396 ms^{-1} . For the numerical algorithm we have taken $\Delta t = \theta/100$, $t_m = 8\theta$; $t_l = 2\theta$ (when $\sigma^2 = 1 \text{ mV}^2/\text{ms}$) and $t_l = \theta$ for the other two values of σ^2 . Largest relative and absolute errors between $g_0(t)$ and $g_2(t)$ in the considered time interval 50θ are also indicated.

Performing substitutions (2.3.44) in Eq. (2.3.36), for $t \geq t_{l+m}$ one obtains:

$$\begin{aligned}
g(t) &\simeq -\psi_0(t) + \int_0^{t_l} \bar{\psi}(t, \tau) \bar{g}(\tau) d\tau + \int_{t_l}^{t-t_m} \bar{\psi}(t, \tau) \bar{g}(\tau) d\tau + \int_{t-t_m}^t \bar{\psi}(t, \tau) \bar{g}(\tau) d\tau \\
&= -\psi_0(t) + \int_{t_l}^{t-t_m} \hat{\psi}(t, \tau) \hat{g}(\tau) d\tau + \int_{t-t_m}^t \psi(t, \tau) \hat{g}(\tau) d\tau \\
&= -\psi_0(t) - a \int_{t_l}^{t-t_m} a e^{-(\tau-t_l)a} d\tau + \int_{t-t_m}^t \psi(t, \tau) \hat{g}(\tau) d\tau \\
&= -\psi_0(t) - a + \hat{g}(t-t_m) + \int_{t-t_m}^t \psi(t, \tau) \hat{g}(\tau) d\tau.
\end{aligned}$$

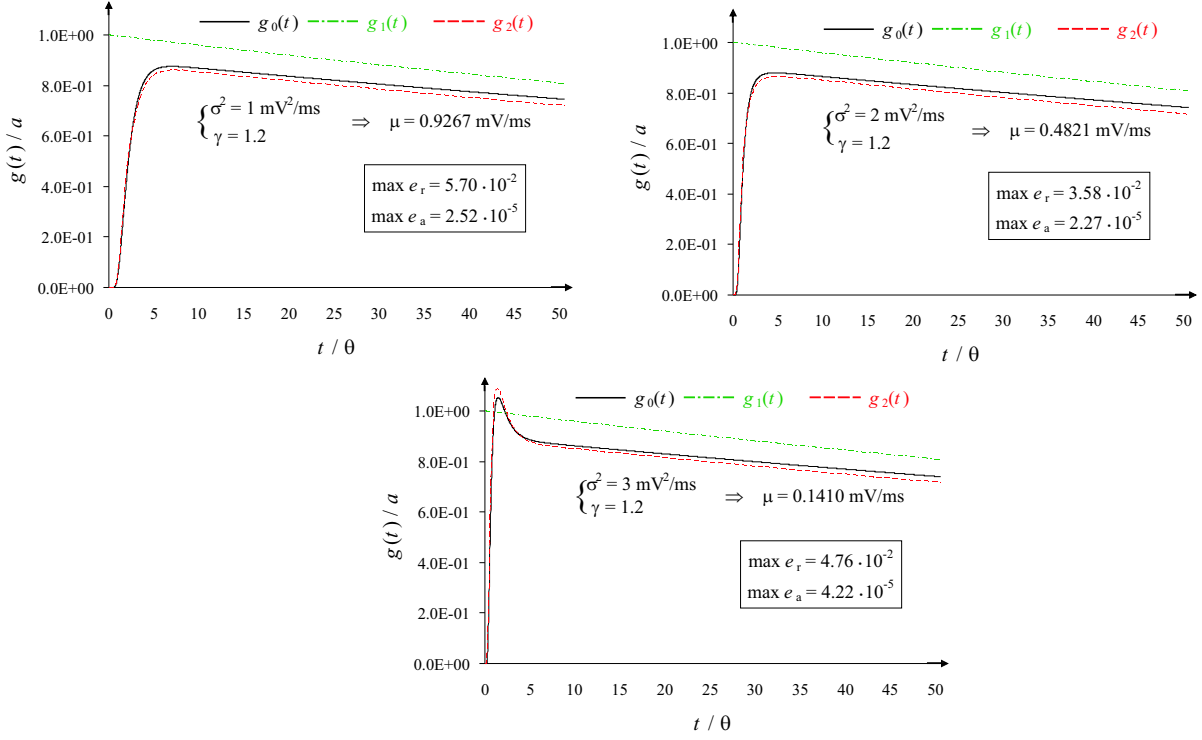


Figure 2.2: As in Figure 2.1, but with $\gamma = 1.2$ and consequently $a = 0.00085 \text{ ms}^{-1}$.

Hence, a new approximation $g_2(t)$ to $g(t)$ at the times t_i defined in (2.3.37) is finally obtained⁴:

$$g_2(t_i) = \begin{cases} -\psi_0(t_i), & 0 \leq i \leq l; \\ -\psi_0(t_i) + \frac{\Delta t}{2} a \psi(t_i, t_l) + \Delta t \sum_{j=l+1}^{i-1} \psi(t_i, t_j) \hat{g}(t_j), & l < i \leq l + m; \\ -\psi_0(t_i) - a + \hat{g}(t_{i-m}) \left[1 + \frac{\Delta t}{2} \psi(t_i, t_{i-m}) \right] \\ \quad + \Delta t \sum_{j=i-m+1}^{i-1} \psi(t_i, t_j) \hat{g}(t_j), & i > l + m. \end{cases} \quad (2.3.45)$$

Figures 2.1–2.3 show approximations $g_0(t)$, $g_1(t)$ and $g_2(t)$ to g for the values of parameters indicated in the captions. In all of them the three parameters S_V , v_0 and θ have been fixed, while in each figure, γ is a constant. Thus, due to (2.3.41), a is also a constant. The graphs show that as γ increases, $g_2(t)$ yields an excellent approximation to $g_0(t)$ for all $t \geq 0$. For instance, for $\gamma = 1.6$, the largest relative error is 5%, while the largest absolute error is $2.30 \cdot 10^{-6} \text{ ms}^{-1}$. It should be pointed out that largest errors occur around time t_l , namely around the time when the approximation is obtained by use of the function $\psi_0(t)$ alone. Hence, it is expected that largest absolute and relative errors can be minimized by suitably choosing t_l .

Finally, it must be explicitly noted that approximation $g_0(t)$ given by (2.3.38) requires that at each instant t_i all previously computed values of $g_0(t)$ be memorized and used, which makes

⁴Here a sum is taken as zero whenever the upper limit is less than the lower limit.

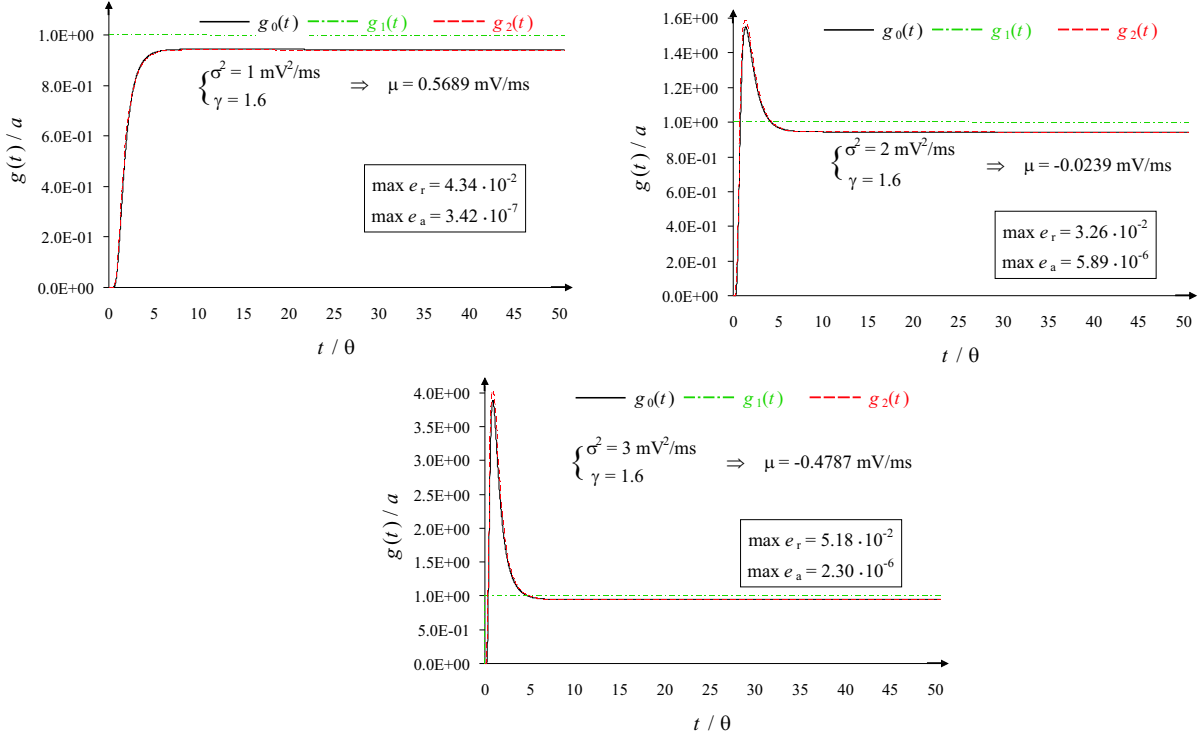


Figure 2.3: Same as Figure 2.1, but with $\gamma = 1.6$ and consequently $a = 0.00013 \text{ ms}^{-1}$. Note that for such value of γ approximations $g_2(t)$ and $g_0(t)$ are excellent.

the computation time grow quadratically with the number of iterations. However, for $t - \tau \geq t_m$, $\psi(t, \tau)$ can be approximated by $-a$. This suggests that a new numerical approximation $g_3(t)$ can be constructed on the considered mesh as follows:

$$g_3(t_i) = \begin{cases} 0, & i = 0; \\ -\psi_0(t_i) + \Delta t \sum_{j=0}^{i-1} \psi(t_i, t_j) g_3(t_j), & 1 \leq i < m; \\ -\psi_0(t_i) - a \Delta t \sum_{j=1}^{i-m} g_3(t_j) + \Delta t \sum_{j=i-m+1}^{i-1} \psi(t_i, t_j) g_3(t_j), & i \geq m. \end{cases} \quad (2.3.46)$$

Hence, the calculation of $g_3(t)$ at each instant t_i only needs to make use of its values at most of previous $m - 2$ instants t_j . This reduces the complexity of the numerical algorithm from quadratic to linear. In addition, the computed values of $g_3(t_j)$ at all instants t_j preceding t_{i-m+1} after contributing to the second sum in the third line of (2.3.46) are eliminated, with consequent saving of storage space. Table 2.8 shows the largest absolute and relative errors between $g_0(t)$ and $g_3(t)$ for all nine cases of Figures 2.1–2.3.

It should be stressed that approximation $g_3(t)$ is not an extension of approximation $g_2(t)$. Indeed, $g_3(t)$ does not rely on the approximation (2.3.40), whereas it is a direct development of $g_0(t)$, and thus unrelated to $g_1(t)$ and $g_2(t)$.

Table 2.8: Maximum absolute and relative errors, e_a and e_r , of $g_3(t)$ with respect to $g_0(t)$ are indicated for the LIF model with constant stimulus. The listed parameters γ , σ^2 and μ , as well as all other parameters, have been chosen as in Figures 2.1–2.3 and it has been taken $t_m = 40$ ms.

γ	σ^2	μ	$\max e_a$	$\max e_r$
0.8	1.000	1.284	$6.29 \cdot 10^{-6}$	$1.55 \cdot 10^{-3}$
0.8	2.000	0.988	$6.45 \cdot 10^{-6}$	$1.59 \cdot 10^{-3}$
0.8	3.000	0.761	$6.79 \cdot 10^{-6}$	$1.62 \cdot 10^{-3}$
1.2	1.000	0.927	$3.70 \cdot 10^{-8}$	$5.08 \cdot 10^{-5}$
1.2	2.000	0.482	$3.72 \cdot 10^{-8}$	$5.10 \cdot 10^{-5}$
1.2	3.000	0.141	$4.21 \cdot 10^{-8}$	$5.72 \cdot 10^{-5}$
1.6	1.000	0.569	$1.20 \cdot 10^{-11}$	$9.89 \cdot 10^{-7}$
1.6	2.000	-0.024	$1.64 \cdot 10^{-11}$	$1.35 \cdot 10^{-6}$
1.6	3.000	-0.479	$3.79 \cdot 10^{-11}$	$3.11 \cdot 10^{-6}$

LIF Model with periodic stimulus

Let P the period of the stimulus. Set:

$$a_V(t) = \frac{h_V(t)}{\theta} \quad (2.3.47)$$

and

$$A_V(t) = \int_0^t a_V(\tau) d\tau, \quad (2.3.48)$$

with $h_V(t)$ defined in (2.3.33). It is not difficult to prove that, if $\gamma \geq 1$, $h_V(t)$ is non-negative. Hence, $A_V(t)$ is also non-negative. In addition, it is strictly increasing, vanishes at $t = 0$, diverges for $t \rightarrow +\infty$ and satisfies $A_V(t + nP) = A_V(t) + nA_V(P)$ for all (positive) integer n .

Recalling that θ is the characteristic time for the relaxation of $S_U(t')$ on $s_U(t')$ and that $s_U(t')$ is also P periodic, we set $\Delta t = \min\{\theta/M, P/M\}$ with M an integer to be specified in such a way that a suitable time parsing is obtained in the numerical computations.

Let now denote by $g_4(t)$ the approximation to $g(t)$ obtained via (2.3.34) under the assumptions $\gamma \geq 1$ and $t \geq t_m \gg \theta$, with m a suitable integer. Then, at the instants representing the considered mesh (2.3.37), one has:

$$g_4(t_i) = a_V(t_i) e^{-A_V(t_i)}, \quad i \geq 0. \quad (2.3.49)$$

In order to obtain an extension of $g_4(t)$ we make use of the algorithm implemented for $g_2(t)$, with the proviso that now $\hat{\psi}(t, \tau)$ and $\hat{g}(t)$ are given by:

$$\hat{\psi}(t, \tau) = -a_V(t)$$

and

$$\hat{g}(t) = a_V(t) e^{-[A_V(t) - A_V(t_i)]},$$

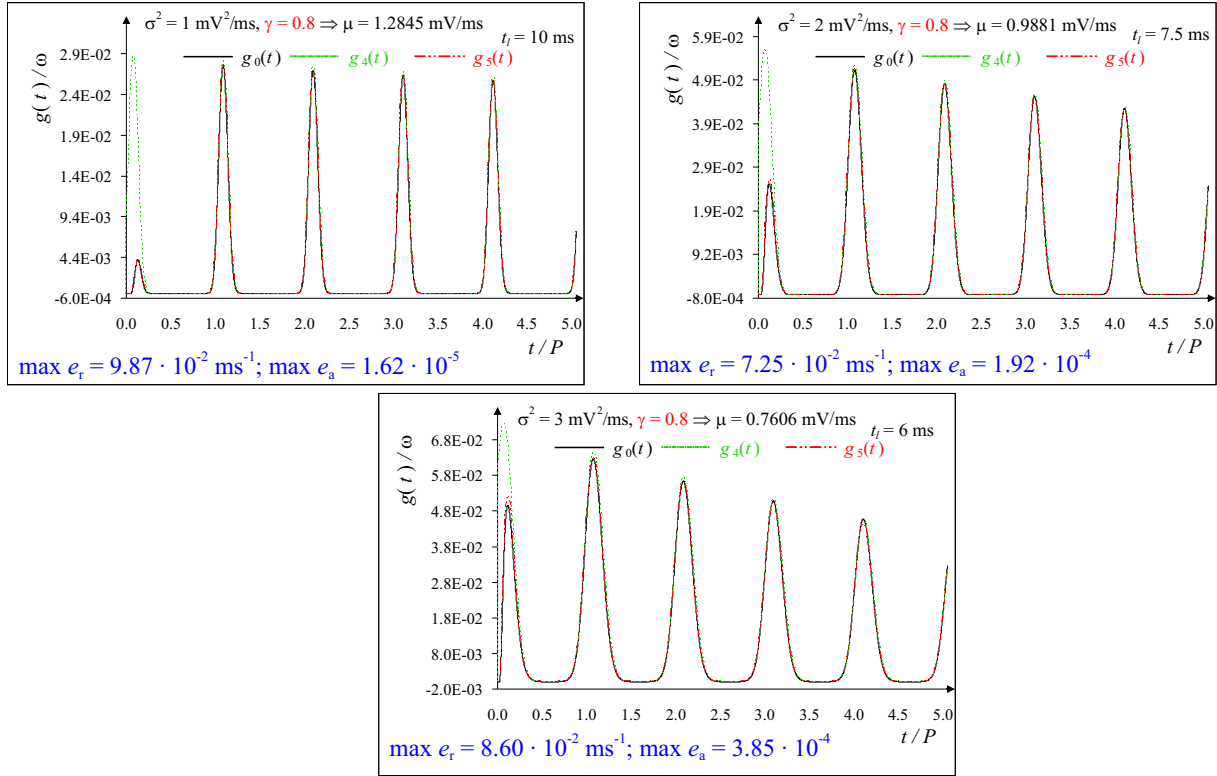


Figure 2.4: The approximations $g_0(t), g_4(t)$ and $g_5(t)$ to FPT pdf $g(t)$, normalized by angular frequency ω , are plotted in the time scale t/P for the LIF model with P -periodic stimulus. Here, $\gamma = 0.8$ and $S = 10$ mV, $v_0 = 2$ mV, $\theta = 5$ ms, $P = 10\theta$, $\varphi = 0$. The values of σ^2 and μ are also indicated. The numerical algorithms have been implemented with $\Delta t = \theta/100$, $t_m = 8\theta$. The values of t_l are indicated in next to each plot. The maximum relative and absolute errors between $g_0(t)$ and $g_5(t)$ in the time interval of duration 50θ are also shown.

respectively. At the considered discrete instants t_i , we thus obtain:

$$g_5(t_i) = \begin{cases} -\psi_0(t_i), & 0 \leq i \leq l \\ -\psi_0(t_i) + \frac{\Delta t}{2} a_v(t_l) \psi(t_i, t_l) + \Delta t \sum_{j=l+1}^{i-1} \psi(t_i, t_j) \hat{g}(t_j), & l < i \leq l + m \\ -\psi_0(t_i) - a_v(t_i) + \hat{g}(t_{i-m}) \left[\frac{h_v(t_i)}{h_v(t_{i-m})} + \frac{\Delta t}{2} \psi(t_i, t_{i-m}) \right] \\ \quad + \Delta t \sum_{j=i-m+1}^{i-1} \psi(t_i, t_j) \hat{g}(t_j), & i > l + m. \end{cases} \quad (2.3.50)$$

Figures 2.4–2.6 show the results of the computations with fixed γ and the following choices of parameters: $\sigma^2 = 1, 2, 3$ (mV^2/ms). The approximations to $g(t)$ are normalized by the threshold angular frequency ω , and time is expressed in units of P . As before, μ is uniquely determined by the pairs (γ, σ^2) .

Remark 2.3.3 Note that the terms depending on y and τ in $\psi_v[S_v(t), t|y, \tau]$ go to zero as fast as $e^{-(t-\tau)/\theta}$. Hence, approximating $\psi_v[S_v(t), t|y, \tau]$ by $-a$ is acceptable as far as the difference

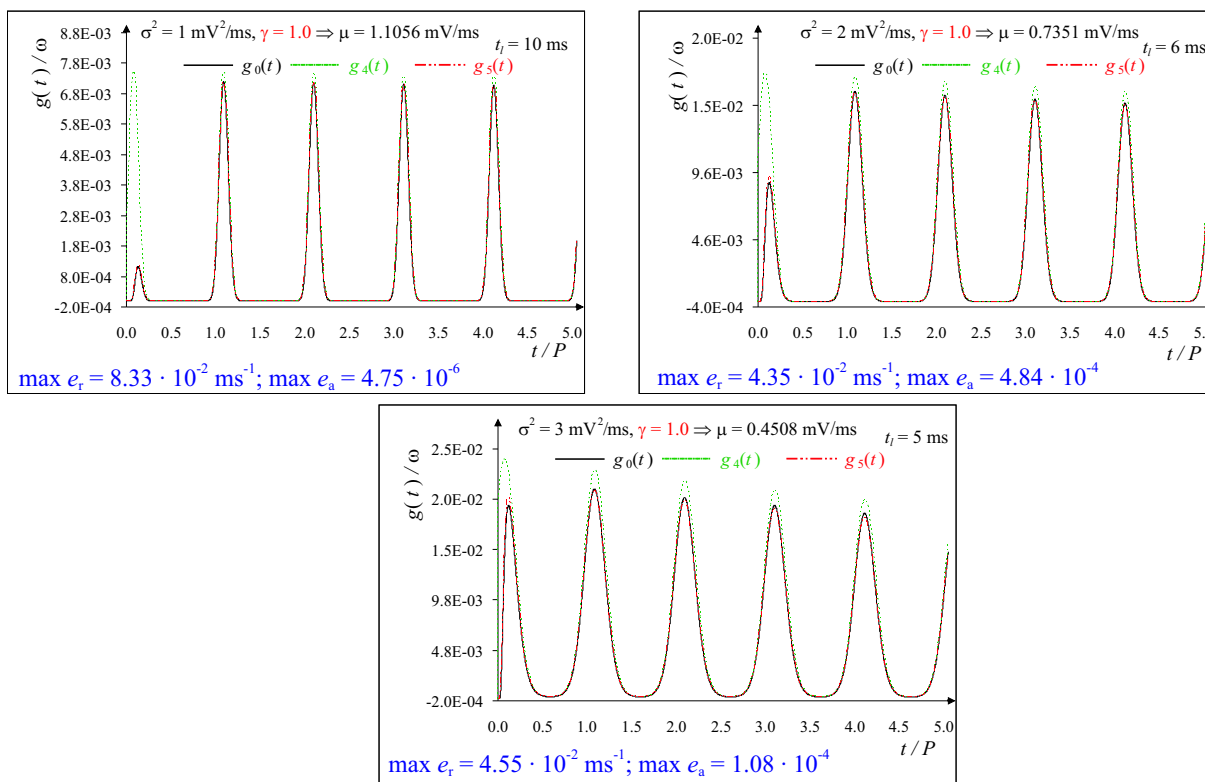


Figure 2.5: As in Fig. 2.4 but with $\gamma = 1.0$.

between t and τ exceeds a few units of θ , thus being overcome the a priori requirement that such an approximation only holds after some multiples of period P .

Use of this remark has been made in constructing the algorithms for obtaining Figures 2.4–2.6 in which $t_m = 8\theta$ and $P = 10\theta$ have been taken.

Remark 2.3.4 *In the case of the LIF model including a periodic stimulus, for the validity of Eq. (2.3.34) condition $\gamma \geq 1$ sometimes can be relaxed. Indeed, the minima of the periodic transformed threshold depend on angular frequency ω , as shown for instance by (2.3.32), thus being always larger than their infimum $2\gamma\sqrt{\zeta^2\vartheta}$, see (2.3.32).*

This remark leads one to the following conclusion. For very low-frequency stimuli, the asymptotic periodicity of the threshold does not play a significant role, so that the considered LIF model does not relevantly differ from that with a constant stimulus. In such cases, condition $\gamma \geq 1$ remains essential for the validity of approximation (2.3.49). Such an approximation may instead turn out to be very satisfactory for large values of the stimulus frequency even for values of γ less than unity. This is shown for instance in Fig. 2.4 in which $\gamma = 0.8$, $\theta = 5$ and $P = 10\theta$, implying $\omega = \pi/25$. The excellent agreement of $g_4(t)$ with $g_0(t)$ for large times is indeed evident. We point out that in Figures 2.4–2.6 the period of the asymptotic threshold has been taken rather large ($P = 10\theta$) to avoid total overlapping of the considered approximations to $g_0(t)$ in the various plots.

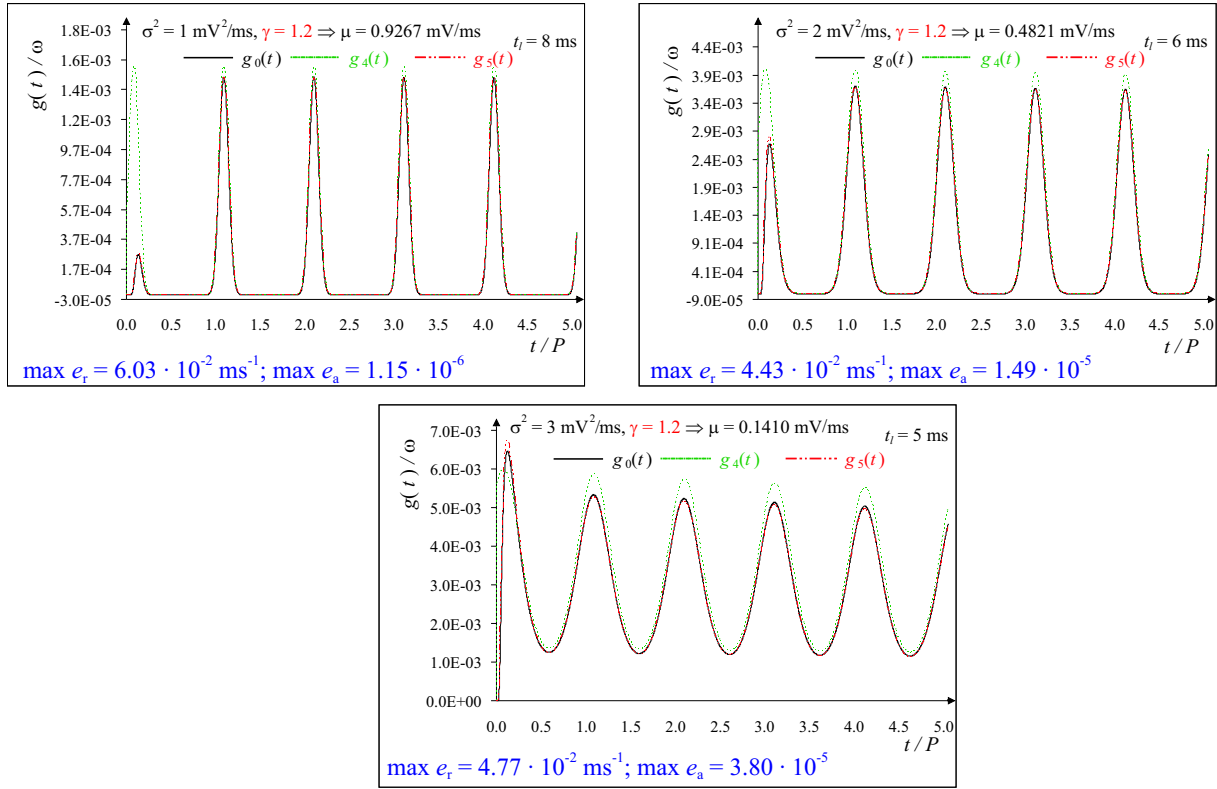


Figure 2.6: As in Fig. 2.4 but with $\gamma = 1.2$.

Similarly to the case of the LIF model with constant stimulus, the algorithm for determining $g_0(t)$ can be improved by substituting $\psi(t, \tau)$ with $-a_v(t)$ whenever $t - \tau \geq t_m$. The resulting approximation, $g_6(t)$ is then:

$$g_6(t_i) = \begin{cases} 0, & i = 0; \\ -\psi_0(t_i) + \Delta t \sum_{j=0}^{i-1} \psi(t_i, t_j) g_6(t_j), & 1 \leq i < m; \\ -\psi_0(t_i) - a_v(t_i) \Delta t \sum_{j=1}^{i-m} g_6(t_j) + \Delta t \sum_{j=i-m+1}^{i-1} \psi(t_i, t_j) g_6(t_j), & i \geq m. \end{cases} \quad (2.3.51)$$

Table 2.9 lists the absolute and relative largest errors between approximations $g_0(t)$ and $g_6(t)$ in the cases of the nine graphs of Figures 2.4–2.6. The advantages offered by approximation $g_6(t)$ are similar to those of the previously considered approximation $g_3(t)$, namely linearity and storage savings.

Table 2.9: For the LIF model with periodic stimulus, maximum absolute and relative errors, e_a and e_r , of $g_6(t)$ with respect to $g_0(t)$ are indicated. The listed parameters γ , σ^2 and μ , as well as all other parameters, have been chosen as in Figures 2.4–2.6 and it has been taken $t_m = 40$ ms.

γ	σ^2	μ	$\max e_a$	$\max e_r$
0.8	1.000	1.284	$3.51 \cdot 10^{-8}$	$2.23 \cdot 10^{-4}$
0.8	2.000	0.988	$4.36 \cdot 10^{-7}$	$4.17 \cdot 10^{-4}$
0.8	3.000	0.761	$1.31 \cdot 10^{-6}$	$5.28 \cdot 10^{-4}$
1.0	1.000	1.106	$3.21 \cdot 10^{-9}$	$5.84 \cdot 10^{-5}$
1.0	2.000	0.735	$5.71 \cdot 10^{-8}$	$1.25 \cdot 10^{-4}$
1.0	3.000	0.451	$2.16 \cdot 10^{-7}$	$1.69 \cdot 10^{-4}$
1.2	1.000	0.927	$1.83 \cdot 10^{-10}$	$1.22 \cdot 10^{-5}$
1.2	2.000	0.482	$5.09 \cdot 10^{-9}$	$3.07 \cdot 10^{-5}$
1.2	3.000	0.141	$2.71 \cdot 10^{-8}$	$4.95 \cdot 10^{-5}$

Chapter 3

Simulation algorithms and comparing analysis

3.1 A simulation procedure

Let us consider a stationary normal process $X(t)$ with zero mean and correlation function $\gamma(t)$. The spectral density $\Gamma(\omega)$ is defined as the Fourier transform of the correlation function $\gamma(t)$:

$$\Gamma(\omega) = \int_{-\infty}^{\infty} \gamma(t) e^{-i\omega t} dt. \quad (3.1.1)$$

The inverse Fourier transform then provides the correlation function if the spectral density is known. In this Section we shall outline a method, essentially proposed by J.N. Franklin [33], to simulate sample paths of a stationary normal process originating from a given state $X(0)$. In the sequel we shall assume $X(0) = 0$; furthermore, we shall take $\gamma(0) = 1$, implying that the variance of the process is unity. The pdf $f[X(t) | X(0) = 0]$ is normal with zero mean and variance $1 - \gamma^2(t)$:

$$f(x, t | 0, 0) = \frac{1}{\sqrt{2\pi[1 - \gamma^2(t)]}} \exp\left\{-\frac{x^2}{2[1 - \gamma^2(t)]}\right\}. \quad (3.1.2)$$

Hereafter we shall refer to various functions that we shall interpret as covariance functions. Any such function $\gamma(t)$ will then have to satisfy the following condition:

$$\gamma(0) = 1, \quad |\gamma(t)| < 1 \quad \text{for } t \neq 0. \quad (3.1.3)$$

Let us now consider a linear filter whose output $X(t)$ is given by

$$X(t) = \int_{-\infty}^t g(t-s) W(s) ds = \int_0^{\infty} g(s) W(t-s) ds. \quad (3.1.4)$$

Equation (3.1.4) can be viewed as a transformation induced by the convolution of the input signal W with the characteristic function of the filter, e.g. its impulse response. The output

signal $X(t)$ at the current time t is thus the sum of the input signals weighted by g up to time t . As is well known, g is said to be the impulse response because if an impulse signal $W(s) = \delta(s)$ (where δ is the Dirac delta function) is the input to the system described by (3.1.4), then the output is $g(t)$:

$$X(t) = \int_0^\infty g(s) \delta(t-s) ds = g(t). \quad (3.1.5)$$

Of course, $g(s) = 0$ for $s < 0$, because for physically realizable systems, such as those that we refer to, the output at any given time cannot depend on inputs at previous times.

Since the convolution operation is linear, if in (3.1.4) the input signal is stationary and normal then also the output $X(t)$ is stationary and normal. Moreover, if g is a real function such are also $X(t)$ and $W(t)$.

Let us denote by $\Gamma_W(\omega)$ and $\Gamma_X(\omega)$ the spectral densities of input $W(t)$ and output $X(t)$ respectively, and let us denote by $G(\omega)$ the Fourier transform of $g(t)$. One can then prove that the following relation holds:

$$\Gamma_X(\omega) = |G(\omega)|^2 \Gamma_W(\omega). \quad (3.1.6)$$

Indeed, recalling (1.2.21) and (3.1.1) one obtains:

$$\Gamma_X(\omega) = \int_{-\infty}^\infty e^{-i\omega\tau} \gamma_X(\tau) d\tau = \int_{-\infty}^\infty e^{-i\omega\tau} E[X(t)X(t-\tau)] d\tau,$$

where by $\gamma_X(t)$ we have denoted the covariance of $X(t)$. Making use of (3.1.4) one then has:

$$\begin{aligned} \Gamma_X(\omega) &= \int_{-\infty}^\infty e^{-i\omega\tau} E \left[\int_0^\infty g(s) W(t-s) ds \int_0^\infty g(\sigma) W(t-\tau-\sigma) d\sigma \right] d\tau \\ &= \int_{-\infty}^\infty e^{-i\omega\tau} d\tau \int_0^\infty g(s) ds \int_0^\infty g(\sigma) E[W(t-s)W(t-\tau-\sigma)] d\sigma. \end{aligned}$$

Making then use of (1.2.21) one finds:

$$\Gamma_X(\omega) = \int_0^\infty g(s) ds \int_0^\infty g(\sigma) d\sigma \int_{-\infty}^\infty e^{-i\omega\tau} \gamma_W(\tau + \sigma - s) d\tau,$$

where in the last integral on the right hand side γ_W denotes the covariance of the process W . Finally, making use of the transformation $\tau = u - \sigma + s$ and recalling (3.1.1) we obtain

$$\begin{aligned} \Gamma_X(\omega) &= \int_0^\infty e^{-i\omega s} g(s) ds \int_0^\infty e^{i\omega\sigma} g(\sigma) d\sigma \int_{-\infty}^\infty e^{-i\omega u} \gamma_W(u) du \\ &= \int_0^\infty e^{-i\omega s} g(s) ds \int_0^\infty \overline{e^{-i\omega\sigma} g(\sigma)} d\sigma \Gamma_W(\omega) \\ &= \int_0^\infty e^{-i\omega s} g(s) ds \overline{\int_0^\infty e^{-i\omega\sigma} g(\sigma) d\sigma} \Gamma_W(\omega) \\ &= G(\omega) \overline{G(\omega)} \Gamma_W(\omega) = |G(\omega)|^2 \Gamma_W(\omega). \end{aligned}$$

Equation (3.1.6) is suggestive of a method to construct a normal process $X(t)$ having a preassigned spectral density $\Gamma_X(\omega) \equiv \Gamma(\omega)$. It is indeed sufficient to make use of (3.1.4) for the case when the input signal $W(t)$ is a normal process having spectral density $\Gamma_W(\omega) \equiv 1$, and then select $g(t)$ in such a way that its Fourier transform $G(\omega)$ satisfies $|G(\omega)|^2 = \Gamma(\omega)$. Hence, substituting $\Gamma_W(\omega) = 1$ and $|G(\omega)|^2 = \Gamma(\omega)$ in (3.1.6), $\Gamma_X(\omega) = \Gamma(\omega)$ is immediately obtained.

By such a procedure we have therefore obtained a process $X(t)$ that is normal due to the linearity of (3.1.4). Moreover, its spectral density $\Gamma_X(\omega)$ is equal to the spectral density $\Gamma(\omega)$ corresponding to the preassigned covariance $\gamma(t)$.

The process $W(t)$ whose spectral density has been assumed to be unit, is a zero-mean stationary normal process. Furthermore, its covariance $\gamma(\tau)$ is the Dirac-delta function $\delta(\tau)$, as is immediately seen from the following relation:

$$\Gamma_W(\omega) = \int_{-\infty}^{\infty} e^{-i\omega\tau} \gamma(\tau) d\tau = 1. \quad (3.1.7)$$

The process $W(t)$, that henceforth we shall denote by $\Lambda(t)$, identifies with the white noise. Hence, it is an ideal process, which is not physically realizable because its variance is infinity at all instants:

$$E[\Lambda^2(t)] = \gamma(0) = \delta(0) = \infty.$$

Furthermore, no matter how close ($t_1 \neq t_2$) are the instants t_1 and t_2 , the random variables $\Lambda(t_1)$ and $\Lambda(t_2)$ are uncorrelated.

We are now left with the problem of determining the Fourier transform $G(\omega)$ such that $|G(\omega)|^2 = \Gamma(\omega)$. This can be done by making use of a result due to Davenport and Root [14]. Namely, if $\Gamma(\omega)$ is a rational function satisfying the condition:

$$0 \leq \Gamma(\omega) \leq \infty, \quad \Gamma(\omega) = \Gamma(-\omega), \quad \lim_{\omega \rightarrow \pm\infty} \Gamma(\omega) = 0, \quad (3.1.8)$$

then it can be written in the form:

$$\Gamma(\omega) = \left| \frac{P(i\omega)}{Q(i\omega)} \right|^2, \quad (\omega \text{ real}), \quad (3.1.9)$$

where $P(z)$ and $Q(z)$ are polynomials with real coefficients such that the degree of P is less than the degree of Q and with the zeroes of $Q(z)$ laying in the complex half-plane $\Re(z) < 0$. It is thus evident that if we take

$$G(\omega) = \frac{P(i\omega)}{Q(i\omega)}, \quad (3.1.10)$$

the relation $\Gamma(\omega) = |G(\omega)|^2$ immediately follows. Substituting (3.1.10) in (3.1.6) we thus obtain:

$$\Gamma_X(\omega) = \left| \frac{P(i\omega)}{Q(i\omega)} \right|^2 \Gamma_W(\omega). \quad (3.1.11)$$

If we now denote by D the operator d/dt , recalling that we have identified the input $W(t)$ with the white noise $\Lambda(t)$, from (3.1.11) we obtain:

$$X(t) = \frac{P(D)}{Q(D)} \Lambda(t). \quad (3.1.12)$$

Equation (3.1.12) should be interpreted in the following way: first we solve the differential equation

$$Q(D) \phi(t) = \Lambda(t) \quad (3.1.13)$$

to obtain the stationary solution $\phi(t)$; the required output

$$X(t) = P(D) \phi(t) \quad (3.1.14)$$

is then expressed as a linear combination of the derivatives of $\phi(t)$ whose order is less than the degree of Q . Assume that P has degree m and the Q has degree n :

$$P(z) = \sum_{i=0}^m b_i z^{m-i} = b_0 z^m + b_1 z^{m-1} + \dots + b_m, \quad (3.1.15)$$

$$Q(z) = \sum_{i=0}^n a_i z^{n-i} = z^n + a_1 z^{n-1} + \dots + a_n, \quad (a_0 = 1). \quad (3.1.16)$$

By virtue of (3.1.15) and (3.1.16) equations (3.1.13) and (3.1.14) become ($n > m$):

$$\phi(t)^n(t) + a_1 \phi(t)^{n-1}(t) + \dots + a_n \phi(t) = \Lambda(t), \quad (3.1.17)$$

$$X(t) = b_0 \phi(t)^m(t) + b_1 \phi(t)^{m-1}(t) + \dots + b_m \phi(t) \quad (3.1.18)$$

respectively. To calculate the desired input signal $X(t)$ it is thus necessary to calculate the derivative of $\phi(t)$ by means of the stochastic equation (3.1.17).

Let us now remark that if we introduce the state vector

$$\mathbf{v}(t) = \begin{pmatrix} \phi(t) \\ \phi'(t) \\ \vdots \\ \phi^{(n-1)}(t) \end{pmatrix}, \quad (3.1.19)$$

then equation (3.1.17) can be re-written in the following compact form:

$$\frac{d}{dt} \mathbf{v}(t) = A \mathbf{v}(t) + \mathbf{y}(t). \quad (3.1.20)$$

Here, matrix A is in canonical form:

$$A = \begin{pmatrix} 0 & 1 & 0 & \cdots & 0 \\ 0 & 0 & 1 & \cdots & 0 \\ \vdots & \vdots & \vdots & \ddots & \vdots \\ 0 & 0 & 0 & \cdots & 1 \\ -a_n & -a_{n-1} & -a_{n-2} & \cdots & -a_1 \end{pmatrix} \quad (3.1.21)$$

and the input vector $\mathbf{y}(t)$ is given by

$$\mathbf{y}(t) = \begin{pmatrix} 0 \\ 0 \\ \vdots \\ 0 \\ \Lambda(t) \end{pmatrix}. \quad (3.1.22)$$

The simulation procedure aims at constructing sample paths of the process $X(t)$ at the instants $t = 0, \Delta t, 2\Delta t, \dots$ where Δt is a constant positive time increment. To this purpose it is necessary to calculate the components of vector $\mathbf{v}(t)$ at the same instants. This can be achieved by solving the system (3.1.20) of linear differential equations. Denoting by $\mathbf{v}(0)$ the vector of the initial conditions, from (3.1.20) one obtains:

$$(3.1.23)$$

Hence,

$$\begin{aligned}
\mathbf{v}(t + \Delta t) &= e^{A(t+\Delta t)} \mathbf{v}(0) + \int_0^{t+\Delta t} e^{A(t+\Delta t-\tau)} \mathbf{y}(\tau) d\tau \\
&= e^{A\Delta t} \left[e^{At} \mathbf{v}(0) + \int_0^t e^{A(t-\tau)} \mathbf{y}(\tau) d\tau \right] \\
&\quad + \int_t^{t+\Delta t} e^{A(t+\Delta t-\tau)} \mathbf{y}(\tau) d\tau \\
&= e^{A\Delta t} \mathbf{v}(t) + \int_0^{\Delta t} e^{A(\Delta t-\tau)} \mathbf{y}(t + \tau) d\tau.
\end{aligned} \tag{3.1.24}$$

If we set

$$\mathbf{r}(t) = \int_0^{\Delta t} e^{A(\Delta t-\tau)} \mathbf{y}(t + \tau) d\tau, \tag{3.1.25}$$

one is led to the following relation:

$$\mathbf{v}(t + \Delta t) = e^{A\Delta t} \mathbf{v}(t) + \mathbf{r}(t). \tag{3.1.26}$$

By calculating the matrix $e^{A\Delta t}$ and the vector $\mathbf{r}(t)$ it is possible to obtain from $\mathbf{v}(t)$ the state vector $\mathbf{v}(t + \Delta t)$. By means of (3.1.26) one can then calculate by iteration the components of the state vector $\mathbf{v}(t)$ at time $t = k\Delta t$ ($k = 1, 2, \dots$).

We still have to show how one can calculate the state vector $\mathbf{v}(t)$ at initial time $t = 0$ and how $\mathbf{r}(t)$ it can be determined at times $t = k\Delta t$ ($k = 1, 2, \dots$). However, it is first necessary to indicate how one can generate a sequence of n -dimensional normal vectors $\mathbf{z}^{(0)}, \mathbf{z}^{(1)}, \mathbf{z}^{(2)}, \dots$ with mean equal to the null vector and covariance matrix M . This can be done by making use of a sample of progressively increasing size generated by a sequence of i.i.d. standard normal random variables $\tilde{\Lambda}_1, \tilde{\Lambda}_2, \tilde{\Lambda}_3, \dots$. Setting

$$\tilde{\Lambda}^{(0)} = \begin{pmatrix} \tilde{\Lambda}_1 \\ \vdots \\ \tilde{\Lambda}_n \end{pmatrix}, \quad \tilde{\Lambda}^{(1)} = \begin{pmatrix} \tilde{\Lambda}_{n+1} \\ \vdots \\ \tilde{\Lambda}_{2n} \end{pmatrix}, \quad \tilde{\Lambda}^{(2)} = \begin{pmatrix} \tilde{\Lambda}_{2n+1} \\ \vdots \\ \tilde{\Lambda}_{3n} \end{pmatrix}, \dots \tag{3.1.27}$$

one obtains samples of independent, n -dimensional normal random variables having zero mean and covariance matrix consisting of the identity matrix. Let now us recall that a real, positive-definite symmetric square matrix M can be factorized as follows:

$$M = B B^T, \tag{3.1.28}$$

where B is a lower triangular matrix with positive elements on the diagonal (cf., for instance, [44]). If we then set

$$\mathbf{z}^{(i)} = B \tilde{\Lambda}^{(i)} \quad (i = 0, 1, 2, \dots) \tag{3.1.29}$$

it turns out that vectors $\mathbf{z}^{(i)}$ are the required vectors. Due to the linearity of the mean value operator and because of (3.1.28) the vectors defined by (3.1.29) are normal, with mean and covariance given by

$$E[\mathbf{z}^{(i)}] = B E[\tilde{\Lambda}^{(i)}] = 0, \tag{3.1.30}$$

$$E[\mathbf{z}^{(i)} (\mathbf{z}^{(i)})^T] = B E[\tilde{\Lambda}^{(i)} (\tilde{\Lambda}^{(i)})^T] B^T = B B^T = M. \tag{3.1.31}$$

We now calculate the state vector $\mathbf{v}(0)$, which is normal with zero mean and covariance matrix

$$M_{\mathbf{v}} = E[\mathbf{v}(0) \mathbf{v}^T(0)] = E[\mathbf{v}(t) \mathbf{v}^T(t)]. \tag{3.1.32}$$

Recalling (3.1.19) we then find that the elements M_{ij} of $M_{\mathbf{v}}$ are given by

$$M_{ij} = E[\phi^{(i)}(t) \phi^{(j)}(t)] \quad (i, j = 0, 1, \dots, n-1). \quad (3.1.33)$$

To calculate the M_{ij} 's we make use of the following formula (cfr. [33]):

$$M_{ij} = \begin{cases} 0, & i+j \text{ odd,} \\ (-1)^{(j-i)/2} m_{(i+j)/2}, & i+j \text{ even,} \end{cases} \quad (3.1.34)$$

where m_0, m_1, \dots, m_{n-1} can be computed by solving the following n linear algebraic equations

$$(-1)^k \sum_{q \in I} (-1)^q a_{n-2q+k} m_q = \begin{cases} 0, & k = 0, 1, \dots, n-2, \\ 1/2, & k = n-1, \end{cases} \quad (3.1.35)$$

with $a_0 = 1$ and $I = \{i \in \mathbf{Z} : k/2 \leq i \leq (n+k)/2\}$. After the matrix $M_{\mathbf{v}}$ has been determined, it can be factored out in the form (3.1.28), for instance by means of Crout's method. One then obtains:

$$M_{\mathbf{v}} = B_{\mathbf{v}} B_{\mathbf{v}}^T \quad (3.1.36)$$

where $B_{\mathbf{v}}$ is a lower triangular matrix. If we then set

$$\mathbf{v}(0) = B_{\mathbf{v}} \tilde{\mathbf{\Lambda}}^{(0)}, \quad (3.1.37)$$

the vector $\mathbf{v}(0)$ thus obtained exhibits the desired features, i.e. is normal, with zero mean and covariance matrix $M_{\mathbf{v}}$. Therefore, we now dispose of the initial condition to be associated to equation (3.1.26). Let us now show how vector $\mathbf{r}(t)$ can be calculated at times $t = k\Delta t$ ($k = 1, 2, \dots$). First of all one can easily see that $\mathbf{v}(t)$ and $\mathbf{r}(t)$, given by (3.1.23) and (3.1.25) respectively, are uncorrelated. Indeed, one has

$$\begin{aligned} E[\mathbf{r}(t) \mathbf{v}^T(t)] = & \int_0^{\Delta t} e^{A(\Delta t - \tau)} E[\mathbf{y}(t + \tau) \mathbf{v}^T(0)] (e^{A\tau})^T d\tau \\ & + \int_0^{\Delta t} e^{A(\Delta t - \tau)} d\tau \int_0^t E[\mathbf{y}(t + \tau) \mathbf{y}^T(\sigma)] (e^{A(t - \sigma)})^T d\sigma. \end{aligned} \quad (3.1.38)$$

Since

$$E[\mathbf{y}(t + \tau) \mathbf{v}^T(0)] = 0 \quad (t + \tau > 0) \quad (3.1.39)$$

and

$$E[\mathbf{y}(t + \tau) \mathbf{y}^T(\sigma)] = C \delta(t + \tau - \sigma) \quad (t + \tau > \sigma), \quad (3.1.40)$$

where C is the positive semi-definite matrix

$$C = \begin{pmatrix} 0 & 0 & \cdots & 0 \\ 0 & 0 & \cdots & 0 \\ \vdots & \vdots & \ddots & \vdots \\ 0 & 0 & \cdots & 1 \end{pmatrix}, \quad (3.1.41)$$

by making use of (3.1.39) and (3.1.40) in (3.1.38), we find that the normal vectors $\mathbf{r}(t)$ and $\mathbf{v}(t)$ are uncorrelated and hence independent. Therefore, $\mathbf{r}(t)$ can be calculated independently of $\mathbf{v}(t)$. To this purpose it is necessary to calculate the covariance matrix

$$M_{\mathbf{r}} = E[\mathbf{r}(t) \mathbf{r}^T(t)]. \quad (3.1.42)$$

From (3.1.25) we have:

$$M_{\mathbf{r}} = \int_0^{\Delta t} d\tau_1 \int_0^{\Delta t} e^{A(\Delta t - \tau_1)} E[\mathbf{y}(t + \tau_1) \mathbf{y}^T(t + \tau_2)] (e^{A(\Delta t - \tau_2)})^T d\tau_2. \quad (3.1.43)$$

Making use of (3.1.40), after the substitution $s = \Delta t - \tau$ from (3.1.43) we obtain

$$M_{\mathbf{r}} = \int_0^{\Delta t} e^{As} C (e^{As})^T ds. \quad (3.1.44)$$

Let us denote by $J(s)$ the function under the integral sign in (3.1.44). Then,

$$\frac{d}{ds} J(s) = A J(s) + J(s) A^T. \quad (3.1.45)$$

Integrating both sides with respect to s in $[0, \Delta t]$ and recalling (3.1.44) we obtain

$$e^{A\Delta t} C (e^{A\Delta t})^T - C = A M_{\mathbf{r}} + M_{\mathbf{r}} A^T. \quad (3.1.46)$$

Since the eigenvalues of A are the roots of polynomial $Q(z)$ and since these have negative real part, equation (3.1.46) admits the unique solution $M_{\mathbf{r}}$. To calculate such matrix one has to solve system (3.1.46). Indeed, denoting by m_{ij} the elements of $M_{\mathbf{r}}$ and by d_{ij} the elements of $e^{A\Delta t}$, equation (3.1.46) can be re-written in the form of a system of n^2 equations in as many unknowns:

$$\sum_{k=1}^n (a_{ik} m_{kj} + a_{jk} m_{ik}) = \begin{cases} d_{in} d_{jn}, & \text{if } i < n \text{ or } j < n, \\ d_{nn}^2 - 1, & \text{if } i = j = n. \end{cases} \quad (3.1.47)$$

However, due to the symmetry of $M_{\mathbf{r}}$ the number of equations and of unknowns reduces to $n(n+1)/2$. System (3.1.47) then becomes:

$$\begin{aligned} \sum_{k \leq j} a_{ik} m_{jk} &+ \sum_{k > j} a_{ik} m_{kj} + \sum_{k \leq i} a_{jk} m_{ik} + \sum_{k > i} a_{jk} m_{ki} \\ &= \begin{cases} d_{in} d_{jn}, & \text{if } i = 1, 2, \dots, n; j = 1, 2, \dots, i (j < n), \\ d_{nn}^2 - 1, & \text{if } i = j = n. \end{cases} \end{aligned} \quad (3.1.48)$$

After the elements m_{ij} have been calculated, $M_{\mathbf{r}}$ can be written in the form (3.1.28):

$$M_{\mathbf{r}} = B_{\mathbf{r}} B_{\mathbf{r}}^T, \quad (3.1.49)$$

with $B_{\mathbf{r}}$ a lower triangular matrix. Setting then

$$\mathbf{r}(t) = B_{\mathbf{r}} \tilde{\mathbf{\Lambda}}^{(k)} \quad \text{for } t = k\Delta t, \quad (k = 1, 2, \dots), \quad (3.1.50)$$

the vector $\mathbf{r}(t)$ is a normal sample with zero mean and covariance matrix $M_{\mathbf{r}}$. We can now calculate the components of the state vector $\mathbf{v}(t)$ at times $t = 0, \Delta t, 2\Delta t, \dots$. From (3.1.26), (3.1.37) and (3.1.50) we obtain the initial condition and the iteration law for the computation of $\mathbf{v}(t)$:

$$\mathbf{v}(0) = B_{\mathbf{r}} \tilde{\mathbf{\Lambda}}^{(0)}, \quad (3.1.51)$$

$$\mathbf{v}[(k+1)\Delta t] = e^{A\Delta t} \mathbf{v}(k\Delta t) + B_{\mathbf{r}} \tilde{\mathbf{\Lambda}}^{(k)}, \quad (k = 0, 1, \dots), \quad (3.1.52)$$

Finally, recalling (3.1.18) and (3.1.19) the sample path of the process $X(t)$ can be obtained as linear combination of the components $v_1(t), v_2(t), \dots, v_n(t)$ of vector $\mathbf{v}(t)$ as follows:

$$X(t) = b_0 v_{m+1}(t) + b_1 v_m(t) + \dots + b_m v_1(t) \quad \text{when } t = 0, \Delta t, 2\Delta t, \dots \quad (3.1.53)$$

Whenever it is required that $X(t)$ originates at a given state $X(0) = x_0$, it is sufficient to calculate m out of the $m+1$ unknowns that appeared on the right hand side of (3.1.53) written for $t = 0$. The $(m+1)$ -th component of $\mathbf{v}(0)$ can be obtained by imposing that the left hand side of (3.1.53) is changed to x_0 . Hence, one can for instance first calculate $v_1(0), v_2(0), \dots, v_m(0)$ from (3.1.51) and then arise to $v_{m+1}(0)$ via (3.1.53) :

$$v_{m+1}(0) = \frac{x_0 - [b_1 v_m(0) + \dots + b_m v_1(0)]}{b_0}. \quad (3.1.54)$$

3.2 Covariance function with damped oscillations

In this Section we shall implement the simulation procedure discussed in the foregoing. Let $X(t)$ be a stationary normal process with zero mean and correlation function ([96])

$$\gamma(\tau) = e^{-\beta\tau} \frac{\cos(\alpha\tau - \psi)}{\cos\psi} \quad (\tau \geq 0), \quad (3.2.1)$$

where α and β are positive real numbers and ψ is a real number such that

$$\psi \leq \arctan \frac{\beta}{\alpha}. \quad (3.2.2)$$

From (3.2.1) we see that $\gamma(0) = 1$. Since $\gamma(\tau)$ is an even function, to check that $|\gamma(\tau)| < 1$ for $\tau \neq 0$ it is sufficient to show that

$$\left. \frac{d}{d\tau} \gamma(\tau) \right|_{\tau=0^+} \leq 0. \quad (3.2.3)$$

Indeed one has

$$\frac{d}{d\tau} \gamma(\tau) = -\frac{e^{-\beta\tau}}{\cos\psi} [\alpha \sin(\alpha\tau - \psi) + \beta \cos(\alpha\tau - \psi)] \quad (\tau \geq 0) \quad (3.2.4)$$

or

$$\left. \frac{d}{d\tau} \gamma(\tau) \right|_{\tau=0^+} = \frac{1}{\cos\psi} (\alpha \sin\psi - \beta \cos\psi) = \alpha \tan\psi - \beta. \quad (3.2.5)$$

From assumptions (3.2.2) it follows that (3.2.5) is not positive, i.e. (3.2.3) follows.

Let us now calculate the spectral density of $X(t)$. Keeping in mind that $\gamma(\tau)$ is an even function one has

$$\begin{aligned} \Gamma(\omega) &\equiv \int_{-\infty}^{\infty} e^{-i\omega\tau} e^{-\beta|\tau|} \frac{\cos(\alpha|\tau| - \psi)}{\cos\psi} d\tau \\ &= \frac{2}{\cos\psi} \int_0^{\infty} \cos(\omega\tau) e^{-\beta\tau} \cos(\alpha\tau - \psi) d\tau, \end{aligned} \quad (3.2.6)$$

or

$$\begin{aligned}\Gamma(\omega) &= \frac{2}{\cos\psi} \int_0^\infty \cos(\omega\tau) e^{-\beta\tau} [\cos(\alpha\tau) \cos\psi + \sin(\alpha\tau) \sin\psi] d\tau \\ &= 2 \int_0^\infty e^{-\beta\tau} \cos(\omega\tau) \cos(\alpha\tau) + 2 \tan\psi \int_0^\infty e^{-\beta\tau} \cos(\omega\tau) \sin(\alpha\tau).\end{aligned}\quad (3.2.7)$$

From this expression we obtain

$$\begin{aligned}\Gamma(\omega) &= \int_0^\infty e^{-\beta\tau} \{\cos[(\omega + \alpha)\tau] + \cos[(\omega - \alpha)\tau]\} d\tau \\ &\quad + \tan\psi \int_0^\infty e^{-\beta\tau} \{\sin[(\omega + \alpha)\tau] + \sin[(\alpha - \omega)\tau]\} d\tau.\end{aligned}\quad (3.2.8)$$

Making use of

$$\int_0^\infty e^{-\beta\tau} \cos(\alpha\tau) = \frac{\beta}{\alpha^2 + \beta^2}, \quad \int_0^\infty e^{-\beta\tau} \sin(\alpha\tau) = \frac{\alpha}{\alpha^2 + \beta^2}, \quad (3.2.9)$$

from (3.2.8) we obtain

$$\Gamma(\omega) = \frac{\beta + (\omega + \alpha) \tan\psi}{\beta^2 + (\omega + \alpha)^2} + \frac{\beta + (\alpha - \omega) \tan\psi}{\beta^2 + (\omega - \alpha)^2} \quad (3.2.10)$$

$$\begin{aligned}\Gamma(\omega) &= \frac{[\beta + \omega \tan\psi + \alpha \tan\psi] [\omega^2 - 2\alpha\omega + \alpha^2 + \beta^2]}{[\omega^2 + 2\alpha\omega + \alpha^2 + \beta^2] [\omega^2 - 2\alpha\omega + \alpha^2 + \beta^2]} \\ &\quad + \frac{[\beta - \omega \tan\psi + \alpha \tan\psi] [\omega^2 + 2\alpha\omega + \alpha^2 + \beta^2]}{[\omega^2 + 2\alpha\omega + \alpha^2 + \beta^2] [\omega^2 - 2\alpha\omega + \alpha^2 + \beta^2]} \\ &= \frac{\omega^2 [\beta + \alpha \tan\psi - 2\alpha \tan\psi + \beta + \alpha \tan\psi - 2\alpha \tan\psi]}{\omega^4 + (\alpha^2 + \beta^2 - 4\alpha^2 + \alpha^2 + \beta^2)\omega^2 + (\alpha^2 + \beta^2)^2} \\ &\quad + \frac{2(\alpha^2 + \beta^2)(\beta + \alpha \tan\psi)}{\omega^4 + (\alpha^2 + \beta^2 - 4\alpha^2 + \alpha^2 + \beta^2)\omega^2 + (\alpha^2 + \beta^2)^2}.\end{aligned}$$

Hence, we are finally led to the following expression:

$$\Gamma(\omega) = \frac{2[(\beta - \alpha \tan\psi)\omega^2 + (\beta + \alpha \tan\psi)(\alpha^2 + \beta^2)]}{\omega^4 + 2(\beta^2 - \alpha^2)\omega^2 + (\alpha^2 + \beta^2)^2}. \quad (3.2.11)$$

Note that (3.2.2) insures that spectral density (3.2.11) is positive.

We now write down $\Gamma(\omega)$ in the form (3.1.9) in the general case when

$$\Gamma(\omega) = \frac{d_1 \omega^2 + d_2}{\omega^4 + c_1 \omega^2 + c_2} \quad (d_1, d_2 > 0; c_1^2 - 4c_2 < 0). \quad (3.2.12)$$

In order to have $\Gamma(\omega) = |P(i\omega)/Q(i\omega)|^2$, from (3.2.12) we see that $P(z)$ is a first degree polynomial while the degree of $Q(z)$ is two:

$$P(z) = b_0 z + b_1, \quad (3.2.13)$$

$$Q(z) = z^2 + a_1 z + a_2. \quad (3.2.14)$$

By imposing

$$\Gamma(\omega) = \frac{d_1 \omega^2 + d_2}{\omega^4 + c_1 \omega^2 + c_2} = \left| \frac{b_0 i \omega + b_1}{(i \omega)^2 + a_1 i \omega + a_2} \right|^2,$$

e.g.

$$d_1 \omega^2 + d_2 = |b_0 \omega i + b_1|^2, \quad (3.2.15)$$

$$\omega^4 + c_1 \omega^2 + c_2 = |a_1 \omega i + a_2 - \omega^2|^2, \quad (3.2.16)$$

from which we obtain

$$\begin{aligned} d_1 \omega^2 + d_2 &= b_0^2 \omega^2 + b_1^2, \\ \omega^4 + c_1 \omega^2 + c_2 &= \omega^4 + \omega^2(a_1^2 - 2a_2) + a_2^2. \end{aligned}$$

Hence,

$$d_1 = b_0^2, \quad d_2 = b_1^2, \quad c_1 = a_1^2 - 2a_2, \quad c_2 = a_2^2. \quad (3.2.17)$$

From (3.2.17) we finally obtain the coefficients of polynomials (3.2.13) and (3.2.14):

$$b_0 = \sqrt{d_1}, \quad b_1 = \sqrt{d_2}, \quad a_1 = \sqrt{c_1 + 2\sqrt{c_2}}, \quad a_2 = \sqrt{c_2}. \quad (3.2.18)$$

In the particular case of the process $X(t)$ having covariance (3.2.1) , by identifying the spectral density (3.2.11) with (3.2.12) , one finds

$$\Gamma(\omega) = |P(i\omega)/Q(i\omega)|^2,$$

with

$$P(z) = \sqrt{2(\beta - \alpha \tan \psi)} z + \sqrt{2(\beta + \alpha \tan \psi)(\alpha^2 + \beta^2)}, \quad (3.2.19)$$

$$Q(z) = z^2 + 2\beta z + \alpha^2 + \beta^2, \quad (3.2.20)$$

where use of (3.2.13), (3.2.14) and (3.2.18) has been made.

To implement the simulation procedure, recalling (3.1.23)-(3.1.25) we have to solve the stochastic differential equation (3.1.21) that is convenient to re-write as:

$$\frac{d}{dt} \mathbf{v}(t) = A \mathbf{v}(t) + \mathbf{y}(t), \quad (3.2.21)$$

in which

$$\mathbf{v}(t) = \begin{pmatrix} \phi(t) \\ \phi'(t) \end{pmatrix}, \quad A = \begin{pmatrix} 0 & 1 \\ -\alpha^2 - \beta^2 & -2\beta \end{pmatrix}, \quad \mathbf{y}(t) = \begin{pmatrix} 0 \\ \Lambda(t) \end{pmatrix}. \quad (3.2.22)$$

By a well known procedure (see, for instance, [10]) the matrix e^{At} can be calculated. The final result is

$$e^{At} = \frac{e^{-\beta t}}{\alpha} \begin{pmatrix} \alpha \cos(\alpha t) + \beta \sin(\alpha t) & \sin(\alpha t) \\ -(\alpha^2 + \beta^2) \sin(\alpha t) & \alpha \cos(\alpha t) - \beta \sin(\alpha t) \end{pmatrix}. \quad (3.2.23)$$

To obtain the matrix $M_{\mathbf{v}} = E[\mathbf{v}(0)\mathbf{v}^T(0)]$, we have to calculate (see (3.1.36) and (3.1.37)) the quantities

$$M_{ij} = \begin{cases} m_i, & i = j = 0, 1, \\ 0, & \text{otherwise,} \end{cases}$$

where m_0 and m_1 are the solutions of the system

$$a_2 m_0 - m_1 = 0, \quad a_1 m_1 = \frac{1}{2}.$$

Hence,

$$m_0 = \frac{1}{2 a_1 a_2} = \frac{1}{4 \beta (\alpha^2 + \beta^2)}, \quad (3.2.24)$$

$$m_1 = \frac{1}{2 a_1} = \frac{1}{4 \beta}, \quad (3.2.25)$$

so that

$$M_{\mathbf{v}} = \begin{pmatrix} \frac{1}{4 \beta (\alpha^2 + \beta^2)} & 0 \\ 0 & \frac{1}{4 \beta} \end{pmatrix}. \quad (3.2.26)$$

Since $M_{\mathbf{v}}$ is diagonal, the factorization $M_{\mathbf{v}} = B_{\mathbf{v}} B_{\mathbf{v}}^T$ is trivial:

$$B_{\mathbf{v}} = \begin{pmatrix} \frac{1}{2 \sqrt{\beta (\alpha^2 + \beta^2)}} & 0 \\ 0 & \frac{1}{2 \sqrt{\beta}} \end{pmatrix}. \quad (3.2.27)$$

To calculate the elements m_{ij} of the matrix $M_{\mathbf{r}} = E[\mathbf{r}(t) \mathbf{r}^T(t)]$, let us remark that the linear system (3.1.48) becomes

$$\begin{pmatrix} d_{11} & d_{12} \\ d_{21} & d_{22} \end{pmatrix} \begin{pmatrix} 0 & 0 \\ 0 & 1 \end{pmatrix} \begin{pmatrix} d_{11} & d_{21} \\ d_{12} & d_{22} \end{pmatrix} - \begin{pmatrix} 0 & 0 \\ 0 & 1 \end{pmatrix} \\ = \begin{pmatrix} 0 & 1 \\ -\alpha^2 - \beta^2 & -2\beta \end{pmatrix} \begin{pmatrix} m_{11} & m_{12} \\ m_{12} & m_{22} \end{pmatrix} + \begin{pmatrix} m_{11} & m_{12} \\ m_{12} & m_{22} \end{pmatrix} \begin{pmatrix} 0 & -\alpha^2 - \beta^2 \\ 1 & -2\beta \end{pmatrix}$$

or:

$$\begin{pmatrix} d_{12}^2 & d_{12} d_{22} \\ d_{12} d_{22} & d_{22}^2 - 1 \end{pmatrix} \\ = \begin{pmatrix} 2m_{12} & m_{22} - m_{11} (\alpha^2 + \beta^2) - 2\beta m_{12} \\ m_{22} - m_{11} (\alpha^2 + \beta^2) - 2\beta m_{12} & -2m_{12} (\alpha^2 + \beta^2) - 4\beta m_{22} \end{pmatrix}, \quad (3.2.28)$$

where we have denoted by d_{ij} the elements of $e^{\Delta t}$.

Solving the system (3.2.28), we obtain:

$$m_{11} = \frac{1}{\alpha^2 + \beta^2} \left\{ \frac{1}{4\beta} [1 - d_{22}^2 - d_{12}^2 (\alpha^2 + \beta^2)] - \beta d_{12}^2 - d_{12} d_{22} \right\}, \quad (3.2.29)$$

$$m_{12} = \frac{d_{12}^2}{2}, \quad (3.2.30)$$

$$m_{22} = \frac{1}{4\beta} [1 - d_{22}^2 - d_{12}^2 (\alpha^2 + \beta^2)]. \quad (3.2.31)$$

It is now necessary to write $M_{\mathbf{r}}$ in the form $M_{\mathbf{r}} = B_{\mathbf{r}}B_{\mathbf{r}}^T$, with $B_{\mathbf{r}}$ a lower triangular matrix. Denoting the elements of $B_{\mathbf{r}}$ by b_{ij} , one has:

$$\begin{pmatrix} b_{11} & 0 \\ b_{21} & b_{22} \end{pmatrix} \begin{pmatrix} b_{11} & b_{21} \\ 0 & b_{22} \end{pmatrix} = \begin{pmatrix} m_{11} & m_{12} \\ m_{12} & m_{22} \end{pmatrix},$$

that is

$$b_{11}^2, \quad b_{11}b_{21} = m_{12}, \quad b_{21}^2 + b_{22}^2 = m_{22}.$$

We thus finally obtain

$$b_{11} = \sqrt{m_{11}}, \quad b_{21} = \frac{m_{12}}{\sqrt{m_{11}}}, \quad b_{22} = \sqrt{m_{22} - \frac{m_{12}^2}{m_{11}}}. \quad (3.2.32)$$

We are now in the position to construct sample paths of the normal process $X(t)$ with covariance (3.2.1). Indeed, we first construct the sequence $\mathbf{v}(k\Delta t)$ ($k = 0, 1, 2, \dots$) and then obtain $X(k\Delta t)$ ($k = 0, 1, 2, \dots$). Recalling (3.1.51) and (3.1.52) one obtains:

$$\mathbf{v}(0) = \begin{pmatrix} v_1(0) \\ v_2(0) \end{pmatrix} = \begin{pmatrix} \frac{1}{2\sqrt{\beta(\alpha^2 + \beta^2)}} & 0 \\ 0 & \frac{1}{2\sqrt{\beta}} \end{pmatrix} \tilde{\mathbf{\Lambda}}^{(0)}, \quad (3.2.33)$$

$$\begin{aligned} \mathbf{v}[(k+1)\Delta t] &= \begin{pmatrix} v_1[(k+1)\Delta t] \\ v_2[(k+1)\Delta t] \end{pmatrix} \\ &= \begin{pmatrix} d_{11} & d_{12} \\ d_{21} & d_{22} \end{pmatrix} \mathbf{v}(k\Delta t) + \begin{pmatrix} b_{11} & 0 \\ b_{21} & b_{22} \end{pmatrix} \tilde{\mathbf{\Lambda}}^{(k)}, \end{aligned} \quad (3.2.34)$$

where the elements d_{ij} of $e^{A\Delta t}$ are obtained from (3.2.23) while the b_{ij} 's are given by (3.2.32). The sequence $\tilde{\mathbf{\Lambda}}^{(k)}$ ($k = 0, 1, 2, \dots$) consists of two-dimensional standard normal samples. The values $X(k\Delta t)$ can then be obtained by (3.1.53).

Recalling that $b_0 = \sqrt{2(\beta - \alpha \tan \psi)}$ and $b_1 = \sqrt{2(\beta + \alpha \tan \psi)(\alpha^2 + \beta^2)}$, for $k = 0, 1, 2, \dots$, one is led to the following expression:

$$X(k\Delta t) = \sqrt{2(\beta - \alpha \tan \psi)} v_2(k\Delta t) + \sqrt{2(\beta + \alpha \tan \psi)(\alpha^2 + \beta^2)} v_1(k\Delta t). \quad (3.2.35)$$

Note that if one wishes to condition the process on the initial state $X(0) = x_0$, $v_2(0)$ must be calculated as indicated by (3.2.33) and then $v_1(0)$ must be taken in such a way that

$$x_0 = X(0) = \sqrt{2(\beta - \alpha \tan \psi)} v_2(0) + \sqrt{2(\beta + \alpha \tan \psi)(\alpha^2 + \beta^2)} v_1(0),$$

that is

$$v_1(0) = \frac{1}{\sqrt{2(\beta + \alpha \tan \psi)(\alpha^2 + \beta^2)}} [x_0 - \sqrt{2(\beta - \alpha \tan \psi)} v_2(0)]. \quad (3.2.36)$$

We stress that the normal process $X(t)$ with correlation function (3.2.1) is m.s. continuous by virtue of the continuity of (3.2.1) in $\tau = 0$. Furthermore, it is m.s. differentiable since $\ddot{\gamma}(0)$ is finite. Indeed, from (3.2.4) one obtains

$$\frac{d^2}{d\tau^2} \gamma(\tau) = -\frac{e^{-\beta\tau}}{\cos \psi} [2\alpha\beta \sin(\alpha\tau - \psi) + (\beta^2 - \alpha^2) \cos(\alpha\tau - \psi)] \quad (\tau \geq 0), \quad (3.2.37)$$

so that

$$\frac{d^2}{d\tau^2}\gamma(\tau)\Big|_{\tau=0^+} = \beta^2 - \alpha^2 - 2\alpha\beta \tan\psi. \quad (3.2.38)$$

From the symmetry of $\gamma(\tau)$ and hence of $\ddot{\gamma}(\tau)$, it follows $d^2\gamma(\tau)/d\tau^2|_{\tau=0} = d^2\gamma(\tau)/d\tau^2|_{\tau=0^+}$. From (3.2.38) one then concludes that $\ddot{\gamma}(0)$ is finite.

We remark that the process $X(t)$ with correlation function (3.2.1) includes some well known processes as a special case. If, for instance, we set $\beta = \alpha$ and $\psi = \pi/4$ in (3.2.1) one is led to the B-2 type autocorrelation function

$$\gamma(\tau) = \sqrt{2} e^{-\alpha\tau} \cos\left(\alpha\tau - \frac{\pi}{4}\right) \quad (\tau \geq 0). \quad (3.2.39)$$

If, instead, we set $\psi = 0$ in (3.2.1) we obtain the following autocorrelation function

$$\gamma(\tau) = e^{-\beta\tau} \cos(\alpha\tau) \quad (\tau \geq 0). \quad (3.2.40)$$

3.2.1 About simulations

The simulation procedure is suitable to be implemented on supercomputers. Indeed, the error induced by Monte Carlo methods is of the order of $1/\sqrt{N}$, where N is the sample size. The latter must therefore be large. Since the sample paths of our process are generated independently of one another, it is possible to construct a vector algorithm to generate simultaneously a preassigned number of sample paths. Hence, by using a supercomputer the computation time is expected to shrink relevantly on the grounds of the mentioned parallel construction of the sample paths of the process.

We have set up a FORTRAN program suitable to be implemented on a supercomputer. We stress that the program has been conceived in a way to generate simultaneously independent sample paths of a Gaussian process. As soon as a sample path crosses the preassigned boundary $S(t)$, the instant when such a crossing takes place is recorded and then used to build up a histogram of the unknown FCT pdf through $S(t)$. Such a sample path is then discarded and the simulation is carried on starting afresh from the initial state $x_0 = 0$ at the initial time $t_0 = 0$.

The simulation procedure consists of constructing the states $X(k\Delta t)$ of $X(t)$ at times $t_k = k\Delta t$ ($k = 1, 2, \dots$). We assume that $t_h = h\Delta t$ is the first crossing time of $S(t)$ if

$$X(h\Delta t) \geq S(h\Delta t), \quad X(k\Delta t) < S(k\Delta t) \quad (k = 0, 1, \dots, h-1).$$

Hence, the error due to the introduced discretization is not larger than Δt . Therefore, the error for a sample of size N (that is of the order $1/\sqrt{N}$) has to be of the same order of magnitude. It is thus convenient to choose $N \approx (\Delta t)^{-2}$.

The program is structured in such a way that after establishing the form of the covariance and of the boundary, the choice of the involved parameters can be made. Input variables are also the total number of sample paths to be simulated, the number of those that must be simultaneously simulated, the discretization step and the histogram's bin. At each step by means of (3.1.53) the states of the simultaneously simulated sample paths are determined. The vector $\tilde{\Lambda}$ of the random numbers necessary to simulate the sample paths is constructed by a

subroutine that adds up twelve pseudo-random numbers that are uniformly distributed in $[0, 1]$. The error committed by exploiting such a subroutine can be disregarded with respect to the intrinsic error of the simulation procedure due to the use of discrete sample paths and of a limited number of samples.

3.2.2 First passage time estimations

In order to widen up the field of investigation and thus reach more general conclusions on the dependence of the shape of the FCT pdf on the boundary's and covariance's oscillations, we referred to the following covariance function:

$$\gamma(t) = \exp\{-\beta t\} \cos \alpha t, \quad t \geq 0, \quad (3.2.41)$$

with $\alpha, \beta > 0$. The corresponding spectral density is then:

$$\Gamma(\omega) = \frac{2\beta(\omega^2 + \alpha^2 + \beta^2)}{\omega^4 + 2\omega^2(\beta^2 - \alpha^2) + (\alpha^2 + \beta^2)^2}. \quad (3.2.42)$$

Differently from the B-2 case, the presence in (3.2.41) of the two independent parameters α and β permit us to assign arbitrarily the period $P = 2\pi/\alpha$ of the periodic component of the covariance as well as the damping time-constant β .

We recall that the covariance (3.2.41) has been included in some models of processes of practical interest. Furthermore, often it turns out to be very useful to approximate certain empirical covariance functions in which positive values are succeeded by negative values, such as in the fading of radio signals received by a radar (see, for instance, [96]).

Since the spectral density (3.2.42) is of rational type, with the denominator a polynomial of degree less than the numerator, Franklyn's method is again applicable; hence, the algorithm can be exploited.

Our simulation results allow us to come to some conclusions on the features of the FPT density. In particular, its shape is seen to depend not only on the barrier, but also on the numerical values of the parameters that characterize the covariance function of the process. Indeed, the density is unimodal, bimodal or multimodal depending on the values of the input parameters.

We then considered the estimation of how much our vector implementation of the simulation algorithm is responsible for inducing distortions on the shape of the FPT densities. Such distortion is indeed due to the limitation of the specified total number $NPMAX$ of sample paths, namely on the programmed stopping of the simulation algorithm. Such an imposed condition implies that the sample paths being simulated, and such that they have not reached the threshold as yet, do not contribute to the characterization of the FPT density. To estimate the induced distortions, our algorithm has been implemented both in vector and in serial ways and the respective results have been compared. In the serial programming modality, $NPARA$ is set to one, so that the algorithm simulates a pre-assigned number of sample paths each of which has eventually reached the barrier. In order to evaluate the effects of exclusion of longer paths, a $TMAX$ parameter is introduced, representing the maximum time for the first crossing of the barrier by a sample path to occur. Then, if the sample path has not reached the barrier

during such a maximum time, it is removed from the set of paths to be used for the density representation, and the consequent change of the density should consequently become apparent.

The conclusions we can draw from the numerous considered cases in which the parameters of covariance function and the parameter $TMAX$ have been made to vary, can be summarized claiming that there is no significant distortion in the shape of the evaluated density even though the set of paths simulated in the presence of $TMAX$ is different from the set of paths obtained without using $TMAX$. In conclusion, it is reasonable to claim that, at least with the parameters and conditions chosen for our simulations, the number of “slower” paths is sufficiently small not to affect significantly the shape of the histogram. The histograms for some of our simulation results are shown in each couple of Figures 3.1-3.6. In each of them, on left-hand-side the histogram with equal width cells is plotted for the serial simulation of 10^4 sample paths of the process, while on the right-hand-side the histogram is plotted for the simulation of the same number of sample paths constructed by using $TMAX$. In these figures, the step size Δt of the simulated process is set to 0.01, whereas the values of the parameters α and β are specified in the captions to the figures.

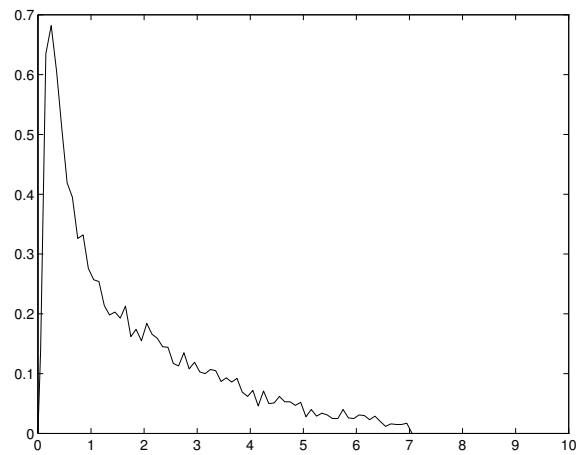
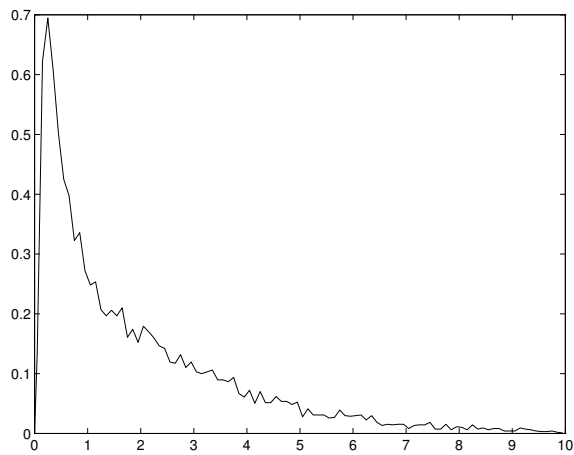


Figure 3.1: On left: $\alpha = 1.0, \beta = 1.0$. On right: $\alpha = 1.0, \beta = 1.0, TMAX = 7.0$

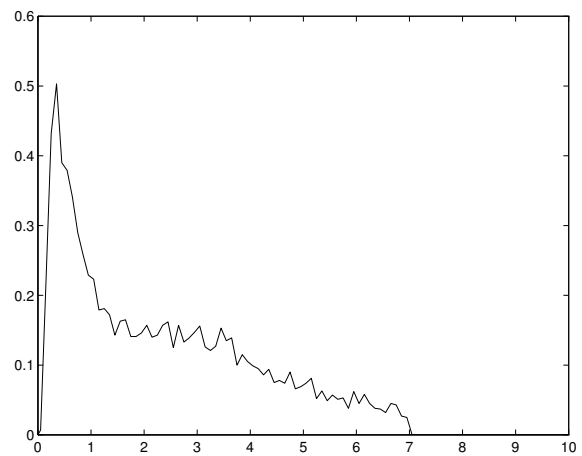
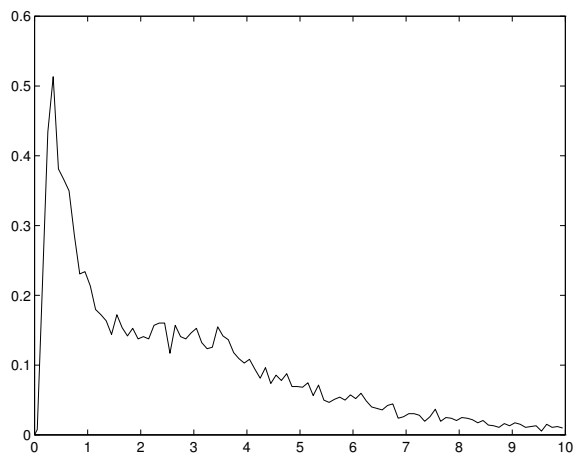


Figure 3.2: On left: $\alpha = 1.0, \beta = 0.5$. On right: $\alpha = 1.0, \beta = 0.5, TMAX = 7.0$

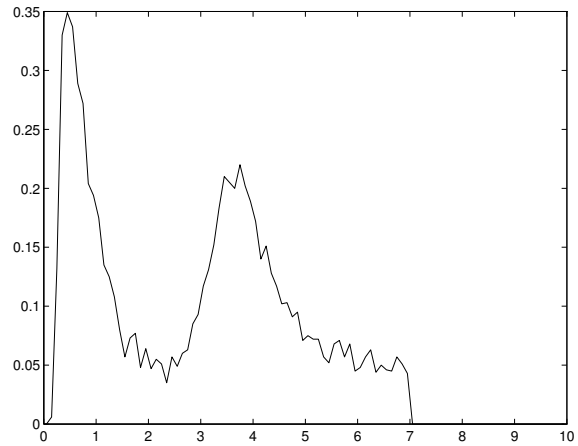
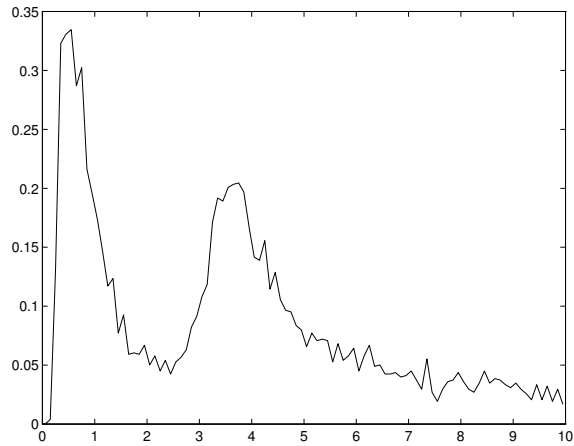


Figure 3.3: On left: $\alpha = 1.0, \beta = 0.1$. On right: $\alpha = 1.0, \beta = 0.1, TMAX = 7.0$

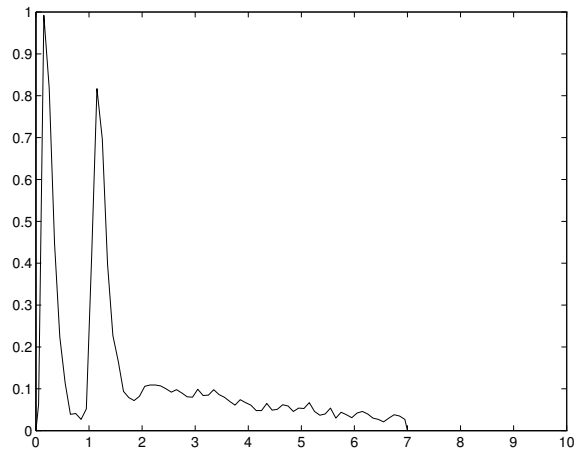
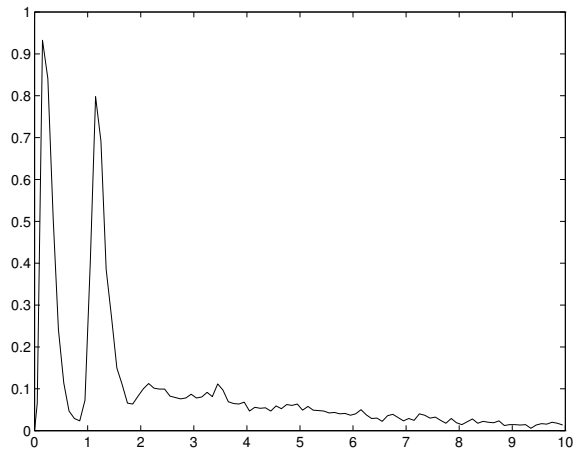


Figure 3.4: On left: $\alpha = \pi, \beta = 0.1$. On right: $\alpha = \pi, \beta = 0.1, TMAX = 7.0$

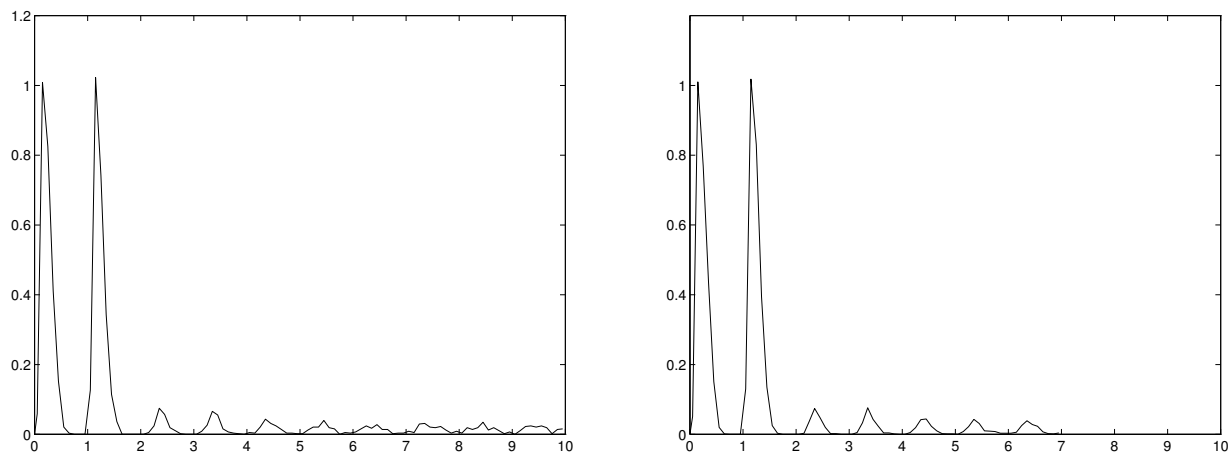


Figure 3.5: On left: $\alpha = \pi$, $\beta = 0.01$. On right: $\alpha = \pi$, $\beta = 0.01$, $TMAX = 7.0$

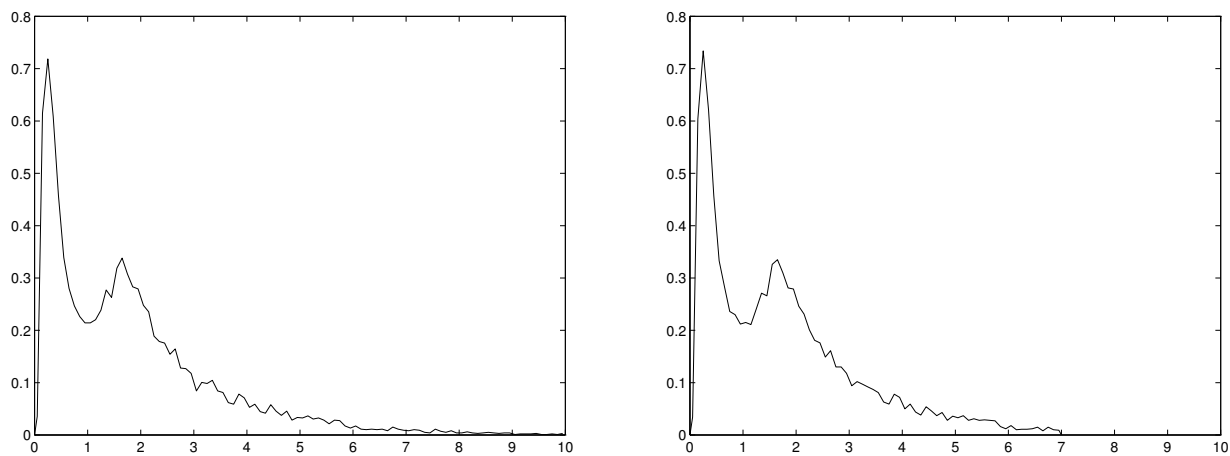


Figure 3.6: On left: $\alpha = (2/3)\pi$, $\beta = 0.5$. On right: $\alpha = (2/3)\pi$, $\beta = 0.5$, $TMAX = 7.0$

3.3 Parallel simulations for upcrossing FPT problem

The specified simulation procedure can be applied to any Gaussian process having rational spectral densities. Since the sample paths of the simulated process are generated independently of one another, this simulation procedure is particularly suited for implementation on supercomputers. Implementation has been made both in vector [20] and parallel modalities [22] after suitable changes required for our computational needs. In particular, the parallel code has been implemented in FORTRAN 90 on a 128-processor IBM SP4 supercomputer, based on MPI language for parallel processing, made available to us by CINECA¹.

To evaluate the upcrossing FPT pdf, we have randomly chosen the initial state x_0 , according to the initial pdf $\gamma_\varepsilon(x_0)$. To this purpose, the following acceptance-rejection method has been implemented (cf. for instance [52]). At first step we generate the rvs U_1, U_2 uniformly distributed in $(0, 1)$. At second step we consider the rv $Y = \ln U_2 + S(0) - \varepsilon$, with pdf

$$f_Y(y) = \begin{cases} e^{y-[S(0)-\varepsilon]}, & \text{if } y < S(0) - \varepsilon \\ 0, & \text{if } y \geq S(0) - \varepsilon. \end{cases}$$

Hence, if $U_1 < \exp\{-(Y+1)^2/2\}$, we set $X_0 = Y$, otherwise we return to first step. Then, X_0 is a rv generated according to the pdf $\gamma_\varepsilon(x_0)$.

Thanks to such simulation procedure, reliable histograms estimating the FPT pdf have been constructed and the different shapes of the FPT pdf as induced by the oscillatory behaviors of covariances and thresholds have been explored (cf. for instance [22] and references therein).

3.3.1 Using the diffusive approximation

Within the context of single neuron's activity modeling, a completely different, apparently not very much known, approach was proposed by Kostyukov ([54]). There, a non-Markov process of a Gaussian type was assumed to describe the time course of the neural membrane potential.

The K-model makes use of [87] notion of correlation time. Namely, let $X(t)$ be a stationary Gaussian process with zero mean, unit variance and correlation function $\rho(t)$. Then,

$$\vartheta = \int_0^{+\infty} |\rho(\tau)| d\tau < +\infty \quad (3.3.1)$$

is the correlation time of $X(t)$. Under the assumption that $\lim_{\varepsilon \rightarrow 0} P\{X(0) < S(0) - \varepsilon\} \simeq 1$, i.e. $\lim_{\varepsilon \rightarrow 0} \gamma_\varepsilon(x_0) \simeq f(x_0)$, Kostyukov works out an approximation $q(t)$ to the upcrossing FPT pdf. Such an approximation is obtained as solution of the integral equation

$$\int_0^t q(\tau) K(t, \tau) d\tau = 1 - \Phi[S(t)]. \quad (3.3.2)$$

This can be solved by standard routine methods, due to the form

$$K(t, \tau) = \begin{cases} \frac{1}{2} & t = \tau \\ 1 - \Phi \left\{ \frac{(t - \tau + \vartheta) S(t) - \vartheta S(\tau)}{\sqrt{(t - \tau + \vartheta)(t - \tau)}} \right\} & t > \tau, \end{cases}$$

¹Interuniversity Consortium of Northeastern Italy for Automatic Computing (<http://www.cineca.it/en/index.htm>)

with $\Phi(z)$ the distribution function of a standard Gauss rv. Equation (3.3.2) stems out of the approximation of the transition density function $P[S(\tau), t - \tau | x, 0]$ of the original process with that of a Wiener process whose infinitesimal variance is the reciprocal of the correlation time:

$$P[S(\tau), t - \tau | x, 0] \approx \frac{1}{\sqrt{2\pi(t-\tau)/\vartheta}} \exp \left\{ -\frac{[x - S(\tau)]^2}{2(t-\tau)/\vartheta} \right\}.$$

Note that, under the above approximation, in equation (3.3.2) the unique parameter ϑ characterizes the considered class of stationary standard Gaussian processes.

The K-model has been analyzed by us to pinpoint similarities and differences with respect to our models, as indicated in the next Section.

3.3.2 Markov versus non-Markov models

In order to analyze how the lack of memory affects the shape of the FPT densities, we have compared the behavior of such densities for Gauss-Markov processes with that of Gauss non-Markov processes ([28]).

Let us consider a zero-mean stationary Gaussian process $X(t)$ with the simplest type of correlation of concrete interest for applications [96]:

$$\rho(t) = e^{-\beta|t|} \cos(\alpha t), \quad \alpha, \beta \in \mathbb{R}^+. \quad (3.3.3)$$

Furthermore, let us assume that the threshold is of the following type:

$$S(t) = d e^{-\beta t} \left\{ 1 - \frac{e^{2\beta t} - 1}{2d^2} \ln \left[\frac{1}{4} + \frac{1}{4} \sqrt{1 + 8 \exp\left(-\frac{4d^2}{e^{2\beta t} - 1}\right)} \right] \right\}, \quad (3.3.4)$$

with $d > 0$.

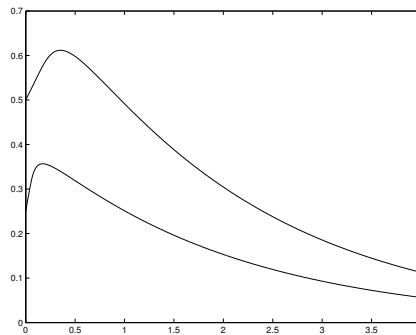


Figure 3.7: Plot of the threshold $S(t)$ given in (3.3.4) for $\beta = 0.5$ and $d = 0.25, 0.50$ (bottom to top).

As shown in Figure 3.7, the threshold (3.3.4) does not sweep the entire state space. Hence, the K-model is not applicable. Moreover due to the form of correlation (3.3.3), $X(t)$ is not mean-square differentiable. Thus, the series expansions (1.3.15) and (1.3.16) do not hold for FPT pdfs. Nevertheless, specific assumptions on parameter α help us characterize the shape of the FPT pdf.

We start assuming $\alpha = 0$, so that the correlation function (3.3.3) factorizes as

$$\rho(t) = e^{-\beta\tau} e^{-\beta(t-\tau)} \quad \beta \in \mathbb{R}^+, 0 < \tau < t.$$

In such case $X(t)$ becomes Gauss-Markov. For thresholds of form (3.3.4), the FPT pdf $g(t)$ of a Gauss-Markov process admits the following closed form:

$$g(t) = \frac{4d\beta e^{\beta t}}{e^{2\beta t} - 1} \frac{\sqrt{1 + 8 \exp\left(-\frac{4d^2}{e^{2\beta t} - 1}\right)}}{1 + \sqrt{1 + 8 \exp\left(-\frac{4d^2}{e^{2\beta t} - 1}\right)}} f[S(t), t | 0, 0], \quad (3.3.5)$$

where $f[S(t), t | 0, 0]$ is the transition pdf of the process.

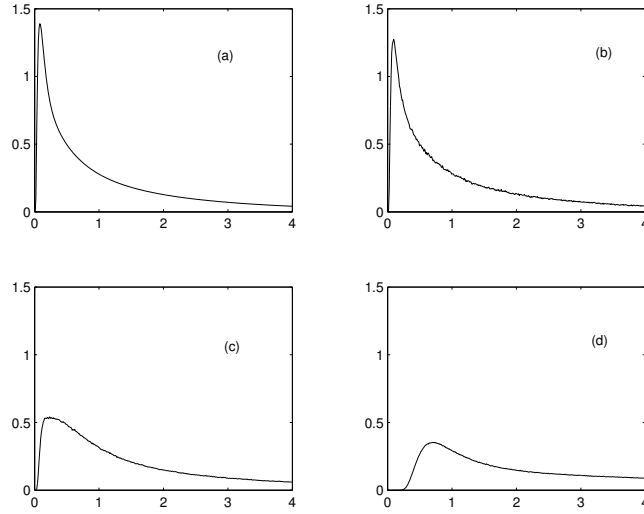


Figure 3.8: Plots refer to FPT pdf of a zero-mean Gaussian process characterized by correlation function (3.3.3), with $\beta = 0.5$, in the presence of the threshold (3.3.4), with $d = 0.25$. In (a), the function $g(t)$ in (3.3.5) has been plotted, corresponding to $\alpha = 0$. The estimated FPT pdf $\tilde{g}(t)$ with $\alpha = 10^{-10}$ is shown in (b), with $\alpha = 0.25$ in (c) and with $\alpha = 0.5$ in (d).

For a zero-mean Gauss-Markov process characterized by the correlation function (3.3.3) with $\beta = 0.5$ and $\alpha = 0$, the FPT pdf given in (3.3.5) for threshold (3.3.4) is plotted in Figure 3.8(a) for $d = 0.25$ and in Figure 3.9(a) for $d = 0.5$. Note that as d increases the mode increases, whereas the corresponding ordinate decreases.

Setting $\alpha \neq 0$ in (3.3.3), the Gaussian process $X(t)$ is no longer Markov. Its spectral density is of a rational type:

$$\Gamma(\omega) = \frac{2\beta(\omega^2 + \alpha^2 + \beta^2)}{\omega^4 + 2\omega^2(\beta^2 - \alpha^2) + (\beta^2 + \alpha^2)^2}. \quad (3.3.6)$$

Since in (3.3.6) the degree of the numerator is less than the degree of the denominator, it is possible to apply the simulation algorithm described in [24] in order to estimate the FPT pdf $\tilde{g}(t)$ of the process. The number of simulated sample paths was set equal to 10^7 . The estimated FPT pdf's $\tilde{g}(t)$ through the threshold (3.3.4) with $d = 0.25$ are plotted in Figures 3.8(b), 3.8(c), 3.8(d) when $\beta = 0.5$ and $\alpha = 10^{-10}, 0.25, 0.5$ respectively. Figures 3.9(b), 3.9(c), 3.9(d) refer to the choice $d = 0.5$. Note that as α increases, the shape of the FPT pdf $\tilde{g}(t)$ becomes flatter and the related mode increases. Furthermore, comparing Figures 3.8(a), 3.8(b) and Figures 3.9(a), 3.9(b), $\tilde{g}(t)$ looks very similar to $g(t)$ for small values of α , since the simulated non-Markov

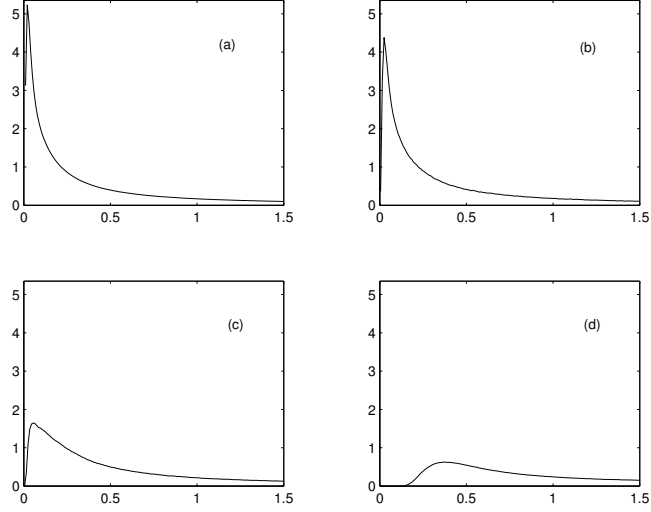


Figure 3.9: Same as in Figure 3.8 with $d=0.5$.

stochastic process $X(t)$ turns out to be approximately an exponentially correlated process. This last circumstance becomes more evident in Figure 3.10, where plots of upcrossing FPT pdf are shown for the same choice of correlation time (3.3.1). Here we refer to the test threshold

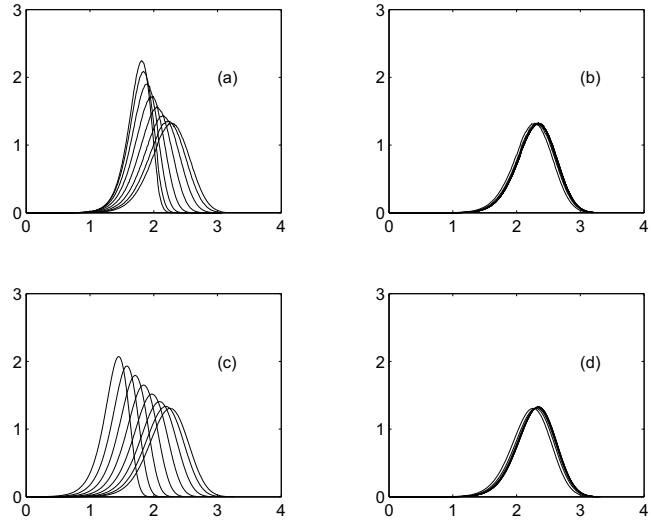


Figure 3.10: For different choices of ϑ in the interval $[0.008, 1.024]$, with threshold $S(t) = -t^2/2 - t + 5$, plots of the estimated $\tilde{g}_u(t)$ are shown in (a) and plots of $\tilde{g}_u(t)$ for the OU-model in (c). Same in (b) and (d) for values of ϑ in $[2.048, 200]$.

$$S(t) = -t^2/2 - t + 5 \quad (3.3.7)$$

and to the following choice of correlation times:

- i)* $\vartheta = 0.008, 0.016, 0.032, 0.064, 0.128, 0.256, 0.512, 1.024$;
- ii)* $\vartheta = 2.048, 4, 8, 16, 32, 64, 100, 200$.

By simulating the stochastic process with correlation function (3.3.3), where $\alpha = 10^{-5}$ and $\beta = \vartheta^{-1}$, plots of estimated upcrossing FPT pdf are shown in Figure 3.10(a) for correlation times i), and in Figure 3.10(b) for correlation times ii). Instead, for the OU model, corresponding to a stationary Gauss-Markov process with

$$m(t) = 0, \quad c(s, t) = e^{-(t-s)/\vartheta} \quad (s < t),$$

upcrossing FPT density approximations $\tilde{g}_u(t)$, evaluated via (1.3.14), are plotted in Figure 3.10(c) for correlation times i) and in Figure 3.10(d) for correlation times ii). Note that plots in Figures 3.10(a), 3.10(b) look similar to plots in Figures 3.10(c), 3.10(d), since the simulated stochastic process $X(t)$ turns out to be approximatively an exponentially correlated process with correlation time $\vartheta = \beta^{-1}$, like as in the case of the OU process. When $\vartheta > 4$, the obtained upcrossing FPT pdf's are practically indistinguishable from a Gaussian with mean 5 and variance 1. A more general asymptotic result holds for a class of diffusion processes with normal standard one-dimensional pdf [21].

We have performed further numerical comparisons, including approximations of the FPT pdf for the Wiener model and for the K-model, by considering a variety of thresholds and of ϑ values [29].

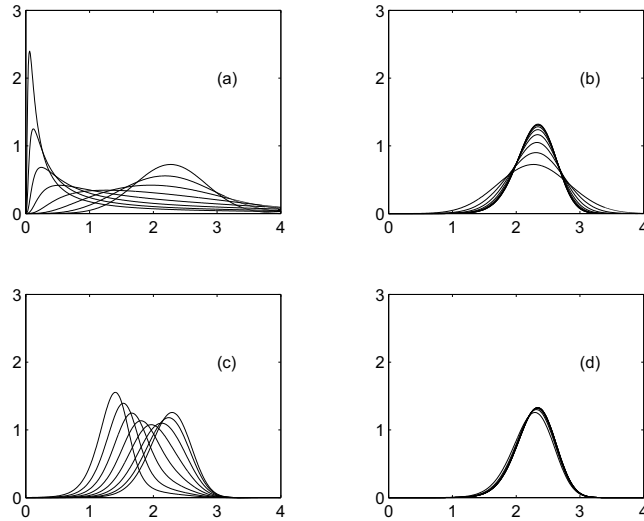


Figure 3.11: For different choices of ϑ in the interval $[0.008, 1.024]$, with the same threshold as in Figure 3.10, plots of $\tilde{g}_u(t)$ for the Wiener model are shown in (a) and plots of $q(t)$ for the Kostyukov-model in (c). Same in (b) and (d) for values of ϑ in $[2.048, 200]$.

Indeed, the Wiener model corresponds to a non stationary Gauss-Markov process with

$$m(t) = 0, \quad c(s, t) = s/\vartheta \quad (s < t).$$

By numerically solving (1.3.14) for the same threshold (3.3.7), plots of the corresponding upcrossing FPT density approximations $\tilde{g}_u(t)$ are shown in Figure 3.11(a) for correlation times i) and in Figure 3.11(b) for correlation times ii). Following the outline given in [55], the results of the numerical solution of equation (3.3.2) are shown in Figure 3.11(c) for correlation times i) and

in Figure 3.11(d) for correlation times ii). Again, growing ϑ induces a continuous displacement of the upcrossing FPT pdf towards a Gaussian with mean 5 and variance 1. This is in agreement with the analytical results obtained in [55] for infinitely large correlation time.

Comparing Figure 3.10 with Figure 3.11, it is evident that for large correlation times the FPT pdf's exhibit similar features, whereas large deviations are present for small correlation times.

Our investigations in this direction suggest that the validity of approximations of the firing densities in the presence of memory effects by the FPT densities of Markov type depends on the magnitude of the correlation time. Some preliminary results on the asymptotics of firing pdf's as the correlation time diverges can be found in [42] for the case of non-stationary Gauss-Markov processes.

3.3.3 Asymptotic results for Gaussian processes

Computational as well as analytical results have indicated that for the class of one-dimensional diffusion processes, admitting steady state densities, the conditioned FPT pdf is susceptible of an excellent non-homogeneous exponential approximation for large thresholds, either asymptotically constant or asymptotically periodic [67, 41]. These results have led us to gain some insight on the asymptotic behavior of the FPT pdf for correlated non-Markov Gaussian stochastic processes of concrete interest for certain applications. Specifically, we have considered the class of zero-mean stationary Gaussian processes characterized by damped oscillatory covariances [87]:

$$\rho(t) = e^{-a|t|} \left[\cos(\omega t) + \frac{a}{\omega} \sin(\omega|t|) \right], \quad (3.3.8)$$

where a and ω are positive real numbers. Functions of form (3.3.8) can be conveniently used to approximate experimental covariance functions that, starting from a unit initial maximum amplitude, asymptotically tend to zero with an exponential envelope. From (3.3.8) one has $\rho(0) = 1$. Furthermore $\dot{\rho}(0) = 0$ and $\ddot{\rho}(0) = -(a^2 + \omega^2) < 0$, since for $t > 0$ there holds:

$$\dot{\rho}(t) = -\dot{\rho}(-t) = -\frac{e^{-at}}{\omega} (a^2 + \omega^2) \sin(\omega t), \quad (3.3.9)$$

$$\ddot{\rho}(t) = \ddot{\rho}(-t) = \frac{e^{-at}}{\omega} (a^2 + \omega^2) \left[a \sin(\omega t) - \omega \cos(\omega t) \right].$$

Gaussian processes with covariances (3.3.8) are mean-square differentiable so that series expansions (1.3.15) and (1.3.16) are available for the FPT pdf. Due to the outrageous complexity of the numerical evaluations of the involved partial sums on account of the form of its terms, we have undertaken a completely different approach to investigate the asymptotic behaviour of FPT pdf [24]. We have estimated the FPT pdf by means of the simulation procedure and then we have made use of the least squares method to fit an exponential density $\lambda e^{-\lambda t}$. The least squares estimate of λ has been determined as

$$\hat{\lambda} = - \frac{\sum_{i=1}^n t_i \ln[1 - \tilde{G}(t_i)]}{\sum_{i=1}^n t_i^2}, \quad (3.3.10)$$

where $\tilde{G}(t)$ is the cumulative FPT distribution function of the random sample (t_1, \dots, t_n) generated by the simulation procedure. The results of our computations have shown that for certain

periodic thresholds of the form

$$S(t) = S_0 + A \sin(2\pi t/Q), \quad S_0, Q > 0, A \geq 0 \quad (3.3.11)$$

and not very distant from the initial value of the process, the FPT pdf soon exhibits damped oscillations having the same period of the threshold. Furthermore, starting from rather small times, the estimated FPT densities $\tilde{g}(t)$ appears to be representable in the form

$$\tilde{g}(t) \simeq \tilde{Z}(t) e^{-\hat{\lambda}t},$$

where $\hat{\lambda}$ is given in (3.3.10) and $\tilde{Z}(t)$ is a periodic function having the same period of the threshold (3.3.11). All forthcoming figures refer to the case $a = \omega = 1$ in (3.3.8). Figures 3.12(a) and

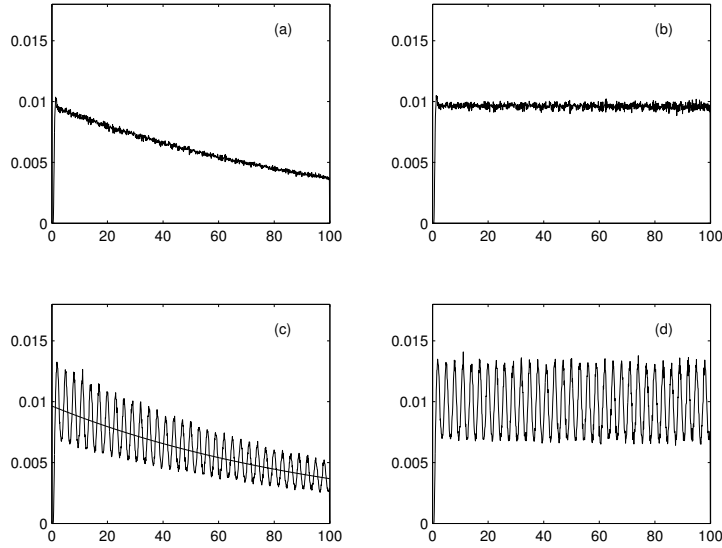


Figure 3.12: The estimated FPT density $\tilde{g}(t)$ is compared with the exponential density $\hat{\lambda} e^{-\hat{\lambda}t}$, for the constant threshold $S = 2.5$ and $\hat{\lambda} = 0.0094905$ in (a) and for the periodic threshold $S(t) = 2.5 + 0.1 \sin(2\pi t/3)$ and $\hat{\lambda} = 0.0096462$ in (c). The corresponding functions $\tilde{Z}(t) = \tilde{g}(t) e^{\hat{\lambda}t}$ are plotted respectively in (b) and in (d).

3.12(c) show the estimated FPT densities $\tilde{g}(t)$, as well as the exponential densities $\hat{\lambda} e^{-\hat{\lambda}t}$ in which the parameter $\hat{\lambda}$ has been evaluated according to (3.3.10). Figures 3.12(b) and 3.12(d) show plots of $\tilde{Z}(t) \simeq \tilde{g}(t) e^{\hat{\lambda}t}$. Their periodic behavior in the cases of periodically varying threshold is apparent.

The goodness of the exponential approximation increases as the threshold is progressively moved farther apart from the starting point of the process. The more the periodic threshold is far from the starting point of the process, the more the exponential approximation improves.

The relevance and the validity of such an unexpected numerical result have been confirmed by rigorous mathematical arguments [27]. Indeed, as threshold (3.3.11) moves away from the initial state of the process, the FPT pdf approaches a non-homogeneous exponential density of the type

$$g(t) \sim h(t) \exp \left\{ - \int_0^t h(\tau) d\tau \right\}, \quad (3.3.12)$$

where $h(t)$ is a function depending on the correlation function and on the threshold. The function $h(t)$ is completely specified by the knowledge of the asymptotic behavior of the first term $W_1(t)$ in the series expansion (1.3.15), within the conditioned FPT problem, and of the first term $W_1^{(\varepsilon)}(t)$ in the series expansion (1.3.16), within the upcrossing one, as we show in some details hereafter.

Let us consider an asymptotically constant threshold

$$S(t) = S_0 + \varrho(t), \quad t \geq 0, \quad (3.3.13)$$

with $S_0 \in \mathbb{R}$ and where $\varrho(t) \in C^1[0, +\infty)$ is a bounded function independent of S_0 such that

$$\lim_{t \rightarrow +\infty} \varrho(t) = 0 \quad \text{and} \quad \lim_{t \rightarrow +\infty} \dot{\varrho}(t) = 0. \quad (3.3.14)$$

If

$$\lim_{t \rightarrow +\infty} \rho(t) = 0 \quad \text{and} \quad \lim_{t \rightarrow +\infty} \dot{\rho}(t) = 0, \quad (3.3.15)$$

then

$$R(S_0) := \lim_{t \rightarrow +\infty} W_1(t) = \frac{\sqrt{-\ddot{\rho}(0)}}{2\pi} \exp\left\{-\frac{S_0^2}{2}\right\}, \quad (3.3.16)$$

i.e. the function $W_1(t)$ in (1.3.15) approaches a constant value as t increases. If we add the hypothesis

$$\lim_{t \rightarrow +\infty} \ddot{\rho}(t) = 0 \quad \lim_{S_0 \rightarrow +\infty} \frac{\varrho\left(\frac{t}{R(S_0)}\right)}{S_0} = 0, \quad (3.3.17)$$

with $R(S_0)$ defined in (3.3.16), then for $S_0 \rightarrow +\infty$ equation (3.3.12) holds with $h(t) = R(S_0)$ for all $t > 0$. When the covariance has the form (3.3.8), hypotheses (3.3.15) hold due to (3.3.9). Moreover, when the threshold is constant, i.e. $S(t) = S_0$, hypotheses (3.3.14) and (3.3.17) are fulfilled so that from (3.3.16) one has

$$R(S_0) = \frac{\sqrt{a^2 + \omega^2}}{2\pi} e^{-S_0^2/2}. \quad (3.3.18)$$

Set $S_0 = 2.5$, as in Figure 3.12(a). From (3.3.16) it follows that, as t increases, $W_1(t)$ approaches the constant value $R(2.5) = 0.00988928$ very near to $\hat{\lambda} = 0.0094905$, estimated via (3.3.10). Recall that $W_1(t)$ is seen to provide an upper bound to the FPT pdf in (1.3.15) as first-order approximation. As Figure 3.13 shows, $W_1(t)$ is a good approximation of g only for small values of t .

Now, let us consider an asymptotically periodic threshold of the form (3.3.13), with

$$\lim_{k \rightarrow +\infty} \varrho(t + kQ) = Z(t), \quad \lim_{k \rightarrow +\infty} \dot{\varrho}(t + kQ) = \dot{Z}(t), \quad (3.3.19)$$

where $Z(t)$ is a periodic function of period $Q > 0$ satisfying

$$\int_0^Q Z(\tau) d\tau = 0. \quad (3.3.20)$$

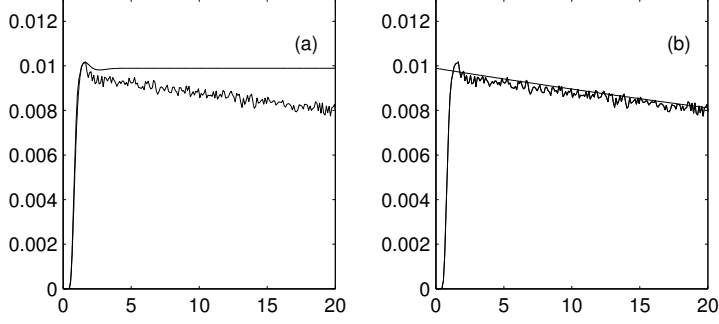


Figure 3.13: For the constant threshold $S(t) = 2$, the estimated FPT density $\tilde{g}(t)$ is plotted with the function $W_1(t)$ in (a) and with the function $R(2) \exp\{-R(2)t\}$ in (b), where $R(2)$ is given in (3.3.18).

If (3.3.15) holds, then

$$R[Z(t)] := \lim_{k \rightarrow +\infty} W_1(t + kQ) = \frac{\sqrt{-\ddot{\rho}(0)}}{2\pi} \exp\left\{-\frac{[S_0 + Z(t)]^2}{2}\right\} \times \left[\exp\left(-\frac{[\dot{Z}(t)]^2}{2[-\ddot{\rho}(0)]}\right) - \sqrt{\frac{\pi}{2[-\ddot{\rho}(0)]}} \dot{Z}(t) \operatorname{Erfc}\left(\frac{\dot{Z}(t)}{\sqrt{2[-\ddot{\rho}(0)]}}\right) \right] \quad (3.3.21)$$

with $\operatorname{Erfc}(z) := 1 - \operatorname{Erf}(z)$, $z \in \mathbb{R}$. Hence, as t increases, $W_1(t)$ becomes a positive periodic function with period Q , providing an upper bound to $g(t)$ for all $t > 0$, as shown in Figure 3.14(a). Since $Z(t)$ does not depend on S_0 , one also has $\lim_{S_0 \rightarrow +\infty} R[Z(t)] = 0$.

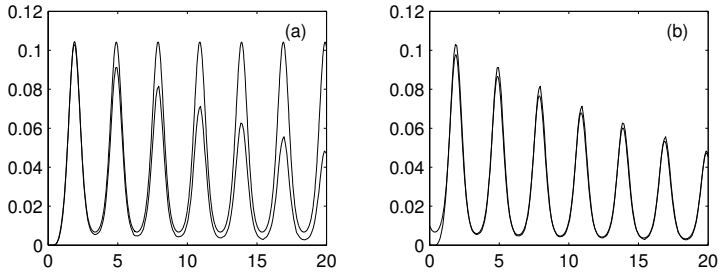


Figure 3.14: In the presence of the periodic threshold $S(t) = 2 + 0.1 \sin(2\pi t/3)$, the estimated FPT density $\tilde{g}(t)$ is compared with the function $W_1(t)$ in (a) and with the asymptotic exponential approximation $R[Z(t)] \exp\left\{-\int_0^t R[Z(\tau)] d\tau\right\}$ in (b).

In order to prove that the FPT pdf exhibits the exponential trend (3.3.12) for large times in the presence of the asymptotically periodic threshold (3.3.13), with $\varrho(t)$ such that (3.3.19) hold, it is necessary to introduce a new function $\varphi(t)$, non-negative and monotonically increasing, that is the solution of

$$\int_0^{\varphi(t)} R[Z(\tau)] d\tau = \alpha t, \quad \forall t > 0 \quad (3.3.22)$$

where

$$\alpha \equiv \alpha(S_0) = \frac{1}{Q} \int_0^Q R[Z(\tau)] d\tau.$$

When (3.3.15) are fulfilled and

$$\lim_{t \rightarrow +\infty} \ddot{\rho}(t) = 0 \quad \lim_{S_0 \rightarrow +\infty} \frac{\varrho\left(\varphi\left(\frac{t}{\alpha}\right)\right)}{S_0 + Z\left(\varphi\left(\frac{t}{\alpha}\right)\right)} = 0, \quad (3.3.23)$$

equation (3.3.12) holds with $h(t) \equiv R[Z(t)]$, given in (3.3.21), and $Z(t) = A \sin(2\pi t/Q)$, as Figure 3.14(b) shows.

Figure 3.15 shows the same non-homogeneous exponential approximations of upcrossing FPT densities for large thresholds, either asymptotically constant or asymptotically periodic.

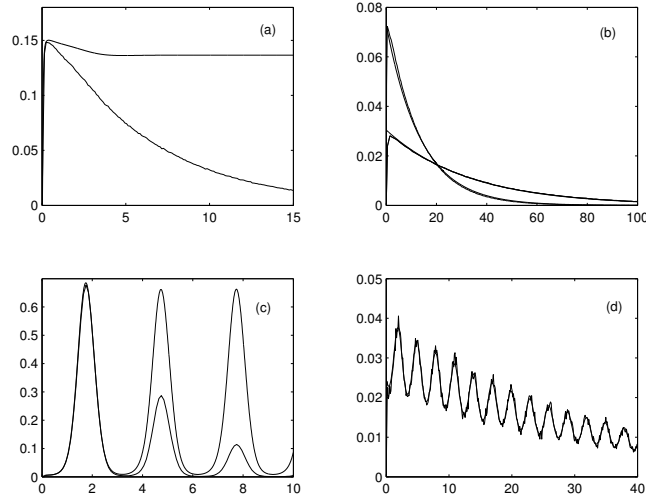


Figure 3.15: For $\varepsilon = 0.1$, the estimated FPT density $\tilde{g}_u^{(\varepsilon)}(t)$ is compared with the function $W_1^{(\varepsilon)}(t)$ for $S(t) = 1.0$ in (a) and for $S(t) = 1 + \sin(2\pi t/3)$ in (c). For the same choice of ε , the estimated FPT density $\tilde{g}_u^{(\varepsilon)}(t)$ is compared with asymptotic exponential approximation $R[Z(t)] \exp\left\{-\int_0^t R[Z(\tau)] d\tau\right\}$ for the constant thresholds $S(t) = S_0 = 1.5$ and $S(t) = S_0 = 2$ in (b) and for the periodic threshold $S(t) = 2 + 0.1 \sin(2\pi t/3)$ in (d).

It should be stressed that the analytic and the simulation results constitutes only a preliminary step towards the construction of neuronal models based on non-Markov processes. Nevertheless, we stress that the unveiling of properties of the asymptotic behavior of FPT may turn out to be useful also for the description of neuronal activities at small times whenever the intrinsic time scale of the microscopic events involved during the neuron's evolution is much smaller than the macroscopic observation time scale, or when the asymptotic regime is exhibited also in the case of firing thresholds not too distant from the resting potential, similarly to what was already pointed out by us in connection with the OU neuronal model [41].

3.4 Upcrossing FPT problem and the correlation time

Upcrossing first passage time problems play a relevant role in various applied contexts including neuronal modeling [56]. Now, for a one-dimensional, non-singular stationary Gaussian process $\{X(t), t \geq 0\}$ with zero mean, unit variance and correlation function $\varrho(t)$, we focus our attention on

$$\tau_c := \int_0^{+\infty} |\varrho(\vartheta)| d\vartheta \quad (3.4.1)$$

defined, as in (3.3.1), as the correlation time of the process.

The available analytical results on upcrossing first-passage-time (FPT) problems are scarce, fragmentary and mainly centered on diffusion processes. Furthermore, if one deals with models involving processes characterized by memory effects the Markov property breaks down, and one is forced to face FPT problems for correlated processes (cf., for instance, [21], [27], [29] and [42]). Hence, in order to construct neuronal models that are based on such processes, we recall that a one-dimensional, non-singular stationary Gaussian process with zero mean, unit variance and correlation function $\varrho(t)$, such that $\varrho(0) = 1$, $\dot{\varrho}(0) = 0$ and $\ddot{\varrho}(0) < 0$, the derivative of $X(t)$, $\dot{X}(t)$, with respect to t , exists in the mean-square sense. Let $S(t) \in C^1[0, +\infty)$ be an arbitrary function such that $X(0) = x_0 < S(0)$, T the FPT random variable and

$$g(t | x_0) = \frac{\partial}{\partial t} P(T < t) \quad (3.4.2)$$

is the FPT pdf of $X(t)$ through $S(t)$ conditional upon $X(0) = x_0$. Furthermore, we recall that $\forall n \in \mathbb{N}$ and $0 < t_1 < t_2 < \dots < t_n$ we denote by $W_n(t_1, t_2, \dots, t_n | x_0) dt_1 dt_2 \dots dt_n$ the joint probability that $X(t)$ crosses $S(t)$ from below in the intervals $(t_1, t_1 + dt_1)$, $(t_2, t_2 + dt_2)$, \dots , $(t_n, t_n + dt_n)$ given that $X(0) = x_0$. The function W_n can be written as:

$$\begin{aligned} W_n(t_1, t_2, \dots, t_n | x_0) &= \int_{\dot{S}(t_1)}^{+\infty} d\xi_1 \int_{\dot{S}(t_2)}^{+\infty} d\xi_2 \dots \int_{\dot{S}(t_n)}^{+\infty} d\xi_n \prod_{i=1}^n [\xi_i - \dot{S}(t_i)] \\ &\times p_{2n}[S(t_1), t_1; S(t_2), t_2; \dots; S(t_n), t_n; \xi_1, t_1; \xi_2, t_2; \dots; \xi_n, t_n | x_0], \end{aligned} \quad (3.4.3)$$

where $p_{2n}(x_1, t_1; x_2, t_2; \dots, x_n, t_n; \xi_1, t_1; \xi_2, t_2; \dots; \xi_n, t_n | x_0)$ is the joint pdf of $x_1 = X(t_1)$, $x_2 = X(t_2)$, \dots , $x_n = X(t_n)$, $\xi_1 = \dot{X}(t_1)$, $\xi_2 = \dot{X}(t_2)$, \dots , $\xi_n = \dot{X}(t_n)$ conditional upon $X(0) = x_0$. Furthermore, we consider the following functions:

$$Q_1(t | x_0) = W_1(t | x_0) \quad (3.4.4)$$

$$\begin{aligned} Q_n(t | x_0) &= \int_0^t dt_1 \int_{t_1}^t dt_2 \dots \int_{t_{n-2}}^t dt_{n-1} W_n(t_1, t_2, \dots, t_{n-1}, t | x_0) \\ &\quad (n = 2, 3, \dots), \end{aligned}$$

with $t_0 > 0$. We note that $Q_n(t | x_0) dt$ gives the probability that $X(t)$ crosses $S(t)$ from below at least n times *and* the last crossing occurs in the interval $(t, t + dt)$ conditional upon $X(0) = x_0$. Denoting by $q_k(t | x_0) dt$ the probability that $X(t)$ crosses $S(t)$ for the k -th time in $(t, t + dt)$, one has (cf. [77]):

$$Q_n(t | x_0) = \sum_{k=n}^{+\infty} \binom{k-1}{n-1} q_k(t | x_0) \quad (n = 1, 2, \dots). \quad (3.4.5)$$

Since $g(t | x_0) \equiv q_1(t | x_0)$, setting $n = 1$ in (3.4.5) one obtains:

$$g(t | x_0) = W_1(t | x_0) - \sum_{k=2}^{+\infty} q_k(t | x_0), \quad x_0 < S(0). \quad (3.4.6)$$

Making use of (3.4.5) and (3.4.6), an alternative expression (to the equation (1.3.15)) for $g(t | x_0)$ can be obtained in terms of the functions $Q_n(t | x_0)$:

$$g(t | x_0) = W_1(t | x_0) - \sum_{n=2}^{+\infty} (-1)^n Q_n(t | x_0), \quad x_0 < S(0). \quad (3.4.7)$$

We stress that although (3.4.7) gives a formal analytical expression for the FPT pdf through arbitrary time-dependent boundaries, no reliable numerical evaluations appear to be feasible due to the complexity of (3.4.4). However, the explicit expression of $W_1(t | x_0)$ can be evaluated ([74]):

$$W_1(t | x_0) = \frac{|\Lambda_3(t)|^{1/2}}{2\pi[1-\varrho^2(t)]} \exp\left\{-\frac{[S(t)-x_0\varrho(t)]^2}{2[1-\varrho^2(t)]}\right\} \\ \times \left[\exp\left\{-\frac{\sigma^2(t|x_0)}{2}\right\} - \sqrt{\frac{\pi}{2}} \sigma(t|x_0) \operatorname{Erfc}\left(\frac{\sigma(t|x_0)}{\sqrt{2}}\right) \right], \quad (3.4.8)$$

where

$$|\Lambda_3(t)| = -\ddot{\varrho}(0)[1-\varrho^2(t)] - [\dot{\varrho}(t)]^2, \quad (3.4.9)$$

$$\sigma(t|x_0) = \left(\frac{1-\varrho^2(t)}{|\Lambda_3(t)|}\right)^{1/2} \left\{ \dot{S}(t) + \frac{\dot{\varrho}(t)[\varrho(t)S(t)-x_0]}{1-\varrho^2(t)} \right\},$$

and

$$\operatorname{Erfc}(z) = \frac{2}{\sqrt{\pi}} \int_z^{+\infty} e^{-y^2} dy, \quad z \in \mathbb{R}. \quad (3.4.10)$$

We note that $W_1(t | x_0)$, providing an upper bound to the FPT pdf in (3.4.7), is a good approximation of $g(t | x_0)$ only for small values of t .

We shall now focus on the upcrossing FPT problem. We assume that a subset of sample paths of $X(t)$ originates at a state X_0 that is a random variable with preassigned pdf

$$\gamma_\varepsilon(x_0) = \begin{cases} f(x_0) \left[\int_{-\infty}^{S(0)-\varepsilon} f(z) dz \right]^{-1}, & x_0 < S(0) - \varepsilon \\ 0, & x_0 \geq S(0) - \varepsilon, \end{cases} \quad (3.4.11)$$

where $\varepsilon > 0$ is a fixed real number and $f(x_0)$ denotes the pdf of $X(0)$:

$$f(x_0) = \frac{1}{\sqrt{2\pi}} \exp\left\{-\frac{x_0^2}{2}\right\}, \quad x_0 \in \mathbb{R}. \quad (3.4.12)$$

Then,

$$T_{X_0}^{(\varepsilon)} := \inf_{t \geq 0} \{t : X(t) > S(t)\} \quad (3.4.13)$$

is the ε -upcrossing FPT of $X(t)$ through $S(t)$. Its pdf is related to the conditional FPT pdf $g(t | x_0)$ as follows [25]:

$$g_u^{(\varepsilon)}(t) = \int_{-\infty}^{S(0)-\varepsilon} g(t | x_0) \gamma_\varepsilon(x_0) dx_0 \quad (t \geq 0). \quad (3.4.14)$$

Making use of (3.4.6) in (3.4.14), one has:

$$g_u^{(\varepsilon)}(t) = W_1^{(\varepsilon)}(t) - \sum_{k=2}^{+\infty} q_k^{(\varepsilon)}(t) \quad (3.4.15)$$

where

$$W_1^{(\varepsilon)}(t) = \int_{-\infty}^{S(0)-\varepsilon} W_1(t | x_0) \gamma_\varepsilon(x_0) dx_0, \quad (3.4.16)$$

$$q_k^{(\varepsilon)}(t) = \int_{-\infty}^{S(0)-\varepsilon} q_k(t | x_0) \gamma_\varepsilon(x_0) dx_0 \quad (k = 2, 3, \dots). \quad (3.4.17)$$

In Section 3.4.1, under suitable assumptions on the correlation function $\varrho(t)$ and on the threshold $S(t)$, the behavior of $g_u^{(\varepsilon)}(t)$ as $\tau_c \rightarrow +\infty$ is analyzed. Furthermore, in Section 3.4.2 two different stationary Gaussian processes are considered and the results of some simulations are finally presented.

3.4.1 Asymptotic results for large correlation times

Proposition 3.4.1 *Let $\{X(t), t \geq 0\}$ be a non-singular stationary Gaussian process with zero mean, unit variance and correlation function $\varrho(t)$ such that $\varrho(0) = 1$, $\dot{\varrho}(0) = 0$ and $\ddot{\varrho}(0) < 0$. Furthermore, let $S(t) \in C^1[0, +\infty)$ be an arbitrary monotonically decreasing function such that $\dot{S}(t) - [S(t) - S(0)]/t \leq 0$. If the correlation function of $X(t)$ satisfies*

$$\lim_{\tau_c \rightarrow +\infty} \varrho(t) = 1, \quad \lim_{\tau_c \rightarrow +\infty} \dot{\varrho}(t) = \lim_{\tau_c \rightarrow +\infty} \ddot{\varrho}(t) = 0, \quad \lim_{\tau_c \rightarrow +\infty} \frac{\dot{\varrho}(t)}{1 - \varrho^2(t)} = -\frac{1}{t}, \quad (3.4.18)$$

then

$$\varphi^{(\varepsilon)}(t) := \lim_{\tau_c \rightarrow +\infty} W_1^{(\varepsilon)}(t) = \begin{cases} -\dot{S}(t) \gamma_\varepsilon[S(t)], & S(t) < S(0) - \varepsilon, \\ 0, & \text{otherwise.} \end{cases} \quad (3.4.19)$$

Proof 3.4.1 *We first note that (3.4.8) can be written as:*

$$\begin{aligned} W_1(t | x_0) &= \frac{1}{\sqrt{2\pi[1-\varrho^2(t)]}} \exp\left\{-\frac{[S(t) - x_0 \varrho(t)]^2}{2[1-\varrho^2(t)]}\right\} \\ &\quad \times \left\{ -\frac{1}{2} \left[\dot{S}(t) + \frac{\dot{\varrho}(t)[\varrho(t)S(t) - x_0]}{1-\varrho^2(t)} \right] \operatorname{Erfc}\left(\frac{\sigma(t | x_0)}{\sqrt{2}}\right) \right. \\ &\quad \left. + \frac{1}{2\pi} \sqrt{\frac{|\Lambda_3(t)|}{1-\varrho^2(t)}} \exp\left[-\frac{\sigma^2(t | x_0)}{2}\right] \right\}, \end{aligned} \quad (3.4.20)$$

with $x_0 < S(0)$, and where $|\Lambda_3(t)|$ and $\sigma(t | x_0)$ are given in (3.4.9). By virtue of assumptions (3.4.18) one has:

$$\lim_{\tau_c \rightarrow +\infty} \frac{|\Lambda_3(t)|}{1 - \varrho^2(t)} = 0, \tag{3.4.21}$$

$$\lim_{\tau_c \rightarrow +\infty} \left\{ \dot{S}(t) + \frac{\dot{\varrho}(t) [\varrho(t) S(t) - x_0]}{1 - \varrho^2(t)} \right\} = \dot{S}(t) - \frac{S(t) - x_0}{t}.$$

Furthermore, by noting that

$$\dot{S}(t) - \frac{S(t) - x_0}{t} < \dot{S}(t) - \frac{S(t) - S(0)}{t} \leq 0$$

and recalling (3.4.18), one is led to:

$$\lim_{\tau_c \rightarrow +\infty} \sigma(t | x_0) = -\infty. \tag{3.4.22}$$

Hence, due to (3.4.21) and (3.4.22), from (3.4.20) one obtains:

$$\lim_{\tau_c \rightarrow +\infty} W_1(t | x_0) = - \left[\dot{S}(t) - \frac{S(t) - x_0}{t} \right] \delta[S(t) - x_0], \tag{3.4.23}$$

where δ denotes the Dirac delta-function. Taking the limit as τ_c diverges in (3.4.16) and making use of (3.4.23), Eq. (3.4.19) immediately follows. \square

Remark 3.4.1 Under the assumptions of Proposition 3.4.1, if $\lim_{t \rightarrow +\infty} S(t) = -\infty$ one has:

$$\int_0^{+\infty} \varphi^{(\varepsilon)}(t) dt = 1. \tag{3.4.24}$$

Proof 3.4.2 Integrating both sides of (3.4.19) with respect to t in $(0, +\infty)$, we obtain:

$$\int_0^{+\infty} \varphi^{(\varepsilon)}(t) dt = - \int_{\mathcal{D}} \dot{S}(t) \gamma_\varepsilon[S(t)] dt,$$

where $\mathcal{D} = \{t : S(t) < S(0) - \varepsilon\}$. Hence, recalling (3.4.11), Eq. (3.4.24) immediately follows. \square

Remark 3.4.1 shows that as $\tau_c \rightarrow +\infty$ the ε -upcrossing probability that, eventually, $X(t)$ crosses $S(t)$ from below at least once is unit. Hence, as $\tau_c \rightarrow +\infty$ the ε -upcrossing probability that $X(t)$ ultimately crosses $S(t)$ for the first time is unit.

Proposition 3.4.2 Under the assumptions of Proposition 3.4.1, if $\lim_{t \rightarrow +\infty} S(t) = -\infty$ one has:

$$\lim_{\tau_c \rightarrow +\infty} g_u^{(\varepsilon)}(t) = \varphi^{(\varepsilon)}(t), \tag{3.4.25}$$

with $\varphi^{(\varepsilon)}(t)$ defined in (3.4.19).

Proof 3.4.3 Taking the limit as $\tau_c \rightarrow +\infty$ in (3.4.15), for all $\varepsilon > 0$ one has:

$$\varphi^{(\varepsilon)}(t) = h^{(\varepsilon)}(t) + \psi^{(\varepsilon)}(t), \quad (3.4.26)$$

where we have set:

$$h^{(\varepsilon)}(t) = \lim_{\tau_c \rightarrow +\infty} g_u^{(\varepsilon)}(t), \quad \psi^{(\varepsilon)}(t) = \lim_{\tau_c \rightarrow +\infty} \sum_{k=2}^{+\infty} q_k^{(\varepsilon)}(t). \quad (3.4.27)$$

Integrating both sides of (3.4.26) with respect to t between 0 and $+\infty$, and making use of Remark 3.4.1, one obtains:

$$\int_0^{+\infty} \psi^{(\varepsilon)}(t) dt = 0.$$

Hence, $\psi^{(\varepsilon)}(t) = 0$, so that (3.4.25) follows from (3.4.26). \square

3.4.2 Simulation results

In this Section, a simulation is used in order to disclose the essential features of the ε -upcrossing FPT pdf for a stationary Gaussian process $X(t)$ and for specified boundaries. Our approach relies on a simulation procedure by which sample paths of the stochastic process are constructed and their upcrossing first passage instants through the boundary are recorded in order to construct reliable histograms estimating the FPT pdf $\tilde{g}_u^{(\varepsilon)}(t)$. Specifically, for the construction of sample paths of the process $X(t)$ we have used the “conditional expectations method” and, to avoid numerical stability problems, we have implemented a regularization technique based on the so-called “doubled algorithm” (see, for instance, [69]). Since the sample paths of the simulated process are generated independently of one another, the simulation procedure is particularly suited for implementation on supercomputers. Hence, the related vector and parallel code has been implemented on an IBM SP-Power4 machine. To evaluate the ε -upcrossing FPT densities, we have chosen X_0 randomly according to the initial pdf $\gamma_\varepsilon(x_0)$. To this purpose, we have made use of the so-called acceptance-rejection method (cf. for instance [78]).

We now consider two stationary Gaussian processes such that the assumptions on the correlation function of Proposition 3.4.1 are satisfied.

(i) Let $\{X_1(t), t \geq 0\}$ be a stationary Gaussian process with zero mean, unit variance and correlation function:

$$\varrho(t) = e^{-\alpha|t|} \left\{ \cos(\alpha \omega t) + \frac{1}{\omega} \sin(\alpha \omega |t|) \right\} \quad (t \in \mathbb{R}) \quad (3.4.28)$$

where $\alpha > 0$ and $\omega \in \mathbb{R}$. Since

$$\begin{aligned} \dot{\varrho}(t) &= -\frac{1+\omega^2}{\omega} \alpha e^{-\alpha|t|} \sin(\alpha \omega t), \\ \ddot{\varrho}(t) &= \frac{1+\omega^2}{\omega} \alpha^2 e^{-\alpha|t|} \left\{ \sin(\alpha \omega |t|) - \omega \cos(\alpha \omega t) \right\}, \end{aligned}$$

one has $\varrho(0) = 1$, $\dot{\varrho}(0) = 0$ and $\ddot{\varrho}(0) = -\alpha^2(1+\omega^2) < 0$, so that the process $X_1(t)$ is mean-square differentiable. Furthermore, the correlation time of $X_1(t)$ is:

$$\tau_c = \frac{2}{\alpha(1+\omega^2)}. \quad (3.4.29)$$

Hence, $\tau_c \rightarrow +\infty$ if and only if $\alpha \rightarrow 0$. It is easily proved that (3.4.18) hold as $\alpha \rightarrow 0$.

(ii) Let $\{X_2(t), t \geq 0\}$ be a stationary Gaussian process with zero mean, unit variance and correlation function:

$$\varrho(t) = \frac{1}{1 + \beta t^2} \quad (t \in \mathbb{R}) \quad (3.4.30)$$

with $\beta > 0$. Since

$$\begin{aligned} \dot{\varrho}(t) &= -\frac{2\beta t}{(1 + \beta t^2)^2}, \\ \ddot{\varrho}(t) &= -\frac{2\beta(1 - 3\beta t^2)}{(1 + \beta t^2)^3}, \end{aligned}$$

one has $\varrho(0) = 1$, $\dot{\varrho}(0) = 0$ and $\ddot{\varrho}(0) = -2\beta < 0$, so that $X_2(t)$ is mean-square differentiable. Furthermore, the correlation time of $X_2(t)$ is:

$$\tau_c = \frac{\pi}{2\sqrt{\beta}}. \quad (3.4.31)$$

Hence, $\tau_c \rightarrow +\infty$ if and only if $\beta \rightarrow 0$. One can easily prove that (3.4.18) hold as $\beta \rightarrow 0$.

In Fig. 3.16(a) the correlation function (3.4.28) is plotted for $\omega = 1$ and for $\alpha = 0.1, 0.5, 1, 2$, whereas in Fig. 3.16(b) the correlation function (3.4.30) is plotted for $\beta = 0.1, 0.5, 1, 2$,

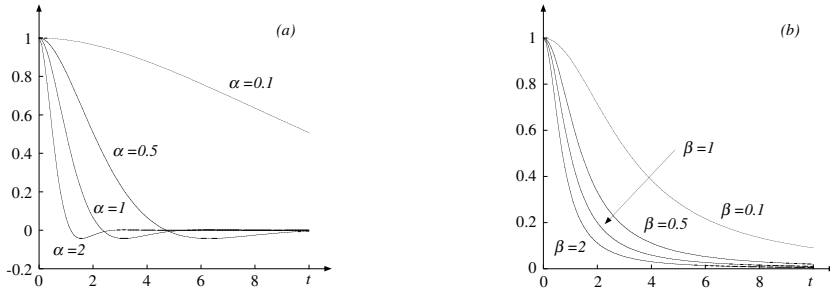


Figure 3.16: Plot of correlation function (3.4.28) in (a) and of correlation function (3.4.30) in (b) as function of t . Figure (a) refers to the case $\omega = 1$ and $\alpha = 0.1, 0.5, 1, 2$; Figure (b) refers to the case $\beta = 0.1, 0.5, 1, 2$.

For both processes $X_1(t)$ and $X_2(t)$, if $S(t)$ is an arbitrary monotonically decreasing function such that (1) $\dot{S}(t) - [S(t) - S(0)]/t \leq 0$ and (2) $\lim_{t \rightarrow +\infty} S(t) = -\infty$, then (3.4.25) holds. For instance, if $S(t) = at + b$ ($a < 0; b \in \mathbb{R}$) conditions (1) and (2) are satisfied, whereas if $S(t) = at^2 + bt + c$ ($a \neq 0; b, c \in \mathbb{R}$) conditions (1) and (2) are satisfied if and only if $a < 0$ and $b < 0$. Furthermore, if $S(t) = ae^{bt}$ ($a, b \in \mathbb{R}$) conditions (1) and (2) hold if and only if $a < 0$ and $b > 0$.

By making use of simulation procedure, we have performed extensive computations on processes $X_1(t)$ and $X_2(t)$ to disclose the behavior of the ε -upcrossing FPT pdf through time-dependent boundaries for large correlation times. The results of the simulations have indicated that $\tilde{g}_u^{(\varepsilon)}(t)$ is susceptible of an excellent approximation for large τ_c . Indeed, under the assumption of Proposition 3.4.2, for large τ_c the following asymptotic relation holds:

$$g_u^{(\varepsilon)}(t) \simeq W_1^{(\varepsilon)}(t) \quad (t > 0), \quad (3.4.32)$$

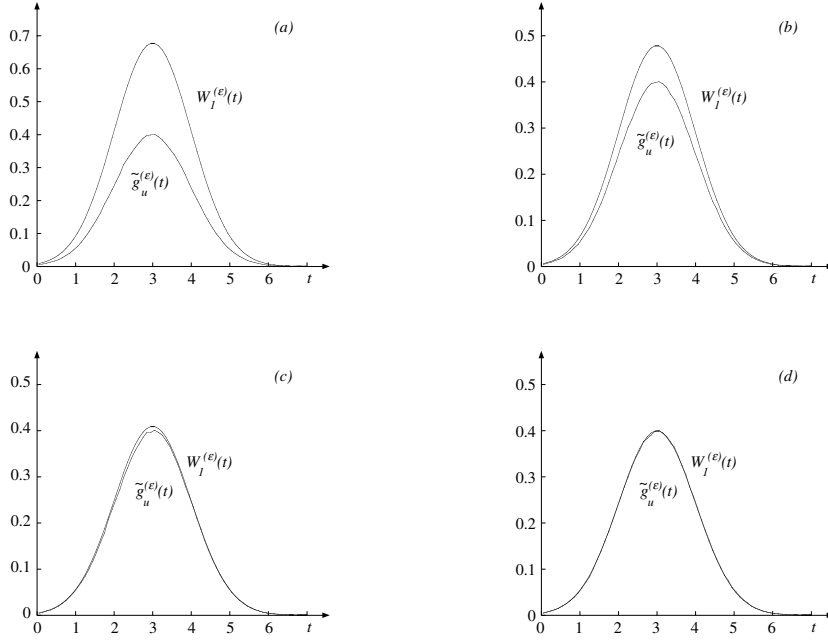


Figure 3.17: Plot of $\tilde{g}_u^{(\varepsilon)}(t)$ and of $W_1^{(\varepsilon)}(t)$ for the Gaussian process with zero mean, unit variance and correlation function (3.4.28) for $S(t) = 3 - t$, $\varepsilon = 0.01$ and $\omega = 1$ in the following cases: (a) $\alpha = 2$, (b) $\alpha = 1$, (c) $\alpha = 0.5$ and (d) $\alpha = 0.1$.

where $W_1^{(\varepsilon)}(t)$, that provides an upper bound for the ε -upcrossing FPT pdf, is given in (3.4.16). This is clearly indicated in Fig. 3.17 and in Fig. 3.18 in which $S(t) = 3 - t$. Indeed, for the Gaussian process $X_1(t)$, in Fig. 3.17 the simulated function $\tilde{g}_u^{(\varepsilon)}(t)$ is compared with $W_1^{(\varepsilon)}(t)$ for $\alpha = 2$ in (a), $\alpha = 1$ in (b), $\alpha = 0.5$ in (c) and $\alpha = 0.1$ in (d), by setting $\varepsilon = 0.01$ and $\omega = 1$. We note that already for $\alpha = 0.1$ (cf. Fig. 3.17(d)) $W_1^{(\varepsilon)}(t)$ provides a good approximation of the simulated ε -upcrossing FPT pdf. Furthermore, Proposition 3.4.1 indicates that $W_1^{(\varepsilon)}(t) \simeq \varphi^{(\varepsilon)}(t)$ for large τ_c , so that $g_u^{(\varepsilon)}(t) \simeq \varphi^{(\varepsilon)}(t)$ for all α such that $0 < \alpha < 0.1$. Instead, for the Gaussian process $X_2(t)$, in Fig. 3.18 the simulated function $\tilde{g}_u^{(\varepsilon)}(t)$ is compared with $W_1^{(\varepsilon)}(t)$ for $\beta = 2$ in (a), $\beta = 1$ in (b), $\beta = 0.5$ in (c) and $\beta = 0.1$ in (d), by setting $\varepsilon = 0.01$. As Fig. 3.18(d) shows, already for $\beta = 0.1$, $W_1^{(\varepsilon)}(t)$ provides a good approximation of $\tilde{g}_u^{(\varepsilon)}(t)$. Hence, $g_u^{(\varepsilon)}(t) \simeq \varphi^{(\varepsilon)}(t)$ for all β such that $0 < \beta < 0.1$.

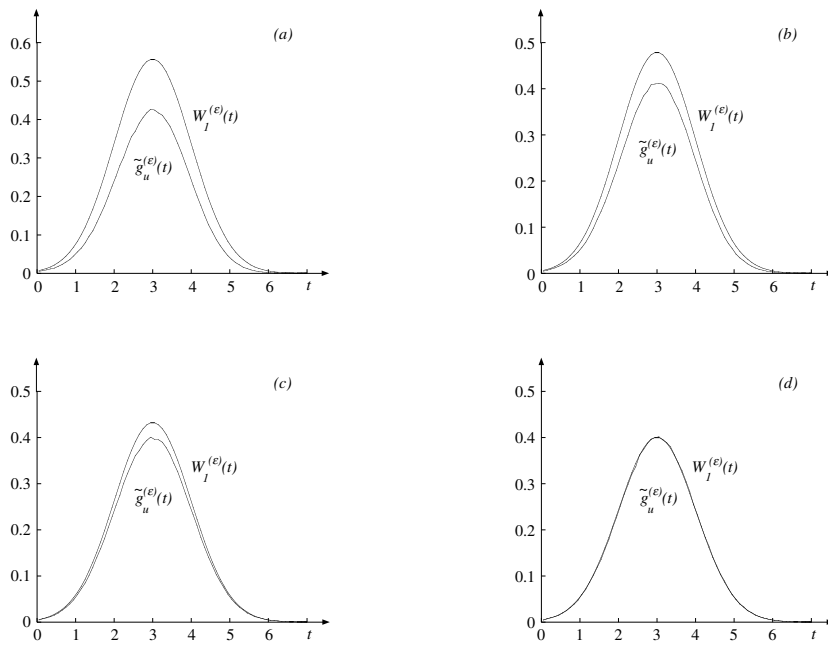


Figure 3.18: Plot of $\tilde{g}_u^{(\epsilon)}(t)$ and of $W_1^{(\epsilon)}(t)$ for the Gaussian process with zero mean, unit variance and correlation function (3.4.30) for $S(t) = 3 - t$, and $\epsilon = 0.01$ in the following cases: (a) $\beta = 2$, (b) $\beta = 1$, (c) $\beta = 0.5$ and (d) $\beta = 0.1$.

Chapter 4

Auxiliary results

4.1 An algorithm for data samples representation

In the descriptive statistic, the *classification methods* are employed for dividing a data sample in cells. Cell grouping is one of the most important and special sector of statistical research. In this field we find the theory of *density estimation* ([92], [84]). If we observe a data sample from a random variable with an unknown density function $f(x)$, the density estimation purpose will be the construction of a function approximating the density function by sampling data. The histogram function is the oldest density estimator (see e.g. [85]). The choice of cell grouping methods is the main problem for the histogram construction, because we lose a part of information on the sample by this procedure. Since we look for a synthetic view of known data, we cannot evaluate all available information. Anyway, there is not a perfect rule by which we could conclude that our deductions from histogram are exact. Nevertheless it is possible to change the choice of the cells so that we could find a better approximation. Generally one prefers dividing the sample range into intervals with the same length (method of equal cell widths). But if we could formulate an hypothesis about the distribution of the random sample, we could also fix cells in which the probability of a data belonging from each of this is equal (method of equal probability cells). There are also other methods: some are more near the cluster analysis (see e.g. [47]), like, for example, the method of natural cells, proposed by Mineo in [60].

We proposed here the RANDOM algorithm ([18]). It constructs histograms of data samples in which the location of the cells is determined by a preassigned fixed number of sample elements. This procedure is substantially innovative with respect to the construction of histograms with equal cell widths [84]. Being based on a different method for choosing histogram cells, it requires only the specification of the number of cells.

We give an outline of the adopted method and analyze its running time. Then we discuss some statistical results obtained by the use of RANDOM and of the standard method of equal cell widths. The statistical analysis of data sample relies on the use of pseudo-random number generators ([52]). Finally, some concluding remarks on the use of RANDOM algorithm are given.

4.1.1 Description of the Random Algorithm

Given an unordered random data sample x_1, x_2, \dots, x_n of size n , we consider the first m ordered data $y_1 < y_2 < \dots < y_m$ and the intervals

$$I_i = (y_i, y_{i+1}) \quad i = 1, 2, \dots, m-1.$$

The middle points

$$z_{i+1} = \frac{y_i + y_{i+1}}{2} \quad i = 1, 2, \dots, m-1$$

of the intervals I_i are the end points of the cells K_i used for the histogram's construction:

$$\begin{aligned} K_1 &=]z_1, z_2], \quad \text{with } z_1 = y_1 + (y_1 - z_2) = 2y_1 - z_2 \\ K_i &=]z_i, z_{i+1}], \quad \text{for } i = 2, 3, \dots, m-1 \\ K_m &=]z_m, z_{m+1}], \quad \text{with } z_{m+1} = y_m + (y_m - z_m) = 2y_m - z_m. \end{aligned}$$

In order to describe the entire data sample and to achieve an estimation of the order of magnitude of its elements, we add two more cells in which the minimum α and the maximum β of the data sample represent the left-hand point of the first cell and the right-hand point of the last cell, respectively

$$K_0 =]\alpha, z_1] \quad K_{m+1} =]z_{m+1}, \beta].$$

It should be emphasized that α and β do not have any direct influence on the cell construction, in the sense that they do not play any role in the specification of the cell width. The addition of the above two intervals is required for the description of the tails of histogram. After the specification of the cells, the number of data falling in each cell is recorded. The algorithm yields two output arrays: the first array includes the cell end points, and the second array includes the ratio of the sample frequencies in each cell over the cell width. The main steps of RANDOM are listed hereafter.

Scheme of the RANDOM algorithm

- R1 . Set $y(i) = x(i)$ for $i = 1, 2, \dots, m$.
- R2 . Sorting the array y by increasing order. [Average running time: $O(m \cdot \log m)$ ([53])].
- R3 . [Construction of the cell end points] Set

$$\begin{aligned} z(1) &= \frac{3 \cdot y(1) - y(2)}{2} \\ z(i+1) &= \frac{y(i) + y(i+1)}{2} \quad i = 1, 2, \dots, m-1 \\ z(m+1) &= \frac{3 \cdot y(m) - y(m-1)}{2}. \end{aligned}$$

- R4 . Find sample maximum and minimum. [Average running time: $O(n)$ ([53])].
- R5 . [Frequencies counting] Set

$$\begin{aligned}
f(0) &= \frac{|\{x(k) : x(k) < z(1), k = 1, \dots, n\}|}{n \cdot [z(1) - \alpha]} \\
f(j) &= \frac{|\{x(k) : z(j) \leq x(k) < z(j+1), j = 1, \dots, m; k = 1, \dots, n\}|}{n \cdot [z(j+1) - z(j)]} \\
&\qquad\qquad\qquad (j = 1, 2, \dots, m) \\
f(m+1) &= \frac{|\{x(k) : x(k) \geq z(m+1), k = 1, \dots, n\}|}{n \cdot [\beta - z(m+1)]}
\end{aligned}$$

For step R5 the uniform binary searching algorithm with two pointers, which is sketched below, has been implemented.

Uniform binary searching algorithm

- B1 . Set $i = 1$.
- B2 . If $i = n$, go to B11: the algorithm terminates.
- B3 . If $x(i) < z(1)$ set $cnt(1) = cnt(1) + 1$;
otherwise if $x(i) > z(m+1)$ set $cnt(m+2) = cnt(m+2) + 1$.
- B4 . Set $Initial = 1$, $Final = m+1$, $Mid = (Initial + Final)/2$.
- B5 . [Test] If $(Final - Initial) \leq 1$ go to B10.
- B6 . If $x(i) < z(Mid)$, set $Final = Mid$; if $x(i) > z(Mid)$, set $Initial = Mid$.
- B7 . If $x(i) = z(Mid)$, go to B9.
- B8 . Go to B5.
- B9 . Set $cnt(Final) = cnt(Final) + 1$.
- B10 . Set $i = i + 1$ and go to B2. [Average running time: $O(n \cdot \log m)$].
- B11 . Carry out

$$\begin{array}{ll}
\alpha, z(1), z(2), \dots, z(m+1), \beta & \text{(cell end points for the histogram)} \\
f(0), f(1), \dots, f(m), f(m+1) & \text{(frequencies over the cells widths).}
\end{array}$$

The overall average running time of the algorithm RANDOM is thus $O(n \cdot \log m)$.

4.1.2 Statistical tests to verify the RANDOM rule

A FORTRAN 77 code for the implementation of algorithm RANDOM has been realized. The data samples have been generated by pseudo-random number routines of the NAG library. We have tested the RANDOM rule by means of 10^5 -size pseudorandom numbers from normal, uniform in $(0, 1)$, exponential with parameter 1 and chi-square (with 5 freedom degrees) distributions. The histograms, constructed by means of RANDOM, provide a good graphic approximation of such densities.

As a statistical check of the results, achieved by RANDOM, a chi-square hypothesis test ([11]) and Kolmogorov-Smirnov test for grouped data ([11, 70]) have been performed. The cell number $2n^{2/5}$ is customarily indicated for the chi-square test, which in our case led to 200 cells for a 10^5 -size sample. However, we have also made use of some other values.

Chi-square test

In the chi-square test, it is necessary to divide the random sample range in m cells to check the H_0 hypothesis. We call n_i the number of observed data in the i -th cell and p_i the probability of a data belonging to the i -th cell when the null hypothesis is true for $i = 1, 2, \dots, m$.

The Pearson statistic is:

$$\chi_n^2 = \sum_{i=1}^m \left(\frac{n_i - np_i}{\sqrt{np_i}} \right)^2. \quad (4.1.1)$$

Generally in order to reject the H_0 hypothesis, the significativity level is fixed to 0.05 or 0.01. In this case, since we fixed a priori the pseudo-random sample distribution, we evaluate the critical level, i.e. the probability that the random variable χ^2 has a greater value than the statistic χ_n^2 calculated numerically by (4.1.1). In this way the chi-square test allows to compare the histogram function, built on the chosen cells, with the theoretical density function, by measuring the fitting degree of the first one. The chi-square test has been made for the grouping RANDOM method and for the grouping method in equal cell widths.

Since the medium value of the chi-square random variable is equal to the cell number reduced by one, from the tables it is possible to deduce that the statistic χ_n^2 approximates its medium value better with the grouping random rule than the equal cell widths grouping. Moreover we observe that after 150 cells, in the random case the critical level is always greater than that in the equal cell widths. This observation confirms the right result of the chi-square test for the chosen rule. Let us note that for the random rule in χ^2 -test it is not necessary any particular choice for the cell number, as it appears in Mann and Wald ([59]).

Some other considerations are made for the exponential random sample distribution with parameter 1. The χ^2 -test, employed with equal cell width grouping, does not reject the null hypothesis only if the thumb rule is adopted. This technique is not necessary for the random sample grouping (see Table 4.3).

In none of the analyzed cases is the hypothesis rejected when RANDOM is used. The same test has also been performed for the cases of equal-width cells. Tables 4.1-4.4 give the χ_n^2 statistics, estimated from the sample, and the probability that the χ^2 estimator is greater than the χ_n^2 statistics for various cell numbers. Table 4.1 refers to a sample taken from a standard normal distribution, Table 4.2 lists the results obtained for a sample generated by means of a uniform distribution over the interval (0,1). Columns 2 and 3 report the χ^2 test results for the case of algorithm RANDOM, and columns 4 and 5 list the corresponding results for the equal-width case. Table 4.3 lists the results obtained for a sample generated by means of an exponential distribution with parameter 1: the results are specified for the case of equal width cells using the thumb rule and when the thumb rule is not used. Finally, the Table 4.4 shows results for a chi-square distribution sample.

Algorithm RANDOM is designed to construct histograms with unequal cell widths. In such a way one can use narrower cells in the regions where density of data is higher and wider cells where the data appear to be more sparse. Hence, not only frequencies but also cell widths characterize the sample distribution.

Although, as in the case of equal cell widths, RANDOM requires a priori specification of the number of cells for the histogram construction, the specification of classes K_1, K_2, \dots, K_m is made possible as soon as the first m sample data are given, without need to inspect the whole sample. Therefore, the choice of the cells takes place after a number of observations that in general is much smaller than the sample size. This appears to be particularly useful

<i>N(0,1)</i>				
	<i>RANDOM</i>		<i>Equal width</i>	
<i>cells number</i>	χ^2_n	$P(\chi^2 > \chi^2_n)$	χ^2_n	$P(\chi^2 > \chi^2_n)$
50	66.4453	0.0490	42.9888	0.2857
100	108.5469	0.2404	106.1527	0.2933
150	162.6406	0.2102	179.0475	0.0470
200	210.1172	0.2807	242.3425	0.0194
300	290.7969	0.6221	347.1316	0.0288
400	391.3828	0.5978	419.1739	0.2339

Table 4.1: Results of χ^2 -test for a normal distribution sample

<i>Uniform in (0,1)</i>				
	<i>RANDOM</i>		<i>Equal width</i>	
<i>cells number</i>	χ^2_n	$P(\chi^2 > \chi^2_n)$	χ^2_n	$P(\chi^2 > \chi^2_n)$
50	61.6328	0.1062	55.5131	0.2427
100	116.9922	0.1047	115.4379	0.1238
150	179.8438	0.0432	156.5202	0.3202
200	220.9609	0.1365	226.4800	0.0882
300	314.5547	0.2570	333.5806	0.0822
400	428.3203	0.1498	403.9240	0.4218

Table 4.2: Results of χ^2 -test for an uniform distribution sample

for statistical observations on sample data occurring over long periods of time: by recording an initial part of the incoming data one is led to specify the histogram cells and hence launch the histogram construction procedure without any further action. All this is greatly advantageous over the standard procedure based on equal cell widths, whereby the whole sample must be recorded in order to specify cell widths on the basis of the observed smallest and largest sample data.

Kolmogorov-Smirnov test for grouped data

The Kolmogorov-Smirnov statistic, usually called D , is used for testing the hypothesis according to which a random sample comes from a fixed discrete distribution (see e.g. [86]). Pettitt and Stephens ([70]) defined the analogous statistic for grouping data with continuous distribution.

Be k the cell number and p_i the probability of a data belonging to the i -th cell. We indicate with $e_i = np_i$ the expected number of the i -th cell observations and with n_i the absolute

<i>Exponential with parameter 1</i>						
	<i>RANDOM</i>		<i>Equal width (thumb rule)</i>		<i>Equal width (no thumb rule)</i>	
<i>cells</i>	χ^2_n	$P(\chi^2 > \chi^2_n)$	χ^2_n	$P(\chi^2 > \chi^2_n)$	χ^2_n	$P(\chi^2 > \chi^2_n)$
50	61.5312	0.1079	80.0565	3.359-E03	34.0543	0.9483
100	116.9844	0.1047	158.4693	1.382-E04	59.7499	0.9993
150	176.6328	0.0606	253.4255	2.036-E07	91.2264	0.9999
200	218.6719	0.1614	340.2742	1.739-E09	113.7131	0.9999
300	312.0938	0.2894	501.4445	1.817-E09	146.7343	0.9999
400	428.5234	0.1482	694.1066	3.909-E18	198.8663	0.9999

Table 4.3: Results of χ^2 -test for an exponential distribution sample

<i>chi-square with 5 freedom degrees</i>				
	<i>RANDOM</i>		<i>Equal width</i>	
<i>cells number</i>	χ^2_n	$P(\chi^2 > \chi^2_n)$	χ^2_n	$P(\chi^2 > \chi^2_n)$
50	46.0781	0.5923	42.9270	0.7165
100	114.2656	0.1399	90.4564	0.7183
150	170.4688	0.1099	169.0036	0.1253
200	225.2969	0.0297	231.8755	0.0550
300	314.8047	0.2538	332.3705	0.0894
400	402.2500	0.4449	469.9254	0.0082

Table 4.4: Results of χ^2 -test for a chi-square distribution sample

$N(0,1)$			
<i>cells</i>	<i>RANDOM</i>	<i>Equal width</i>	<i>Equal probability</i>
100	132.9808	124.5460	133.0000
150	132.9808	131.0362	132.9987
200	139.2207	124.5460	137.0000
300	138.9666	131.0359	132.9991
400	138.9666	138.4010	137.0000

Table 4.5: Results of Kolmogorov-Sminorv test for a normal distribution sample

observed frequencies. If y_1, y_2, \dots, y_{k+1} are the endpoints of the given cells, let:

$$F_n(y) = \begin{cases} 0 & \text{for } y < y_1 \\ \sum_{i=1}^j \frac{n_i}{n} & \text{for } y_j \leq y < y_{j+1} \text{ for } j = 1, \dots, k \\ 1 & \text{for } y > y_{k+1} \end{cases} \quad (4.1.2)$$

is the cumulated distribution function of the histogram related to the observed data and let

$$F_r(y) = \begin{cases} 0 & \text{for } y < y_1 \\ \sum_{i=1}^j \frac{e_i}{n} & \text{for } y_j \leq y < y_{j+1} \text{ for } j = 1, \dots, k \\ 1 & \text{for } y > y_{k+1} \end{cases} \quad (4.1.3)$$

is the cumulated distribution function for grouped data.

The Kolmogorov-Smirnov statistic for grouping data is:

$$S = \max_{1 \leq j \leq k} \left| \sum_{i=1}^j (n_i - e_i) \right|. \quad (4.1.4)$$

The statistic (4.1.4) allows to compare the empirical distribution function (4.1.2) with the theoretical one in (4.1.3), both defined for a fixed grouping. The test has a good power when the grouping is made with equal probability cells (see e.g. [39]). For this reason, it is necessary to compare the value of S obtained by taking equal probability cells with that obtained for equal cells widths and for random cells. In the sequel, we give the tables of the results.

Let us observe that the computation of statistic S does not require more than 5 observed data in each cell, differently from the χ^2 -test. This requirement is very advantageous for densities with shape very similar to the exponential one.

By Tables 4.5-4.8 we do not see very different behavior between the statistic values calculated for random cells, for equal cell widths and for equal probability cells.

<i>Uniform in (0,1)</i>			
<i>cells</i>	<i>RANDOM</i>	<i>Equal width</i>	<i>Equal probability</i>
100	198.3109	235.9438	236.0000
150	227.6627	235.9462	236.0012
200	227.6627	235.9438	236.0000
300	238.1205	235.9462	236.0012
400	240.3350	235.9438	236.0000

Table 4.6: Results of Kolmogorov-Sminorv test for an uniform distribution sample

<i>Exponential with parameter 1</i>			
<i>cells</i>	<i>RANDOM</i>	<i>Equal width</i>	<i>Equal probability</i>
100	192.5839	147.7309	236.0000
150	227.7742	192.2722	235.9981
200	238.1558	237.2067	236.0000
300	240.6874	192.2722	235.9981
400	240.6874	229.4807	236.0000

Table 4.7: Results of Kolmogorov-Sminorv test for an exponential distribution sample

<i>chi-square with 5 freedom degrees</i>			
<i>cells</i>	<i>RANDOM</i>	<i>Equal width</i>	<i>Equal probability</i>
100	187.3853	200.6175	202.0000
150	187.3853	209.9221	205.6688
200	209.7770	200.6184	211.0000
300	215.3498	209.9230	208.3356
400	209.5713	207.0301	216.0000

Table 4.8: Results of Kolmogorov-Sminorv test for a chi-square distribution sample

4.1.3 Modified RANDOM rule

In [19] the Random rule is tested by samples of numerically generated (distinct) data. After the reliability of Random rule has been proved, we have applied it on samples of data whose density function was unknown. More specifically, we have constructed histograms with random cells for simulated times of the first passage of 10^5 sample paths of a stationary Gaussian process characterized by a covariance function with damped oscillations (3.2.41), and for a constant threshold. In this case the samples consist of data that are not all distinct. In such a case, the Random algorithm, originally devised for distinct data, has been suitably modified. It now may build a number of histogram cells less than that required in input. For instance, if 100 cells are required, the algorithm chooses the first k (< 100) separate elements among the first 100, that are those present once in the initial subsample, and it constructs k cells centred in these k points. This algorithm is denoted as the Modified Random rule with Unknown number of cells, the MRU rule for short. Alternatively, we have also implemented the Random rule choosing the first 100 data that have a frequency greater than or equal to 2 (we call this algorithm Modified Random rule with Fixed number of cells, i.e. MRF rule). In this way, we were able to take note of the changes in the density histogram for different choices of number of cells. To this end, we have carried out simulations for the specified processes and we have applied both modified Random rules to the array of the simulated first passage times. The histograms thus obtained are shown in the Figures 4.9-4.20 and each of them is compared with the histograms obtained by applying the equal width cells rule. The graphs were constructed by resorting to Matlab tools. We can draw the following conclusions:

1. the Random Rule, in its both variants, appears to be more stable than that for the equal width cells, in the sense that with a smaller number of cells it provides a good approximation of the density, which is not significantly affected by a class number increase;
2. the results obtained by applying the modified versions of Random rule, MRU and MRF, show that the MRU provides a more detailed approximation than that available by applying the MRF criterion. The reason is that the first k most frequent data belong to high density areas, and the MRF criterion yields a discrete approximation that is good in such areas but rather poor in low probability areas.

4.1.4 Comparing histograms

In the following Figures histograms for data sample of 10^5 size from assigned probability distributions are plotted. For each data sample 3 histograms are constructed: by 100 RANDOM cells, by 100 equal width cells and by 100 equal probability cells.

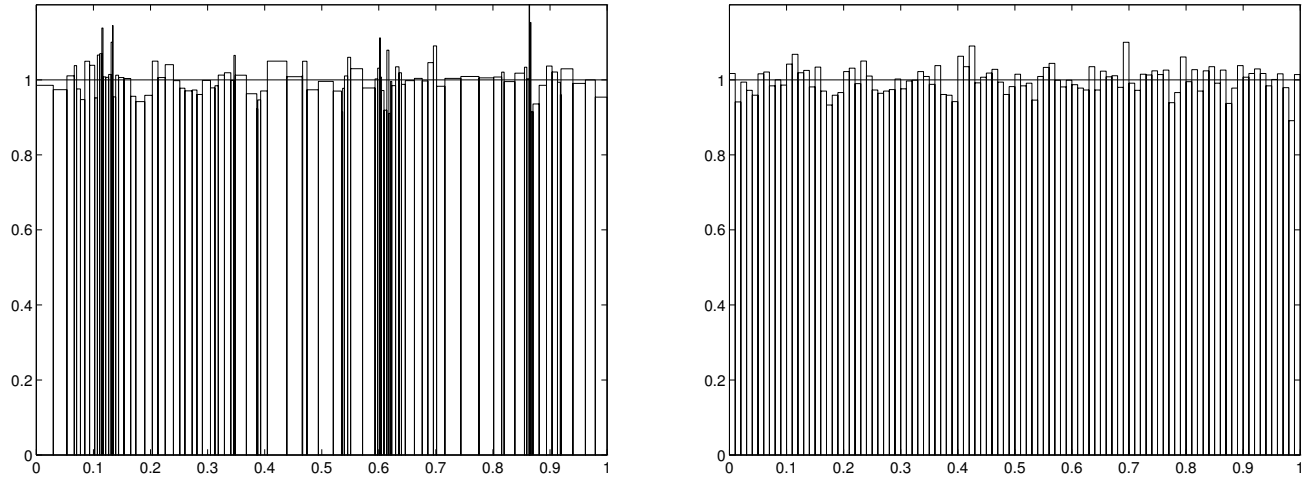


Figure 4.1: Uniform sample. On left: RANDOM cells. On right: equal width cells

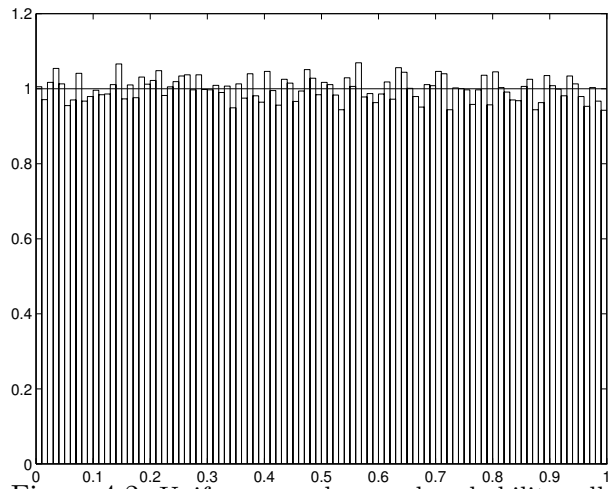


Figure 4.2: Uniform sample: equal probability cells

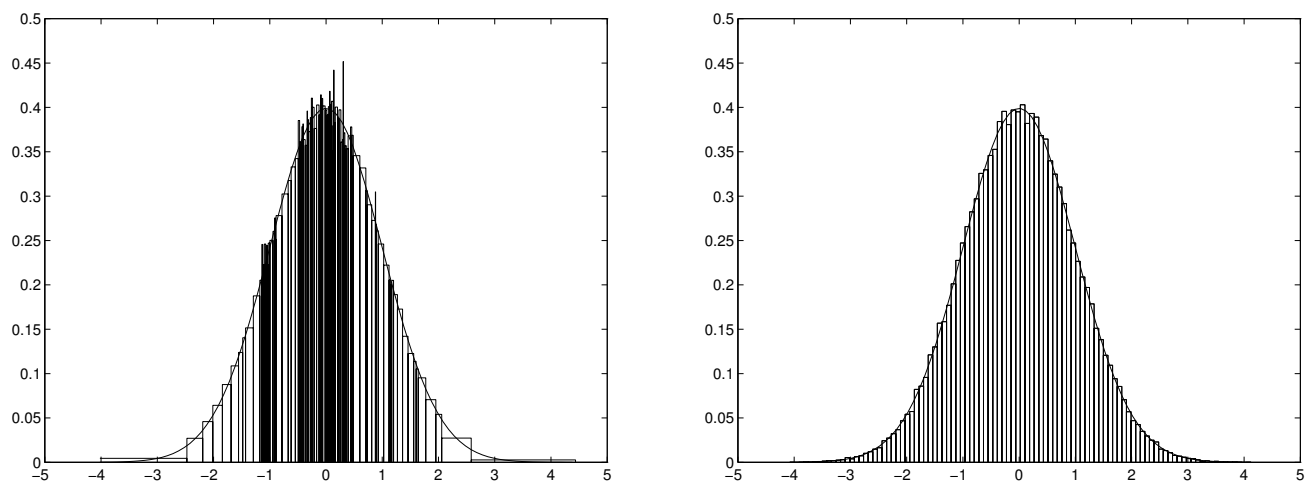


Figure 4.3: Normal sample. On left: RANDOM cells. On right: equal width cells

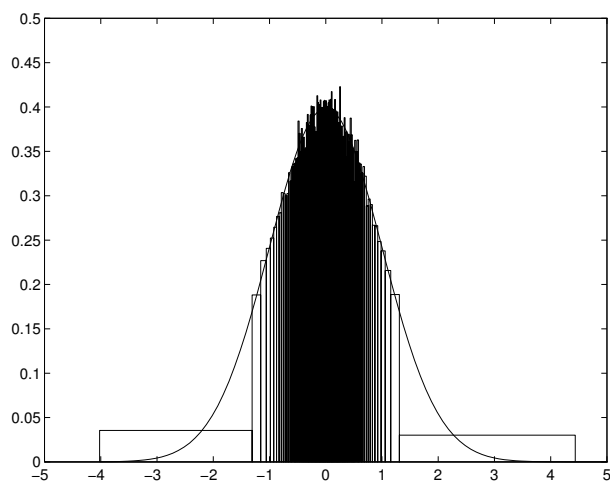


Figure 4.4: Normal sample: equal probability cells

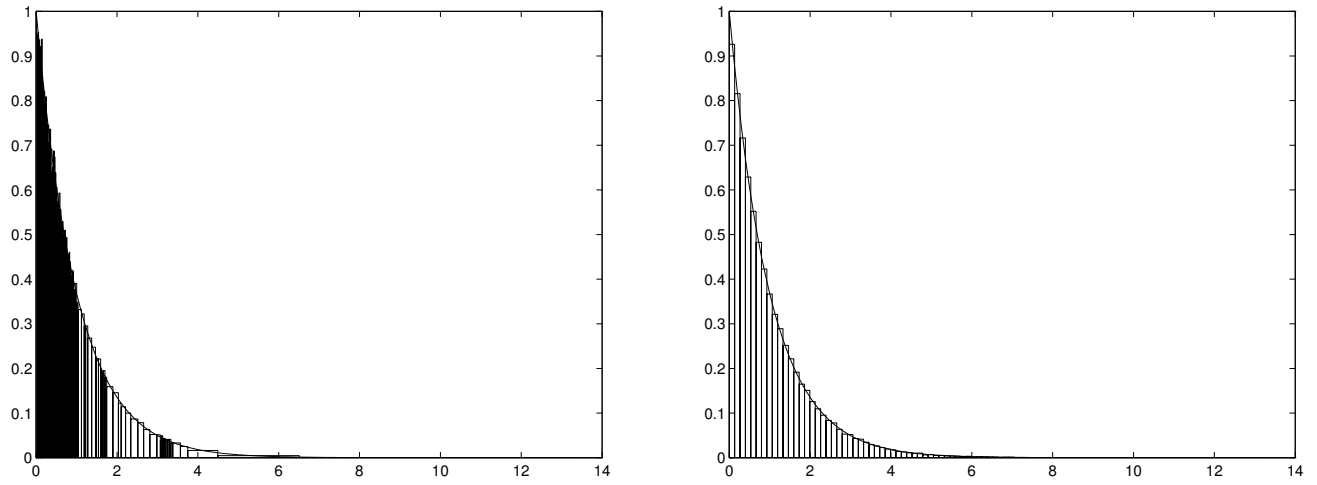


Figure 4.5: Exponential(1) sample. On left: RANDOM cells. On right: equal width cells

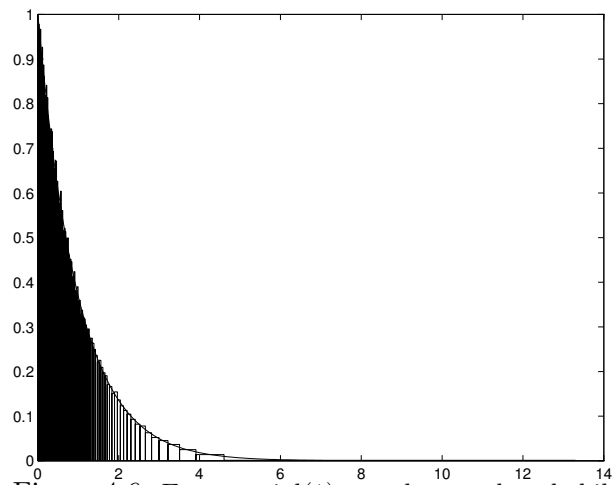


Figure 4.6: Exponential(1) sample: equal probability cells

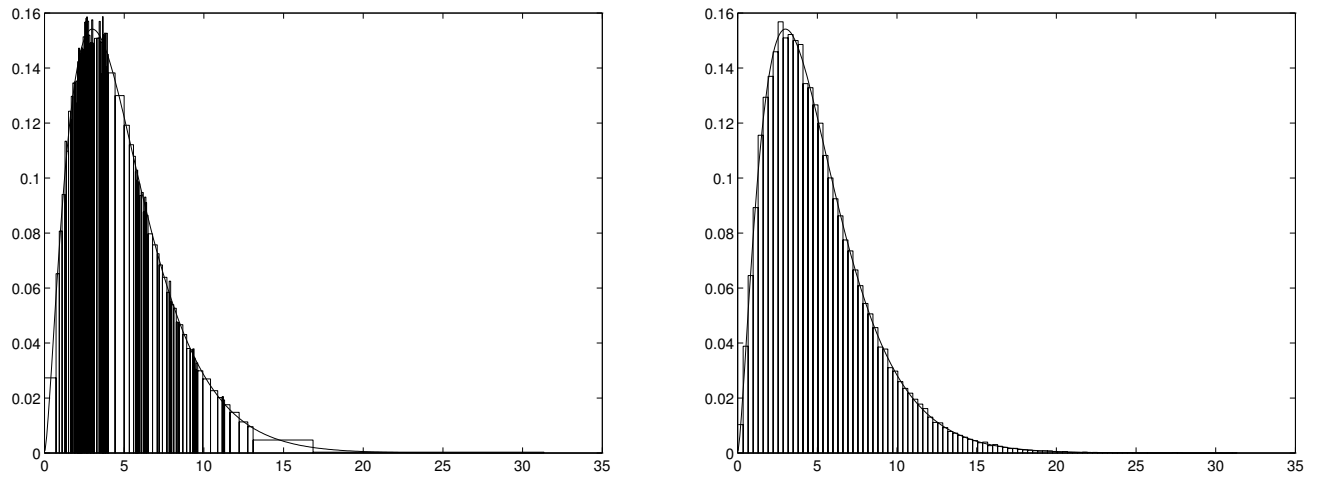


Figure 4.7: Chi-square(5) sample. On left: RANDOM cells. On right: equal width cells

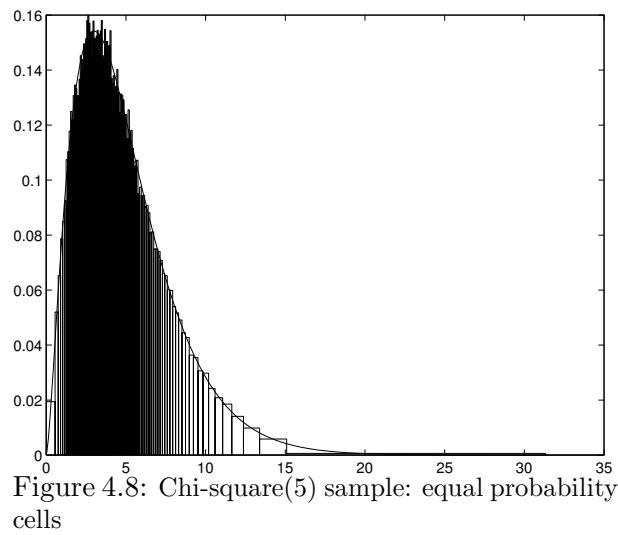


Figure 4.8: Chi-square(5) sample: equal probability cells

In particular, in Figures 4.9 and 4.10 the histograms by MRU and MRF rules, and by equal width cell (EWC) rules are plotted. At first algorithm MRU rule has been implemented, and 39 distinct elements in the first 200 data have been found. Consequently, also in the other 2 cases (by MRF and EWC rules), histograms with 39 cells had to be constructed. The covariance function (3.2.41) contains the parameters $\alpha = 1.0$ and $\beta = 1.0$ and the barrier is set equal to 1. In Figures 4.11-4.14 are listed three graphs: the first is the histogram constructed with the MRU rule, the second one depicts the histogram with cells obtained by MRF rule and the third one shows the EWC histogram.

The number of classes is set as described above, and therefore it varies from case to case. The barrier is constant, while the parameters α and β of the covariance function are specified for each figure.

As further investigations, we have constructed histograms with different numbers of cells in order to verify if the shape of the approximated density would vary as the number of cells increases. Our numerous simulations have led us to the conclusion that the number of the histogram cells required by applying MRU rule is the number of cells sufficient to provide a satisfactory representation of the density. Indeed its shape does not undergo significant changes as the number of cells varies. In the Figures 4.15-4.20, for these three Rules, histograms with 100 cells are finally shown.

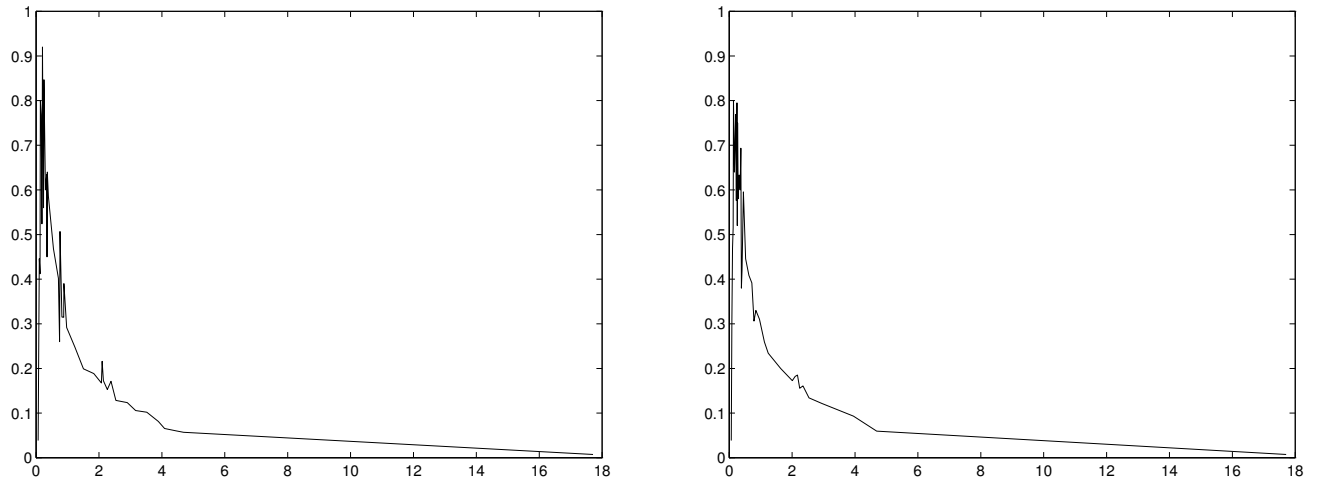


Figure 4.9: Number of cells = 39, $\alpha = 1.0$, $\beta = 1.0$. On left: MRU cells. On right: MRF cells.

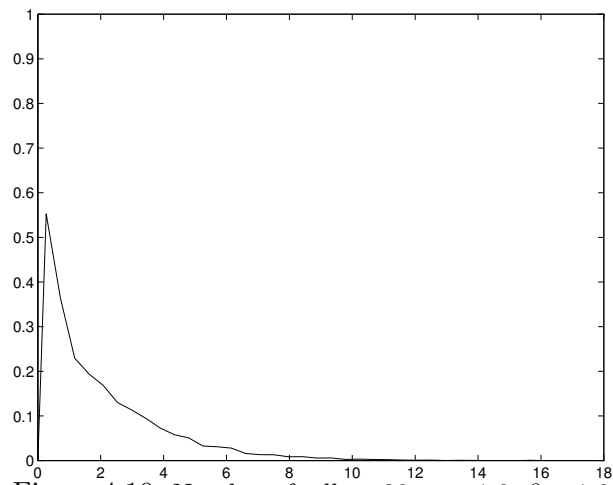


Figure 4.10: Number of cells = 39, $\alpha = 1.0$, $\beta = 1.0$. Equal width cells.

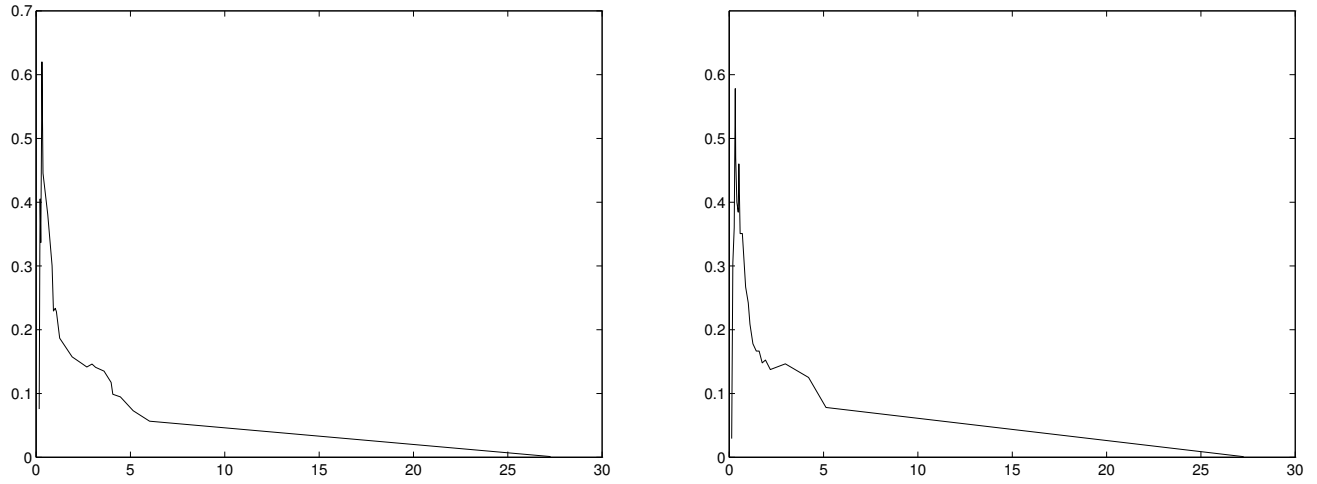


Figure 4.11: Number of cells = 24, $\alpha = 1.0$, $\beta = 0.5$. On left: MRU cells. On right: MRF cells.

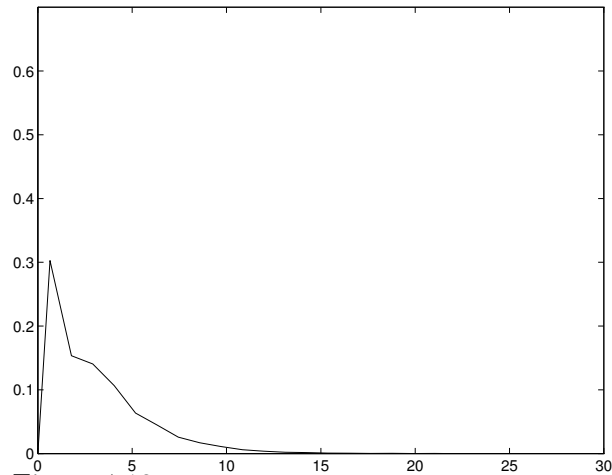


Figure 4.12: Number of cells = 24, $\alpha = 1.0$, $\beta = 0.5$. Equal width cells.

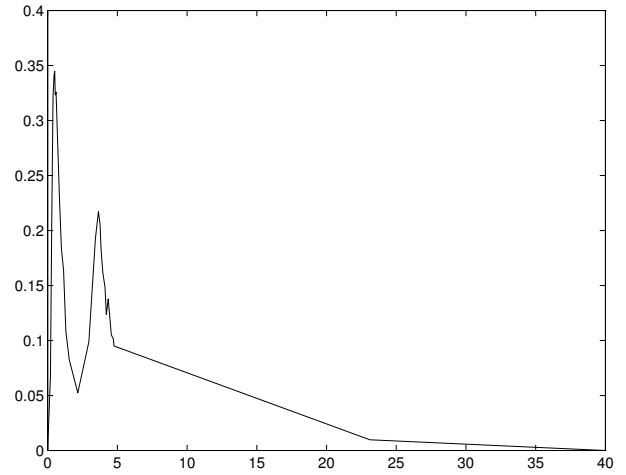
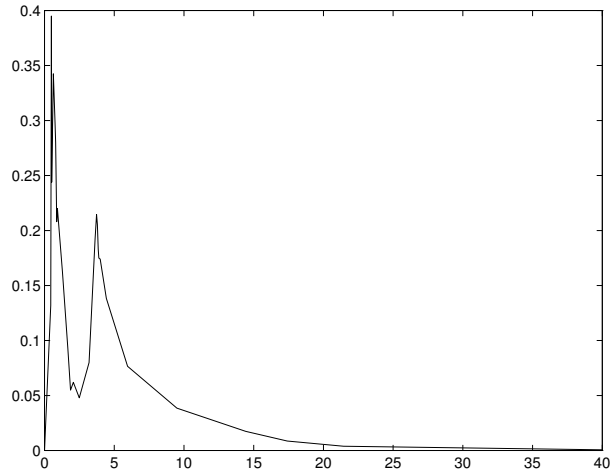


Figure 4.13: Number of cells = 26, $\alpha = 1.0$, $\beta = 0.1$. On left: MRU cells. On right: MRF cells.

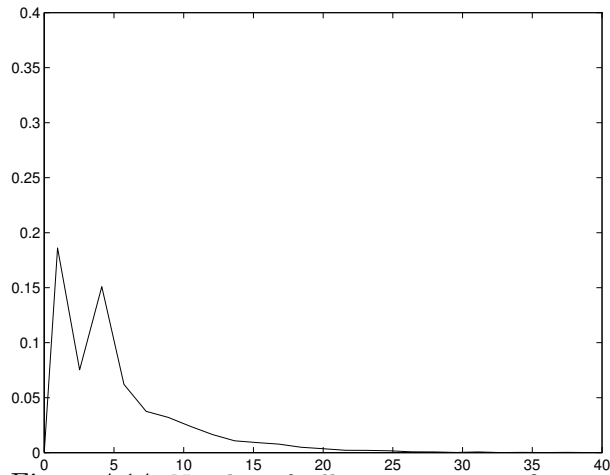


Figure 4.14: Number of cells = 26, $\alpha = 1.0$, $\beta = 0.1$. Equal width cells.

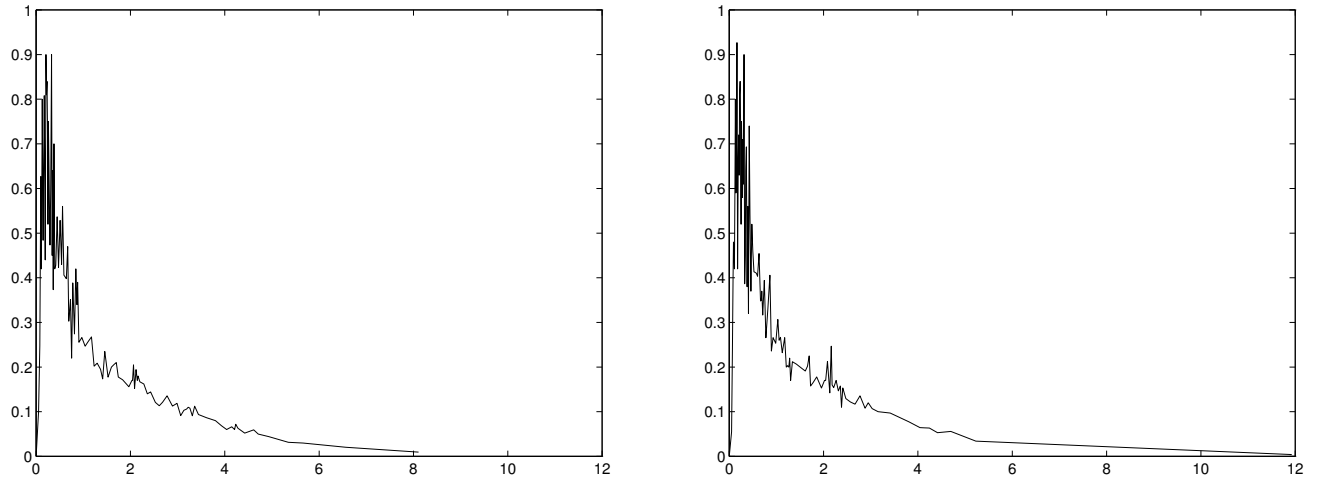


Figure 4.15: Number of cells = 100, $\alpha = 1.0$, $\beta = 1.0$. On left: MRU cells. On right: MRF cells.

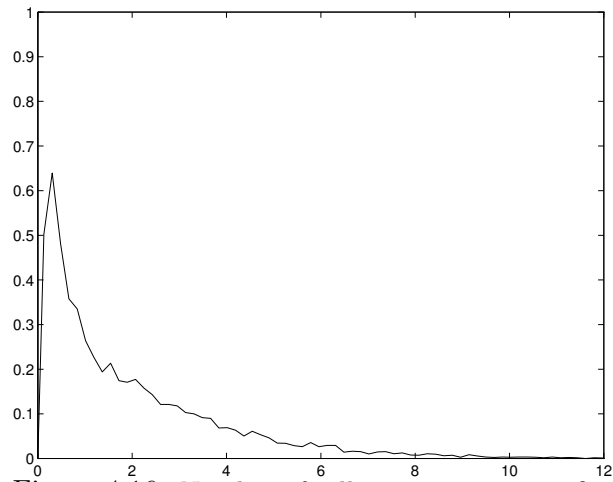


Figure 4.16: Number of cells = 100, $\alpha = 1.0$, $\beta = 1.0$. Equal width cells.

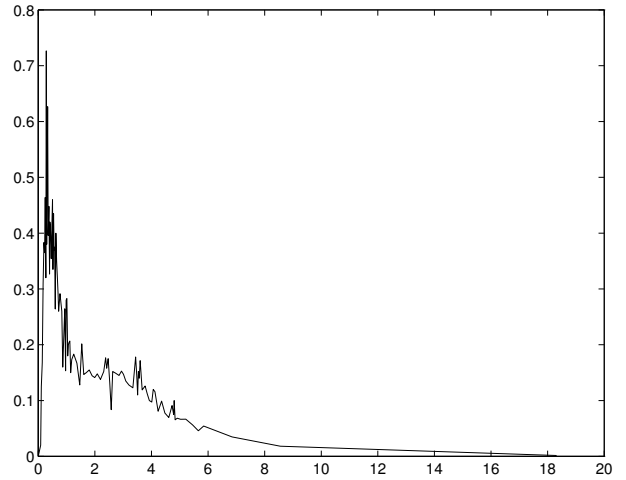
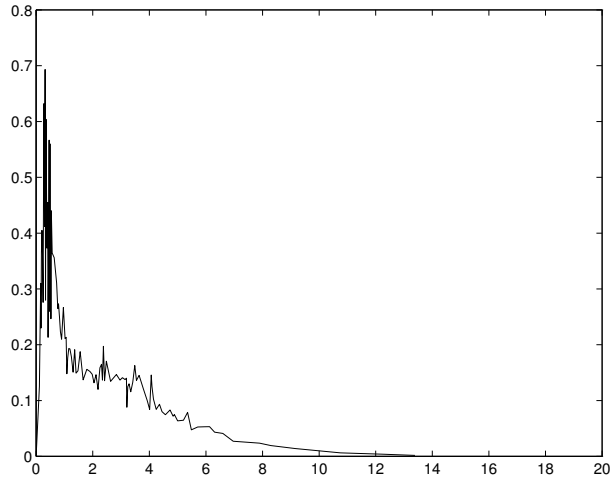


Figure 4.17: Number of cells = 100, $\alpha = 1.0$, $\beta = 0.5$. On left: MRU cells. On right: MRF cells.

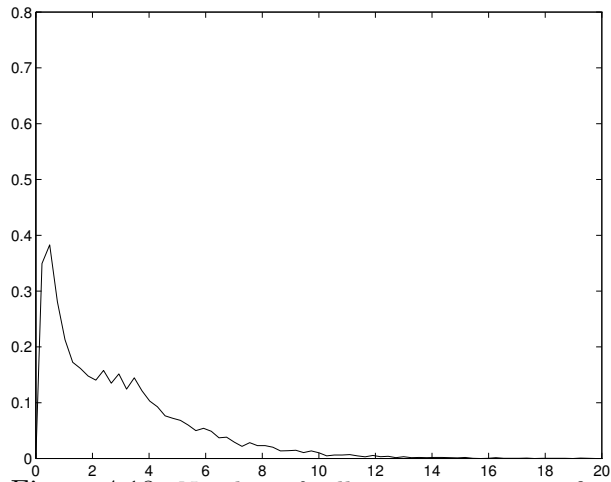


Figure 4.18: Number of cells = 100, $\alpha = 1.0$, $\beta = 0.5$. Equal width cells.

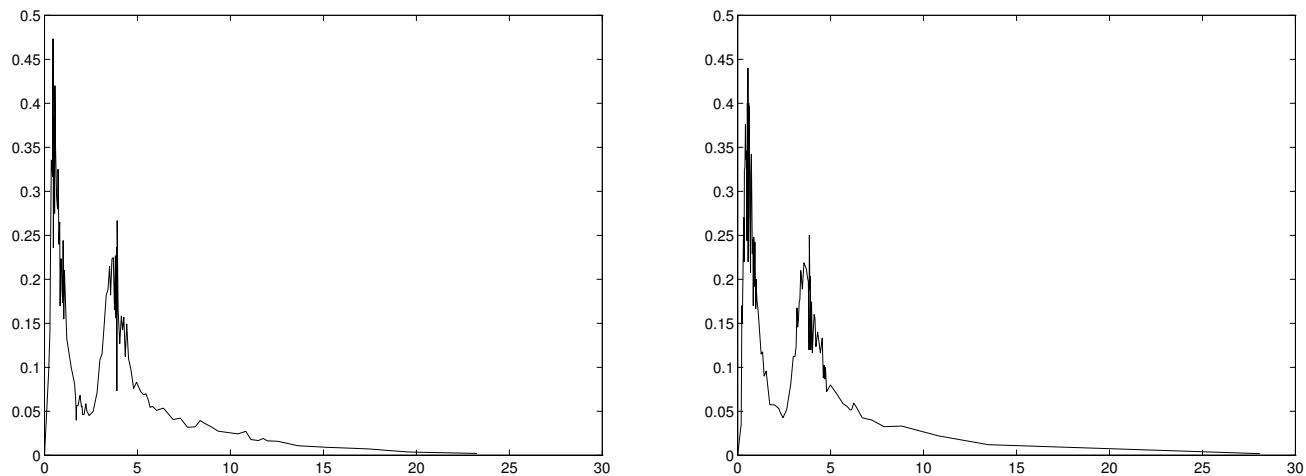


Figure 4.19: Number of cells = 100, $\alpha = 1.0$, $\beta = 0.1$. On left: MRU cells. On right: MRF cells.

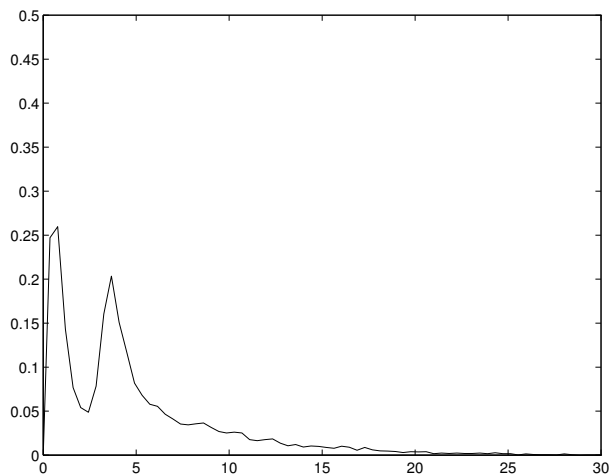


Figure 4.20: Number of cells = 100, $\alpha = 1.0$, $\beta = 0.1$. Equal width cells.

4.2 A quadrature technique

A recursive method for the numerical integration is used here. The idea is to implement the moments method [35] not in original formulation, but introducing a recurrence formula of moments that solves the ill-conditioning problem. Due to recurrence form, we use a recursive algorithm, which well adapts to given formula of moments [62]. Starting with a specified initial value, the algorithm constructs the moments, by which the coefficients of recursive formula for orthogonal polynomials are obtained [88]. The Brent algorithm [1] finds the zeros of the orthogonal polynomials with respect to weight function and finally a gaussian quadrature rule [38] is applied using the new nodes with relative weights. The integrals considered may have different weight functions always characterized by an exponential term.

We give the general recurrence formulas to evaluate the moments used to build up the feasible family of orthogonal polynomials with respect to several specific weight functions and some of them have been suggested by a paper of Piessen [71].

The application of the method to the numerical treatment of contact problems shows some interesting results.

Now, specifically a special recursive algorithm is built by a three-term recursive formula with coefficients evaluated by the moments method. A functional $c(\cdot)$ is studied over any function space that contains the polynomial space and it is shown that such a functional is positive definite, enabling us to use the advantages of such a property on the zeros of orthogonal polynomials for such a functional. A comparison is presented of the numerical advantages of such a method with respect to the Laguerre polynomials. This technique is an extension of the method already established for numerical integrations over finite domains [62, 63] and it is a variant of classic quadrature methods [35], [61], [43].

Furthermore, several recurrence formulas for moments related to different weight functions are given. These formulas are used to carry out numerical integrations within a domain corresponding to the whole positive real axis. Benefits of the procedure are shown for particular cases with comparison of results obtained by other integration rules.

4.2.1 The moments method

Given a function $l(x)$ defined over $(0, +\infty)$, positive over such an interval, with

$$\int_0^{+\infty} l(x)e^{-\alpha x} dx < +\infty, \quad \alpha \in \mathbb{R}^+ \quad (4.2.1)$$

let us consider a system of orthogonal polynomials $\{P_n(x)\}_{n=0}^{\infty}$ in $(0, +\infty)$ with respect to the weight function $l(x)e^{-\alpha x}$, namely such that $\forall n$

$$\int_0^{+\infty} l(x)e^{-\alpha x} P_n(x)P_i(x) dx = 0 \quad i = 0, 1, \dots, n-1, \quad (4.2.2)$$

and the Gaussian quadrature formula

$$\int_0^{+\infty} l(x)e^{-\alpha x} f(x) dx \approx \sum_{k=1}^n A_k^{(n)} f(x_k) \quad (4.2.3)$$

where x_1, x_2, \dots, x_n are the zeros of the polynomial $P_n(x)$ and the $A_k^{(n)}$ are the respective weights in the quadrature formula.

It is known that the Gaussian quadrature formulas are stable, convergent and very precise when one is able to determine the appropriate family of orthogonal polynomials $\{P_n(x)\}_{n=0}^{\infty}$.

The classical treatment may be found in [88], using an orthogonalization procedure and determinantal representation of the polynomials. In [62] it is shown that the numerical procedure coming from determinantal ratios is very ill conditioned.

With the method due to Brezinski [2] one defines over the space of the complex polynomials the functional c ,

$$c(f(x)) = \int_0^{+\infty} f(x)l(x)e^{-\alpha x} dx \quad \alpha \in \mathbb{R}^+; \quad (4.2.4)$$

completely determined by the moments

$$c_i = c(x^i) = \int_0^{+\infty} x^i l(x) e^{-\alpha x} dx \quad i = 0, 1, \dots \quad (4.2.5)$$

In such case, the family of orthogonal polynomials $\{P_k(x)\}$ with respect to the functional c , i.e. the family for which $\forall k \in \mathbb{N}$ and $x \in (0, +\infty)$

$$P_k(x) = p_0^{(k)} + p_1^{(k)}x + \dots + p_k^{(k)}x^k \quad \text{has the degree } k \text{ and} \quad (4.2.6)$$

$$c(x^i P_k) = 0 \quad \text{for } i = 0, 1, \dots, k-1,$$

is determined by the moments (4.2.5) and the following three-term recurrence formula:

$$P_{k+1}(x) = (A_{k+1}x + B_{k+1})P_k(x) - C_{k+1}P_{k-1}(x), \quad k = 0, 1, \dots,$$

with

$$P_{-1}(x) = 0, \quad P_0(x) = \text{any arbitrary constant different from zero,}$$

and

$$A_{k+1} = \frac{p_{k+1}^{(k+1)}}{p_k^{(k)}}, \quad B_{k+1} = -\frac{p_{k+1}^{(k+1)}\alpha_k}{p_k^{(k)}h_k}, \quad C_{k+1} = \frac{p_{k-1}^{(k-1)}p_{k+1}^{(k+1)}}{(p_k^{(k)})^2} \cdot \frac{h_k}{h_{k-1}} \quad (4.2.7)$$

where

$$\alpha_k = p_k^{(k)}c(x^{k+1}P_k) + p_{k-1}^{(k)}c(x^k P_k) \quad \text{and} \quad (4.2.8)$$

$$h_k = c(P_k^2). \quad (4.2.9)$$

Choosing the polynomials P_k as monic polynomials, a simplified recurrence formula is obtained:

$$P_{k+1}(x) = (x + B_{k+1})P_k(x) - C_{k+1}P_{k-1}(x), \quad k = 0, 1, \dots, \quad (4.2.10)$$

$$P_{-1}(x) = 0, P_0(x) = 1,$$

having $\forall k$

$$A_{k+1} = 1, \quad B_{k+1} = -\frac{\alpha_k}{h_k}, \quad C_{k+1} = \frac{h_k}{h_{k-1}}, \quad (4.2.11)$$

with

$$\alpha_k = c(x^{k+1}P_k) + p_{k-1}^{(k)}c(x^k P_k), \quad h_k = c(x^k P_k). \quad (4.2.12)$$

By linearity of the functional, one has

$$h_k = \sum_{i=0}^k c_{k+i} p_i^{(k)}, \quad \gamma_k = \sum_{i=0}^k c_{k+i+1} p_i^{(k)}, \quad (4.2.13)$$

$$\alpha_k = \gamma_k + p_{k-1}^{(k)} h_k \quad \text{for } k = 0, 1, \dots \quad (4.2.14)$$

and finally

$$p_i^{(k+1)} = p_{i-1}^{(k)} + B_{k+1} p_i^{(k)} - C_{k+1} p_i^{(k-1)} \quad i = 0, 1, \dots, k, \quad (4.2.15)$$

which allows the evaluation of the coefficients of the polynomial of degree $k + 1$ starting from the initial data:

$$p_{-1}^{(-1)} = p_0^{(-1)} = 0, \quad p_{-1}^{(0)} = p_1^{(0)} = 0, \quad p_0^{(0)} = 1, \quad h_{-1} = 1. \quad (4.2.16)$$

Chebyshev in [8] used a method based on moments, that, unfortunately, is ill conditioned; he used a recurrence formula, which is analogous to (4.2.10) but involving the quantities

$$z_{k,i} = c(x^i P_k), \quad k, i = 0, 1, 2, \dots$$

In [62] it has been shown that the numerical results by the moments method are better than those of [8].

4.2.2 A recursive relation for moments

The moments method has been applied by various authors to evaluate integrals over finite intervals (see [34], [61], [62], [63]). In the following, we consider the infinite interval and take as a special case $l(x) = \ln(x + 1)$. In particular, we want to evaluate the integral

$$\int_0^{+\infty} f(x) \ln(x + 1) e^{-\alpha x} dx \quad \text{with } \alpha \in \mathbb{R}^+. \quad (4.2.17)$$

• Let us consider the functional

$$c(f(x)) = \int_0^{+\infty} f(x) \ln(x + 1) e^{-\alpha x} dx, \quad \alpha \in \mathbb{R}^+; \quad (4.2.18)$$

the moments c_n are defined as

$$c_n = \int_0^{+\infty} x^n \ln(x + 1) e^{-\alpha x} dx, \quad \forall n \in \mathbb{N}. \quad (4.2.19)$$

The following relations hold

$$(i) \quad c_0 = \frac{e^\alpha}{\alpha} E_1(\alpha) \quad (4.2.20)$$

$$(ii) \quad c_n = \sum_{i=0}^{n-1} (-1)^i \frac{(n-1-i)!}{\alpha^{n-i+1}} + (-1)^n c_0 + \frac{n}{\alpha} c_{n-1} \quad \text{for } n = 1, 2, \dots \quad (4.2.21)$$

It is easy to prove (i):

$$\begin{aligned} c_0 &= \int_0^{+\infty} \ln(x+1)e^{-\alpha x} dx = \left[-\frac{1}{\alpha} e^{-\alpha x} \ln(x+1) \right]_0^{+\infty} + \frac{1}{\alpha} \int_0^{+\infty} \frac{e^{-\alpha x}}{x+1} dx = \\ &= \frac{1}{\alpha} \int_0^{+\infty} \frac{e^{-\alpha x}}{x+1} dx \end{aligned}$$

(setting $y = \alpha(x+1)$)

$$= \frac{e^\alpha}{\alpha} \int_\alpha^{+\infty} \frac{e^{-y}}{y} dy = \frac{e^\alpha}{\alpha} E_1(\alpha),$$

where $E_1(x) = \int_x^{+\infty} \frac{e^{-y}}{y} dy$ is the *exponential integral*, available in tabular form.

We prove now the (ii):

$$c_n = \int_0^{+\infty} x^n \ln(x+1)e^{-\alpha x} dx = [\ln(x+1)I_n]_0^{+\infty} - \int_0^{+\infty} \frac{I_n}{x+1} dx$$

where

$$I_n = \int x^n e^{-\alpha x} dx.$$

From mathematical tables [45] we have that

$$I_n = -\frac{e^{-\alpha x}}{\alpha} \sum_{i=0}^n \frac{x^{n-i} n!}{\alpha^i (n-i)!},$$

therefore

$$\begin{aligned} c_n &= \left[\ln(x+1) \left(-\frac{e^{-\alpha x}}{\alpha} \sum_{i=0}^n \frac{x^{n-i} n!}{\alpha^i (n-i)!} \right) \right]_0^{+\infty} + \int_0^{+\infty} \frac{\frac{e^{-\alpha x}}{\alpha} \sum_{i=0}^n \frac{x^{n-i} n!}{\alpha^i (n-i)!}}{x+1} dx \\ &= \int_0^{+\infty} \frac{e^{-\alpha x} x^n}{\alpha(x+1)} dx + \int_0^{+\infty} \frac{e^{-\alpha x}}{\alpha(x+1)} \sum_{i=1}^n \frac{x^{n-i} n!}{\alpha^i (n-i)!} dx \\ &= \int_0^{+\infty} \frac{e^{-\alpha x} x^n}{\alpha(x+1)} dx + \frac{n}{\alpha} \int_0^{+\infty} \frac{e^{-\alpha x}}{\alpha(x+1)} \sum_{i=0}^{n-1} \frac{x^{n-1-i} (n-1)!}{\alpha^i (n-1-i)!} dx \\ &= \int_0^{+\infty} \frac{e^{-\alpha x} x^n}{\alpha(x+1)} dx - \frac{n}{\alpha} \int_0^{+\infty} \frac{I_{n-1}}{x+1} dx \\ &= \int_0^{+\infty} \frac{e^{-\alpha x} x^n}{\alpha(x+1)} dx + \frac{n}{\alpha} c_{n-1}. \end{aligned} \tag{4.2.22}$$

Recalling that

$$\frac{x^n}{x+1} = \sum_{i=0}^{n-1} (-1)^i x^{n-1-i} + \frac{(-1)^n}{x+1} \tag{4.2.23}$$

we can write

$$\int_0^{+\infty} \frac{e^{-\alpha x} x^n}{\alpha(x+1)} dx = \sum_{i=0}^{n-1} (-1)^i \frac{1}{\alpha} \int_0^{+\infty} e^{-\alpha x} x^{n-1-i} dx + (-1)^n \int_0^{+\infty} \frac{e^{-\alpha x}}{\alpha(x+1)} dx =$$

$$\frac{1}{\alpha} \sum_{i=0}^{n-1} (-1)^i \frac{(n-1-i)!}{\alpha^{n-i}} + (-1)^n c_0.$$

Substituting the last one in (4.2.22)

$$c_n = \sum_{i=0}^{n-1} (-1)^i \frac{(n-1-i)!}{\alpha^{n-i+1}} + (-1)^n c_0 + \frac{n}{\alpha} c_{n-1}. \quad (4.2.24)$$

Now we prove that the following recurrence formula for the moments holds:

$$c_n = c_{n-1} \left(\frac{n}{\alpha} - 1 \right) + \frac{n-1}{\alpha} c_{n-2} + \frac{(n-1)!}{\alpha^{n+1}} \quad n = 1, 2, \dots \quad (4.2.25)$$

with $c_{-1} = c_0 = \frac{e^\alpha}{\alpha} E_1(\alpha)$. To this aim, we rewrite the (ii) for c_{n-1}

$$(iii) \quad c_{n-1} = \sum_{i=0}^{n-2} (-1)^i \frac{(n-2-i)!}{\alpha^{n-i}} + (-1)^{n-1} c_0 + \frac{n-1}{\alpha} c_{n-2}. \quad (4.2.26)$$

Adding (ii) to the (iii) and recalling that

$$\sum_{i=1}^{n-1} (-1)^i \frac{(n-1-i)!}{\alpha^{n-i+1}} = - \sum_{i=0}^{n-2} (-1)^i \frac{(n-2-i)!}{\alpha^{n-i}}, \quad (4.2.27)$$

it obtains

$$c_n + c_{n-1} = \frac{(n-1)!}{\alpha^{n+1}} + \frac{n}{\alpha} c_{n-1} + \frac{(n-1)}{\alpha} c_{n-2} \quad (4.2.28)$$

and finally

$$c_n = c_{n-1} \left(\frac{n}{\alpha} - 1 \right) + \frac{(n-1)}{\alpha} c_{n-2} + \frac{(n-1)!}{\alpha^{n+1}} \quad n = 1, 2, \dots \quad (4.2.29)$$

Specifications on the functional

To apply the moments method we need to verify that

$$h_k \neq 0 \quad k = 0, 1, \dots, \quad (4.2.30)$$

but from [2] $h_k = c(P_k^2)$ and in our case $c(P_k^2)$ is positive, being

$$h_k = c(P_k^2) = \int_0^{+\infty} P_k^2(x) e^{-\alpha x} l(x) dx > 0. \quad (4.2.31)$$

In [2] the determinant involving the moments c_n is considered

$$H_k(c_0) = \begin{vmatrix} c_0 & c_1 & c_2 & \dots & c_{k-1} \\ c_1 & c_2 & c_3 & \dots & c_k \\ \dots & \dots & \dots & \dots & \dots \\ c_{k-1} & c_k & c_{k+1} & \dots & c_{2k-2} \end{vmatrix}. \quad (4.2.32)$$

If $H_k(c_0) \neq 0 \quad \forall k$, the functional c is *definite*.

If $H_k(c_0) \geq 0 \quad \forall k$, the functional c is *positive*.
If $H_k(c_0) > 0 \quad \forall k$, the functional c is *positive definite*.
Furthermore, from [2], one has

$$P_k(x) = D_k \begin{vmatrix} c_0 & c_1 & \dots & c_k \\ c_1 & c_2 & \dots & c_{k+1} \\ \dots & \dots & \dots & \dots \\ c_{k-1} & c_k & \dots & c_{2k-1} \\ 1 & x & \dots & x^k \end{vmatrix} \quad \text{for } k = 1, 2, \dots \quad (4.2.33)$$

and $P_0(x) = D_0$, where D_k for $k = 0, 1, 2, \dots$ are constants different from zero.
Widder in [93] has shown that if $c(P_k^2(x)) > 0$ for all k , the functional c is positive definite.
The proof in [2] for the case of the family of monic polynomials $\{P_k(x)\}$ is given using the following identity

$$c(P_k^2) = c((p_0^{(k)} + p_1^{(k)}x + \dots + p_k^{(k)}x^k)P_k(x)) \quad (4.2.34)$$

$$= p_0^{(k)}c(P_k) + p_1^{(k)}c(xP_k) + \dots + p_k^{(k)}c(x^kP_k). \quad (4.2.35)$$

By the orthogonality of the polynomials P_k , one has

$$c(P_k^2) = p_k^{(k)}c(x^kP_k). \quad (4.2.36)$$

From (4.2.32) and (4.2.33) the coefficient of maximal degree of $P_k(x)$ is given by

$$p_k^{(k)} = D_k H_k(c_0) \quad \text{and} \quad c(x^kP_k) = D_k H_{k+1}(c_0). \quad (4.2.37)$$

Therefore

$$0 < c(P_k^2) = p_k^{(k)}c(x^kP_k) = D_k^2 H_k(c_0) H_{k+1}(c_0), \quad \forall k. \quad (4.2.38)$$

Hence $H_k(c_0) > 0 \quad \forall k$ or $H_k(c_0) < 0 \quad \forall k$.

We note that $c_0 = c(x^0) = c(1) = c(p_0^{(0)}) = c(P_0^2(x)) > 0$, but we also have that $c_0 = H_1(c_0)$ and for $k = 1$ one has that $H_1(c_0) > 0$, from which also $H_2(c_0) > 0$, $H_3(c_0) > 0, \dots$; finally

$$H_k(c_0) > 0 \quad \forall k. \quad (4.2.39)$$

In our case $c(P_k^2(x)) > 0 \quad \forall k$ and in particular

$$c_0 = \frac{e^\alpha}{\alpha} E_1(\alpha) > 0 \quad (4.2.40)$$

with $\alpha \in \mathbb{R}^+$. Therefore the functional (4.2.18) is *positive definite*.

Evaluation of nodes and weights

The determination of the nodes is made by using the Brent algorithm [1], which combining the methods of the linear interpolation, the quadratic inverse interpolation and the bisection, allows to obtain results with high precision. Note that this algorithm requires the specification of the values of extremes a and b of the interval where the polynomial has a zero, namely where $P(a) \cdot P(b) < 0$. Using the properties of roots separation [88] of the orthogonal polynomials,

there is not any problem in the case of a bounded interval containing all the roots of the polynomials. For the case of the unbounded integration domain, it is useful to find an upper bound M for the zeros of the polynomial P_n that makes the interval $[x_{n-1}^{(n-1)}, M]$ not too much larger in such a way to obtain the last zero $x_n^{(n)}$ of P_n in not too many steps. Using the Hadamard-Gershgorin theorem [2], the zeros are localized in the union of balls with center $-B_i$ and radius $r = 1 + |C_i|$ for $i = 1, \dots, k$, where B_i and C_i $i = 1, \dots, k$ are the coefficients appearing in the recurrence formula for P_k . Being the zeros real and separated, namely two consecutive zeros of P_{k+1} are separated by a zero of P_k and vice versa, one can apply the algorithm for searching all zeros without any problem; therefore it is possible to use the Brent algorithm in a Fortran version, as it is in the IMSL Library [48] with H-Float precision. The scheme to find the zeros is the following:

Step 1. The zeros $x_1^{(2)}$ and $x_2^{(2)}$ of $P_2(x)$ are determined (with $x_1^{(2)} < x_2^{(2)}$)

Step 2. For $k = 3, \dots, n$, $x_1^{(k)}$ is evaluated in such a way $0 < x_1^{(k)} < x_1^{(k-1)}$ and for $j = 2, \dots, k-1$ the zeros $x_j^{(k)}$ are evaluated taking in account that $x_{j-1}^{(k-1)} < x_j^{(k)} < x_j^{(k-1)}$;

Step 3. Finally, the last zero $x_k^{(k)}$ of $P_k(x)$ is evaluated recalling that $x_{k-1}^{(k-1)} < x_k^{(k)} < b$, where b is determined by the theorem of Hadamard-Gershgorin.

For the weights, as in [63], the following expression

$$A_i^{(k)} = \frac{h_{k-1}}{P'_k(x_i)P_{k-1}(x_i)} \quad \text{for } i = 1, \dots, k \quad (4.2.41)$$

is used, where x_1, \dots, x_k are the zeros of $P_k(x)$.

The algorithm and numerical results

The algorithm in Fortran-77 has been implemented with the H-Float storage to obtain a sufficient number of significant digits (about 33 significant decimal digits). A brief scheme of the algorithm is the following:

Step 1. The value of α and the maximum number of nodes for the quadrature are required.

Step 2. Initialize the coefficients of $P_{-1}(x)$ and of $P_0(x)$ by the (4.2.16).

Step 3. Set $c_{-1} = c_0 = \frac{e^\alpha}{\alpha} E_1(\alpha)$.

Step 4. For $k = 1, \dots, n-1$

- Compute the moments c_{2k-1} and c_{2k} , by (4.2.29);
- Compute B_{k+1} and C_{k+1} by the (4.2.7) to determine the coefficients of $P_{k+1}(x)$ by the (4.2.15)
- Compute all zeros of $P_{k+1}(x)$ as above described.

As example of application let us consider the following integral

$$\int_0^{+\infty} e^{-\alpha x} \ln(x+1) \frac{\alpha(x+1)\ln(x+1) - 2}{x+1} dx. \quad (4.2.42)$$

We compare its obtained evaluation by the proposed method with its evaluation by the Gauss-Laguerre quadrature formula, known its zero value [45]. The Gauss-Laguerre quadrature formula

Table 4.9: For $\alpha = 0.5$

n. of exact digits	n. of P_n nodes	n. of Laguerre nodes
2	3	4
3	6	9
4	11	14
5	17	22
6	24	30

Table 4.10: For $\alpha = 1.0$

n. of exact digits	n. of P_n nodes	n. of Laguerre nodes
2	2	2
3	3	5
4	6	8
5	9	12
6	13	16

is applied being:

$$\int_0^{+\infty} e^{-\alpha x} \ln(x+1) \frac{\alpha(x+1)\ln(x+1) - 2}{x+1} dx = \frac{1}{\alpha} \int_0^{+\infty} e^{-x} \ln(x/\alpha + 1) \frac{(x+1/\alpha)\ln(x/\alpha + 1) - 2}{(x/\alpha) + 1} dx.$$

In the Tables 4.9-4.11 the number of nodes to obtain the specified number of exact digits are presented for different α values.

From tables results, the method shows its efficiency essentially based on the construction of optimized nodes and weights for the quadrature.

4.2.3 Examples

For a *weight* function such that

$$w(x) = l(x)e^{-\alpha x} \quad \alpha \in \mathbb{R}^+ \tag{4.2.43}$$

defined over $(0, +\infty)$, positive over such interval, with

$$\int_0^{+\infty} w(x) dx < +\infty \tag{4.2.44}$$

we consider the functional

$$c(f(x)) = \int_0^{+\infty} f(x)w(x) dx \tag{4.2.45}$$

Table 4.11: For $\alpha = 1.5$

n. of exact digits	n. of P_n nodes	n. of Laguerre nodes
2	1	2
3	3	4
4	4	6
5	6	8
6	8	11

and the *moments*

$$c_n = \int_0^{+\infty} x^n w(x) dx \quad \forall n \in \mathbb{N}. \quad (4.2.46)$$

We require the related functional is positive definite to allow the implementation of the specified algorithm; this request is satisfied if $c_0 > 0$. For the given *weight* function $w(x)$ we can write a recurrence formula for moments more general, but that needs to be specialized for specified cases, than that presented in [64]

$$c_n = \int_0^{+\infty} \frac{e^{-\alpha x} x^n}{\alpha} \frac{d}{dx} l(x) dx + \frac{n}{\alpha} c_{n-1} + K \quad n = 1, 2, \dots \quad (4.2.47)$$

where K is a constant.

The problem is to find a way to rewrite the integral on the right hand side of (4.2.46) as a function of moments of degree less than n ; we would like to represent the same integral as a function of very few moments. When it is possible, the specified recurrence formula allows to use a recursive algorithm and to evaluate, with high precision, the integral

$$\int_0^{+\infty} f(x) w(x) dx \quad (4.2.48)$$

where $f(x)$ is a real function to be specified.

From c_0 and from the recurrence formula for moments, we can construct B_{k+1} and C_{k+1} involved in the recurrence formula for the coefficients of polynomials, namely

$$p_i^{(k+1)} = p_{i-1}^{(k)} + B_{k+1} p_i^{(k)} - C_{k+1} p_i^{(k-1)} \quad i = 0, 1, \dots, k, \forall k. \quad (4.2.49)$$

The family of polynomials $\{P_n(x)\}_{n=0}^{\infty}$ in $(0, +\infty)$ are orthogonal respect to $l(x)e^{-\alpha x}$, i.e. the polynomials are such that $\forall n$

$$\int_0^{+\infty} l(x) e^{-\alpha x} P_n(x) P_i(x) dx = 0 \quad i = 0, 1, \dots, n-1. \quad (4.2.50)$$

It is not necessary to apply any transformation of infinite integration domain into a finite one, because the aim of this technique is to construct new systems of orthogonal polynomials with respect to specified weight functions over an infinite domain. The gain is to obtain a larger class of orthogonal polynomial systems useful in different fields such as in Volterra analysis

of linear or non linear systems, approximation rules, pseudospectral methods, etc. Though analytical expression for these polynomials is not available, we have an algorithm to construct them. Hence, if we know the recurrence formula for the moments, by using them we can build a different systems of polynomials for different problems.

In order to use the recursive algorithm, we give the recurrence formulas for moments related to the following weight functions:

$$\begin{aligned} w_1(x) &= x^\beta e^{-\alpha x} & \alpha \in \mathbb{R}^+ & \beta > -1 \\ w_2(x) &= e^{-\alpha x}(\sin \beta x + \lambda) & \beta \in \mathbb{R}, \lambda \geq 1, & \alpha \in \mathbb{R}^+ \\ w_3(x) &= e^{-\alpha x}(\cos \beta x + \lambda) & \beta \in \mathbb{R}, \lambda \geq 1, & \alpha \in \mathbb{R}^+ \end{aligned}$$

Case $w_1(x)$

It could be seen as the generalized Laguerre weight function

$$w(x) = x^\beta e^{-x} \quad \beta > -1 \quad (4.2.51)$$

where a simple transformation is applied. We have considered also this case to show that the recursive algorithm gives the generalized Laguerre polynomials. The recurrence formula for the moments is the following:

$$c_n = \frac{n + \beta}{\alpha} c_{n-1} \quad n = 1, 2, \dots \text{ with } c_0 = \frac{(n + \beta)!}{\alpha^{n+\beta+1}}. \quad (4.2.52)$$

This relation has easily derived from (4.2.46) applying the integration by parts.

Case $w_2(x)$

Starting from integral definition of the moment c_n and applying the integration by parts, the equation (4.2.47) becomes

$$c_n = \frac{\beta}{\alpha} \int_0^{+\infty} \frac{e^{-\alpha x} x^n}{\alpha} \cos \beta x dx + \frac{n}{\alpha} c_{n-1} \quad n = 1, 2, \dots \quad (4.2.53)$$

Let us consider the integral in the r.h.s.

$$\begin{aligned} \frac{\beta}{\alpha} \int_0^{+\infty} \frac{e^{-\alpha x} x^n}{\alpha} \cos \beta x dx &= \left[\frac{\beta}{\alpha} I_n \cos \beta x \right]_0^{+\infty} + \frac{\beta^2}{\alpha} \int_0^{+\infty} I_n \sin \beta x dx = \\ \frac{n! \beta}{\alpha^{n+2}} + \frac{\beta^2}{\alpha} \int_0^{+\infty} I_n \sin \beta x dx + \frac{\beta^2 \lambda}{\alpha} \int_0^{+\infty} I_n dx - \frac{\beta^2 \lambda}{\alpha} \int_0^{+\infty} I_n dx &= \\ \frac{n! \beta}{\alpha^{n+2}} + \frac{\beta^2}{\alpha} \int_0^{+\infty} I_n (\sin \beta x + \lambda) dx - \frac{\beta^2 \lambda}{\alpha} \int_0^{+\infty} I_n dx &= \\ \frac{n! \beta}{\alpha^{n+2}} + \frac{\beta^2}{\alpha} \int_0^{+\infty} I_n (\sin \beta x + \lambda) dx - \frac{\beta^2 \lambda}{\alpha} \int_0^{+\infty} \left(-\frac{e^{-\alpha x}}{\alpha} \sum_{i=0}^n \frac{x^{n-i} n!}{\alpha^i (n-i)!} \right) dx &= \\ \frac{n! \beta}{\alpha^{n+2}} + \frac{\beta^2}{\alpha} \int_0^{+\infty} \left(-\frac{e^{-\alpha x}}{\alpha} \sum_{i=0}^n \frac{x^{n-i} n!}{\alpha^i (n-i)!} \right) (\sin \beta x + \lambda) dx &+ \end{aligned}$$

$$\begin{aligned}
& \frac{\beta^2 \lambda}{\alpha^2} \sum_{i=0}^n \frac{n!}{\alpha^i (n-i)!} \frac{(n-i)!}{\alpha^{n-i+1}} = \\
& \frac{n! \beta}{\alpha^{n+2}} - \frac{\beta^2}{\alpha^2} \sum_{i=0}^n \frac{c_{n-i} n!}{\alpha^i (n-i)!} + \frac{\beta^2 \lambda (n+1)!}{\alpha^2 \alpha^{n+1}} = \\
& \frac{n! \beta}{\alpha^{n+2}} - \frac{\beta^2}{\alpha^2} c_n - \frac{\beta^2}{\alpha^2} \sum_{i=1}^n \frac{c_{n-i} n!}{\alpha^i (n-i)!} + \frac{\beta^2 \lambda (n+1)!}{\alpha^{n+3}}, \tag{4.2.54}
\end{aligned}$$

where $I_n = \int e^{-\alpha x} x^n dx = -\frac{e^{-\alpha x}}{\alpha} \sum_{i=0}^n \frac{x^{n-i} n!}{\alpha^i (n-i)!}$.

Finally, substituing (4.2.54) and (4.2.53), we have

$$c_n = \frac{n!}{\alpha^2 + \beta^2} \left[\frac{\beta}{\alpha^n} + \frac{(n+1)\beta^2 \lambda}{\alpha^{n+1}} - \beta^2 \sum_{i=1}^n \frac{c_{n-i}}{\alpha^i (n-i)!} + \frac{\alpha}{(n-1)!} c_{n-1} \right]. \tag{4.2.55}$$

Writing the same relation for c_{n-1} , and subtracting it from (4.2.55), one has

$$c_n = c_{n-1} \frac{n}{\alpha} + \frac{n! \beta^2 \lambda}{(\alpha^2 + \beta^2) \alpha^{n+1}} - \frac{n! \beta^2 c_{n-1}}{(\alpha^2 + \beta^2) \alpha (n+1)!} - \frac{n(n-1) c_{n-2}}{(\alpha^2 + \beta^2)} + \frac{n \alpha c_{n-1}}{(\alpha^2 + \beta^2)}. \tag{4.2.56}$$

So we can write the following three terms recurrence formula for the moments:

$$c_n = \frac{1}{(\alpha^2 + \beta^2)} \left[2n \alpha c_{n-1} - n(n-1) c_{n-2} + \frac{n! \beta^2 \lambda}{\alpha^{n+1}} \right] \quad n = 2, 3, \dots \tag{4.2.57}$$

To apply the (4.2.57) it is sufficient to know the values of c_0 and c_1 , available on the tables [45].

Case $w_3(x)$

This case is similar the previous one, since the recurrence formula is the same of (4.2.57), while the formula derived from (4.2.47) is a little bit different.

By applying the (4.2.47), we obtain

$$c_n = -\beta \int_0^{+\infty} \frac{e^{-\alpha x}}{\alpha} x^n \sin \beta x dx + \frac{n}{\alpha} c_{n-1}. \tag{4.2.58}$$

Developing the above integral, by using same technique, we also obtain:

$$\begin{aligned}
& -\frac{\beta}{\alpha} \int_0^{+\infty} e^{-\alpha x} x^n \sin \beta x dx = \\
& - \left[\frac{\beta}{\alpha} I_n \sin \beta x \right]_0^{+\infty} + \frac{\beta^2}{\alpha} \int_0^{+\infty} I_n \cos \beta x dx + \frac{\beta^2 \lambda}{\alpha} \int_0^{+\infty} I_n dx - \frac{\beta^2 \lambda}{\alpha} \int_0^{+\infty} I_n dx = \\
& \frac{\beta^2}{\alpha} \int_0^{+\infty} I_n (\cos \beta x + \lambda) dx - \frac{\beta^2 \lambda}{\alpha} \int_0^{+\infty} I_n dx,
\end{aligned}$$

where $I_n = \int e^{-\alpha x} x^n dx = -\frac{e^{-\alpha x}}{\alpha} \sum_{i=0}^n \frac{x^{n-i} n!}{\alpha^i (n-i)!}$.

Hence, the recurrence formula is given by

$$c_n = \frac{n!}{\alpha^2 + \beta^2} \left[\frac{(n+1)\beta^2\lambda}{\alpha^{n+1}} - \beta^2 \sum_{i=1}^n \frac{c_{n-i}}{\alpha^i(n-i)!} + \frac{\alpha}{(n-1)!} c_{n-1} \right]. \quad (4.2.59)$$

A comparing example

We have applied the proposed recursive algorithm to the following integral:

$$\int_0^{+\infty} (\sin x + 1)e^{-\alpha x} \ln(x) dx \quad (4.2.60)$$

The Figure 4.21 shows the graphic of the integrand function with $\alpha = 0.01$. It is a difficult case for the classical gaussian quadrature method, but the recursive algorithm appears to be more convenient. The recursive formula for moments (4.2.57) has been used with $\beta = \lambda = 1$.

To evaluate the precision of the algorithm, we used the precision index

$$\tau = -\log \left(\frac{A - B}{B} \right) \quad (4.2.61)$$

where A is the numerical result and B the analytical value. In the Figure 4.22 the precision indexes are plotted as nodes number increases for the recursive algorithm and for the IMSL [48] routines of Gauss-Laguerre quadrature rule applied to

$$\frac{1}{\alpha} \int_0^{+\infty} \left(\sin \frac{x}{\alpha} + 1 \right) e^{-x} \ln \left(\frac{x}{\alpha} \right) dx. \quad (4.2.62)$$

The real value B of the integral, taken from tables [45], has been evaluated by Mathematica [94] to obtain its value in multiple precision. The algorithm is in Q-Float precision. On the left of Figure 4.22 the recursive algorithm shows an increasing precision for the approximation to the integral as the number of nodes increases, with two values of $\alpha = 0.01$ (the lower curve) and $\alpha = 0.001$ (the higher curve). On the right of Figure 4.22, with $\alpha = 0.01$, we see how the result of application of the Gauss-Laguerre quadrature rule is affected by high oscillations.

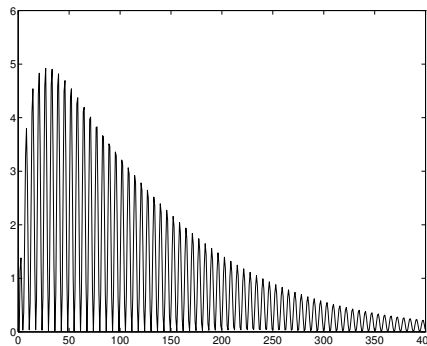


Figure 4.21: $f(x) = (\sin x + 1)e^{-\alpha x} \ln(x)$

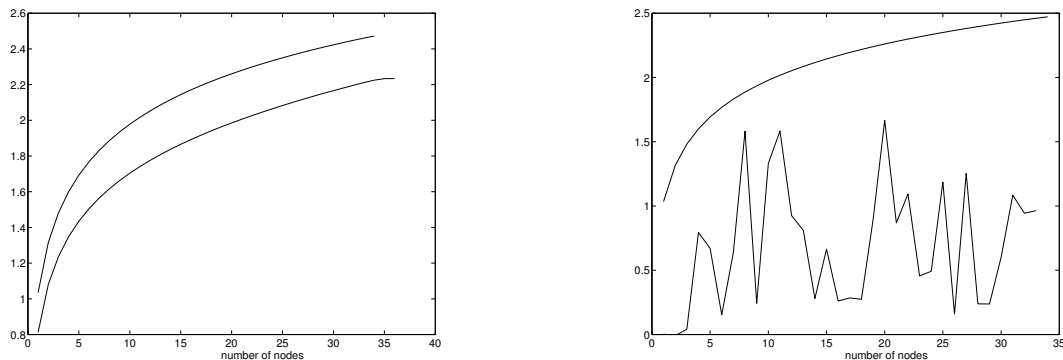


Figure 4.22: On the left: precision index τ for $\alpha = 0.01$ (the lower curve) and $\alpha = 0.001$. On the right: precision indexes for recursive (regular curve) and classical methods with $\alpha = 0.01$.

4.2.4 Application to a contact problem

The analysis of mechanisms that rule the mechanical and thermal behavior of contacting surfaces has been carried out in the past almost exclusively on experimental bases. Theoretical models have also been built up, but their application was limited to very simple geometries. The problem has been revisited by employing numerical methods within the framework of the finite element methods [97], [98], [99]. Experimental methods should be used to characterize in statistical way the microscopic geometry and the micro-mechanical parameters of the contacting surfaces. Different statistical parameters and different mechanical hypotheses can be used to build up such models, see also [9], [46] and [80]. Statistical variables of the surface micro-geometry are extracted from experimental measurements of the surface profile.

Such models usually require the numerical evaluation of quite complex integral relationships. The evaluation of such integrals has shown low precision if standard quadrature rules are adopted hence the development of specific methods is mandatory.

In [65] we have considered the numerical evaluation of integrals over an infinite interval, which plays a key rule in this kind of problem; in order to achieve numerical results with degree of extremal precision it has been necessary to build quadrature rule similar but more general than that of the Gauss-Laguerre type.

Physical contact models has been adapted in [83, 95, 99] to build up high precision contact elements that permit to treat the problem within the framework of the finite element technique. The behavior of such elements is ruled both by the geometrical relationships between contact nodes of the discretisation and by macroscopical laws extrapolated from the microscopical ones. Here we discuss the problems encountered by adapting the elastic model proposed by Greenwood-Williamson [46]. The model is built up by combining statistical relationships with the basic Hertz relationships [50] for contact between two elastic spheres:

$$a_H = (\beta w)^{1/2} \tag{4.2.63}$$

$$A_H = \pi \beta w \tag{4.2.64}$$

$$P_H = \frac{4}{3}E^*\beta^{1/2}w^{3/2} \quad (4.2.65)$$

where a_H is the contact radius, β is the original radius of the spheres, w is the compliance, A_H is the contact area, P_H is the contact force and E^* is the elastic modulus of contacting surfaces. From the statistical point of view we can represent the surface profile by employing a statistical function which represents the distribution of the asperities heights. If the deformation of the microscopical surfaces profile is disregarded the probability that the contact of the two mean planes takes place for a certain compliance, d , is given by

$$\text{prob. of contact} = \text{prob}(z_s > d) = \int_d^\infty \phi(z_s)dz_s \quad (4.2.66)$$

where $\phi(z_s)$ is a chosen statistical function and z_s is the summit height. The number of contacting asperities can be also expressed as a function of the compliance, d , if the total number N of asperities is known

$$n_c = N \int_d^\infty \phi(z_s)dz_s \quad (4.2.67)$$

The Greenwood and Williamson model is based on the hypothesis that the geometry of the top of the asperities have a spherical shape. Hence combining a statistical distribution function with the Hertz equations the authors [46] are able to express the real contact area, A_r , and the contact force, P , as functions of the compliance and of the characteristic values of the asperities:

$$A_r = N\pi\beta \int_d^\infty (z_s - d) \phi(z_s)dz_s \quad (4.2.68)$$

$$P = \frac{4}{3}NE^*\beta^{1/2} \int_d^\infty (z_s - d)^{3/2} \phi(z_s)dz_s. \quad (4.2.69)$$

A typical statistical function considered for height and summits distributions is the normal distribution density function

$$\phi(z_s) = \frac{1}{\sigma_s\sqrt{2\pi}} e^{-\frac{z_s^2}{2\sigma_s^2}} \quad (4.2.70)$$

with σ_s is the standard deviation of the summits. The integrals involved do not admit a closed form solution, hence the relationships are usually normalized to permit their hand calculation by employing table of standard integrals. Such normalization is still convenient also in our case. We define the normalized variable

$$x_s = \frac{z_s}{\sigma_s}. \quad (4.2.71)$$

By using (4.2.70) in the (4.2.67), (4.2.68) and (4.2.69), applying the normalization and by using

$$G_n(d_\sigma) = \sigma_s^n \int_{d_\sigma}^{\infty} (x_s - d_\sigma)^n \frac{1}{\sqrt{2\pi}} e^{-\frac{x_s^2}{2}} dx_s = \int_d^{\infty} (z_s - d)^n \frac{1}{\sigma_s \sqrt{2\pi}} e^{-\frac{z_s^2}{2\sigma_s^2}} dz_s \quad (4.2.72)$$

the (4.2.67-4.2.69) become

$$n_c = NG_0(d_\sigma) \quad (4.2.73)$$

$$A_r = N\pi\beta G_1(d_\sigma) \quad (4.2.74)$$

$$P = \frac{4}{3}NE^*\beta^{1/2}G_{3/2}(d_\sigma). \quad (4.2.75)$$

To set up a contact constitutive law suitable to finite element discretisation we need to determine a relationship between nodal forces and surfaces approach (see also [83, 97]). The Greenwood and Williamson model in last equations presents a nonlinear relationship between such parameters. The equations should be translated at element level

$$F_N = A\frac{4}{3}\eta E^*\beta^{1/2}G_{3/2}(d_\sigma) \quad (4.2.76)$$

where F_N is the element contact force, η is the known density of summits per unit of contact area Λ and d_σ is the contact area element.

The constitutive law should be linked to a chosen contact geometry, which defines the surfaces approach, see [99] for more details. The linearisation of the equation system containing the equation (4.2.76) involves the terms $G_0(d_\sigma)$, $G_1(d_\sigma)$, $G_{\frac{3}{2}}(d_\sigma)$ and also $G_{\frac{1}{2}}(d_\sigma)$, being

$$\frac{\partial F_N}{\partial d} = -2\eta AE^*\beta^{1/2}\sigma_s^{1/2} \int_{d_\sigma}^{\infty} (x_s - d_\sigma)^{1/2} \frac{1}{\sqrt{2\pi}} e^{-\frac{x_s^2}{2}} dx_s = -2\eta AE^*\beta^{1/2}G_{1/2}(d_\sigma). \quad (4.2.77)$$

The Gaussian quadrature is applied setting $t_s = e^{-x_s}$ in such a way the

$$G_n(d_\sigma) = \sigma_s^n \int_0^{e^{-d_\sigma}} (-\ln(t_s) - d_\sigma)^n \frac{1}{\sqrt{2\pi}} e^{-\frac{(-\ln(t_s))^2}{2}} \frac{1}{t_s} dt_s \quad (4.2.78)$$

is approximated by

$$G_n(d_\sigma) = \sigma_s^n \frac{e^{-d_\sigma}}{2} \sum_{k=1}^{N \text{ punti di Gauss}} B_k \left[-\ln\left(\frac{e^{-d_\sigma}}{2}x_k + \frac{e^{-d_\sigma}}{2}\right) - d_\sigma \right]^n \frac{e^{-\frac{1}{2}\left[-\ln\left(\frac{e^{-d_\sigma}}{2}x_k + \frac{e^{-d_\sigma}}{2}\right)\right]^2}}{\left(\frac{e^{-d_\sigma}}{2}x_k + \frac{e^{-d_\sigma}}{2}\right)} \quad (4.2.79)$$

where B_k are the weights and x_k the Gaussian points (nodes).

The numerical integration performed has shown a not satisfactory numerical precision, even if a high number of Gauss points has been used. Tables 4.12 and 4.13 report the number of significant

digits, delimited by the vertical bar, for $G_n(d_\sigma)$ computed at $d = 3.0$ with $\sigma_s = 1.0$. It is evident that the numerical integration of $G_0(3.0)$ and $G_1(3.0)$ presents an almost satisfactory number of correct digits. On the opposite, $G_{\frac{1}{2}}(3.0)$ and $G_{\frac{3}{2}}(3.0)$, which are both involved in the proposed contact numerical model, do not gain a satisfactory number of exact digits, even if a high number of Gauss points would be used. The transformation of the integration limits between zero and infinite and the employment of Gauss-Laguerre quadrature rule have also shown a poor precision.

Then integration has been carried out by employing the proposed method on the range $(0, +\infty)$: Tables 4.12 and 4.13 show the number of the obtained exact digits. The numerical results are achieved by using the recursive algorithm [64] with recurrence formula (4.2.52) for the moments. The integral (4.2.72) under investigations has been transformed in

$$\frac{1}{\sqrt{2\pi}} e^{-\frac{d^2}{2}} \int_0^\infty e^{-\frac{z_s^2}{2}} z_s^n e^{-z_s d} dz_s. \quad (4.2.80)$$

Table 4.12: Exact digits for $G_0(3.0)$ and for $G_1(3.0)$

N. of Nodes	$G_0(3.0)$ (*10 ⁻²)	$G_1(3.0)$ (*10 ⁻²)
2	0.13	0.038
3	0.134	0.038
4	0.1349	0.03821
5	0.1349	0.03821
6	0.13498	0.038215
7	0.134989	0.038215
8	0.1349898	0.0382154
9	0.13498980	0.03821543
10	0.13498980	0.03821543
11	0.134989803	0.038215431
13	0.1349898031	0.038215431
15	0.13498980316	0.03821543170
18	0.13498980316	0.0382154317047
20	0.134989803163	0.03821543170477
26	0.13498980316300945	0.0382154317047723
28	0.134989803163009452	0.03821543170477235
34	0.13498980316300945266	0.0382154317047723595
40	0.1349898031630094526651	0.038215431704772359564

Table 4.13: Exact digits for $G_{\frac{1}{2}}(3.0)$ and for $G_{\frac{3}{2}}(3.0)$

N. of nodes	$G_{\frac{1}{2}}(3.0)$ (*10 ⁻²)	$G_{\frac{3}{2}}(3.0)$ (*10 ⁻²)
2	0.064	0.026
3	0.0641	0.0263
4	0.0641	0.02639
5	0.06418	0.02639
6	0.06418	0.026396
7	0.0641850	0.026396
8	0.0641850	0.0263967
9	0.06418504	0.0263967
10	0.06418504	0.02639675
11	0.06418504	0.02639675
13	0.0641850439	0.0263967554
15	0.06418504393	0.02639675542
18	0.0641850439348	0.026396755426
20	0.06418504393485	0.0263967554269
26	0.0641850439348550	0.0263967554269467
28	0.06418504393485507	0.02639675542694672
34	0.0641850439348550793	0.0263967554269467273
40	0.064185043934855079312	0.0263967554269467273

Bibliography

- [1] Brent R.P. (1971) An Algorithm with Guaranteed Convergence for Finding a Zero of a Function , *Comput. J.*, 14 (4), 422-425.
- [2] Brezinski C. (1980) Padé-type Approximation and General Orthogonal Polynomials, *ISNM* vol.50 Birkhäuser-Verlag, Basel.
- [3] Buonocore A., Nobile AG and Ricciardi LM (1987) A new integral equation for the evaluation of first-passage-time probability densities, *Adv. Appl. Prob.* 19: 784–800.
- [4] Buonocore A., Giorno V., Nobile A.G. and Ricciardi L.M. (1990) On the two-boundary first-crossing-time problem for diffusion processes. *J. Appl. Prob.* **27** , 102–114.
- [5] Buonocore A. and Visentin F. (1992) On the numerical evaluation of first-passage-time probability densities for one dimensional diffusion processes. *Ricerche di Matematica.* **41** -1, 147–161.
- [6] Buonocore A., Caputo L., Pirozzi E. (2008) On the evaluation of firing densities for periodically driven neuron models. *Math Biosci* 214:122–133
- [7] Capocelli R.M. and Ricciardi L.M. (1971) Diffusion approximation and first passage time problem for a model neuron. *Kybernetik* 8: 214–223.
- [8] Chebyshev P.L. (1879) Sur les fractions continues , *J.Math.Pures Appl.*,
- [9] Cooper M.G., Mikic B. B., Yovanovich M.M. (1969) Thermal contact conductance, *Int. J. of Heat and Mass Transfer*, 12:279.
- [10] Coppel W.A. (1965) *Stability and Asymptotic Behavior of Differential Equations.* D.C. Heath and Company, Boston.
- [11] D’Agostino R. and Stephens M.A. (1986) *Goodness of Fit Techniques*, Marcel Dekker,Inc. New York.
- [12] Daniels, H.E. (1969) The minimum of a stationary Markov process superimposed on a U-shaped trend. *J. Appl. Prob.* **6**, 399–408.
- [13] Daniels, H.E. (1996) Approximating the first crossing-time density for a curved boundary. *Bernoulli* **2** (2), 133-143.

- [14] Davenport W.B. Jr. and Root W.L. (1958) *An Introduction to the Theory of Random Signals and Noise*, Mc Graw-Hill, New York.
- [15] Delves, L.M. and Walsh J. (1974) *Numerical solution of integral equations*. Clarendon Press, Oxford.
- [16] Di Crescenzo, A., Giorno, V., Nobile A.G. and Ricciardi L.M. (1997) On first-passage-time and transition densities for strongly symmetric diffusion processes. *Nagoya Math. J.* **145**, 143–161.
- [17] Di Crescenzo A, Di Nardo E, Nobile AG, Pirozzi E and Ricciardi LM (2000) On some computational results for single neurons' activity modeling. *BioSystems* 58: 19–26.
- [18] Di Nardo E., Pirozzi E. (1995) Algorithm for data sample representation by histograms with unequal cell widths, *Cybernetics and Systems*, 26, 343-348.
- [19] Di Nardo E. e Pirozzi E. (1996) On the grouping rule for random samples. *Series on Advances in Mathematics for Applied Sciences*, 40, 248-253.
- [20] Di Nardo E., Nobile A.G., Pirozzi E. and Ricciardi L.M. (1997) Vectorized simulations of normal processes for first crossing-time problems. *Lecture Notes in Computer Science* 1333: 177–188.
- [21] Di Nardo, E., Nobile, A.G., Pirozzi, E., Ricciardi, L.M. (1998) On a non-Markov neuronal model and its approximation. *BioSystems* 48, 29-35.
- [22] Di Nardo E., Nobile A.G., Pirozzi E., Ricciardi L.M. and Rinaldi S. (2000) Simulation of Gaussian processes and first passage time densities evaluation. *Lecture Notes in Computer Science* 1798: 319–333.
- [23] Di Nardo E., Nobile A.G., Pirozzi E. and Ricciardi L.M. (2001a) A computational approach to first-passage-time problem for Gauss-Markov processes. *Adv. Appl. Prob.* 33: 453–482.
- [24] Di Nardo E., Nobile A.G., Pirozzi E. and Ricciardi L.M. (2001b) Computer-aided simulations of Gaussian processes and related asymptotic properties. *Lecture Notes in Computer Science* 2178: 67–78.
- [25] Di Nardo E., Nobile A.G., Pirozzi E. and Ricciardi L.M. (2001c) Parallel simulations in FPT problems for Gaussian processes. In: Garofalo F, Moretti M and Voli M (eds) *Science and Supercomputing at CINECA - Report 2001*, pp 405–412.
- [26] Di Nardo E., Nobile A.G., Pirozzi E. and Ricciardi L.M. (2002) Gaussian processes and neuronal models: an asymptotic analysis. In: Trappl R (ed) *Cybernetics and Systems 2002*, Vol. 1, pp 313–318. Austrian Society for Cybernetics Studies, Vienna.
- [27] Di Nardo E., Nobile A.G., Pirozzi E. and Ricciardi L.M. (2003a) On the asymptotic behavior of first passage time densities for stationary Gaussian processes and varying boundaries. *Methodology and Computing in Applied Probability* 5: 211–233.

- [28] Di Nardo E., Nobile A.G., Pirozzi E. and Ricciardi L.M. (2003b) Towards the Modeling of Neuronal Firing by Gaussian Processes. *Scientiae Mathematicae Japonicae* 58: 255–264.
- [29] Di Nardo E., Nobile A.G., Pirozzi E. and Ricciardi L.M. (2003c) Computational Methods for the evaluation of Neuron’s Firing Densities. *Lecture Notes in Computer Science* 2809: 394–403.
- [30] Doob J. (1949) Heuristic approach to the Kolmogorov-Smirnov theorems. *Ann. Math. Statist.* 20:393–403.
- [31] Durbin, J. (1992) The first–passage density of the brownian motion process to a curved boundary. *J. Appl. Prob.* **29**, 291–304.
- [32] Fortet R. (1943) Les fonctions aléatoires du type de Markoff associées à certaines équations linéaires aux dérivées partielles du type parabolique. *J. Math. Pures Appl.* **22** 177–243.
- [33] Franklin J.N. (1965) Numerical simulation of stationary and non stationary gaussian random processes. *SIAM Review* 7: 68–80.
- [34] Gautschi W., (1968) Costruction of Gauss-Christoffel quadrature formulas, *Math. Comp.*, vol. 22, 251-270
- [35] Gautschi W., (1982) On Generating Orthogonal Polynomials , *SIAM J. Sci. Stat. Comput.* vol. 3, No. 3, 280-317.
- [36] Gerstein G., Mandelbrot B. (1964) Random walk models for the spike activity of a single neuron. *Biophys J.* 4:41–68.
- [37] Gerstner W. and Kistler W.M. (2002) *Spiking neuronmodels: single neurons, populations, plasticity*. Cambridge University Press, Cambridge.
- [38] Ghizzetti A., Ossicini A. (1970) Quadrature Formulae *ISNM*, vol.13, Birkhäuser Verlag Basel und Stuttgart.
- [39] Gibbons J.D., (1983) Kolmogorou-Smirnov symmetry test, *Encyclopedia of Statistical Sciences*, 4, Kotz and Johnson, New York, pp. 396-398.
- [40] Giorno V., Nobile A.G., Ricciardi L.M. and Sato S. (1989) On the evaluation of first-passage-time probability densities via non-singular integral equations. *Adv. Appl. Prob.* **21** 20–36.
- [41] Giorno V., Nobile A.G. and Ricciardi L.M. (1990) On the asymptotic behavior of first-passage-time densities for one-dimensional diffusion processes and varying boundaries. *Adv. Appl. Prob.* 22: 883–914.
- [42] Giorno V., Nobile A.G., Pirozzi E. and Ricciardi L.M. (2004) Non-Stationary Gauss-Markov Processes and Neuronal Modeling. In: Trappl R (ed) *Cybernetics and Systems 2004*, Vol. 1., pp 211–215. Austrian Society for Cybernetics Studies, Vienna.

- [43] Golub G.H. and Welsch J.H., (1969) Calculation of Gauss quadrature rules, *Math. Comp.*, vol. 23, 221-230.
- [44] Golub G.H. and Van Loan C.F. (1983) *Matrix Computations*. The Johns Hopkins University Press Baltimore, Maryland.
- [45] Gradshteyn I.S., Ryzhik I.M. (1980) *Table of Integrals, Series and Products*, Academic Press, New York.
- [46] Greenwood J.A., Williamson J.B.P., (1966) The contact of nominally-flat surfaces, *Proc. R. Soc. London*, 295-A:300.
- [47] Hartigan J. A., (1975) *Clustering Algorithms*, Wiley Series in Probability and Mathematical Statistics.
- [48] IMSL Math/Library - FORTRAN *Subroutines for Mathematical Applications* , IMSL User's Manual.
- [49] Jazwinski A.H. (1970) *Stochastic processes and filtering theory*. Academic Press, New York.
- [50] Johnson K.L., (1987) *Contact Mechanics* , Cambridge University Press, Cambridge.
- [51] Keilson J. and Ross H.F. (1975) Passage times distributions for Gaussian Markov (Ornstein-Uhlenbeck) statistical processes. In *Selected Tables in Mathematical Statistics*, Vol.III, 233-327. Amer. Math. Soc., Providence, R.I.
- [52] Knuth D.E. (1973) *The Art of Computer Programming*, Vol. 2: Seminumerical Algorithms. Reading, M.A. Addison Welsey.
- [53] Knuth, D.E. (1973) *The Art of Computer Programming*, Vol. 3. Addison-Wesley.
- [54] Kostyukov, A.I. (1978) Curve-Crossing Problem for Gaussian Stochastic Processes and its Application to Neural Modelling. *Biol. Cybernetics* 29, 187-191.
- [55] Kostyukov, A.I., Ivanov, Y. N., Kryzhanovsky, M.V. (1981) Probability of Neuronal Spike Initiation as a Curve-Crossing Problem for Gaussian Stochastic Processes. *Biol. Cybernetics* 39, 157-163.
- [56] Lánský P. and Smith C.E. (1989) The effect of a random initial value in neural first-passage-time models. *ath. Biosci.* 93, 191-215.
- [57] Lánský P. (1997) Sources of periodical force in noisy integrate-and-fire models of neuronal dynamics. *Phys Rev E* 55(2):2040-2043
- [58] Mehr C.B. and McFadden J.A. (1965) Certain Properties of Gaussian Processes and their First-Passage Times. *J. R. Statist. Soc., B*, 27: 505-522.
- [59] Mann H.D. and Wald A., (1942) On the Choice of the Number of Class Intervals in the Application of the Chi Square Test, *Annals of Mathematical Statistics*, 13, pp. 306-17.

- [60] Mineo A., (1978) Un Nuovo Criterio di Raggruppamento in Classi, *Atti XXIX Riunione Scientifica SIS*, 2, Bologna, pp. 205-210.
- [61] Morandi Cecchi M. (1967) L'Integrazione Numerica di una Classe di Integrali Calcoli Quantomeccanici , *Calcolo*, 4, 3, 363-368.
- [62] Morandi Cecchi M., Redivo Zaglia M. (1991) A New Recursive Algorithm for a Gaussian Quadrature Formula Via Orthogonal Polynomials , IMACS Transactions on Orthogonal Polynomials and Their Applications, Editors C. Brezinski, Gori L. et al., Baltzer AG, Basel, pp. 353-358.
- [63] Morandi Cecchi M., Redivo Zaglia M. (1993) Computing the Coefficients of Recurrence Formula for Numerical Integration by Moments, *J. of Comp. and App. Math.*, Vol. 49, 1-3, 207-216.
- [64] Morandi Cecchi M., Pirozzi E. (1995) A Recursive Algorithm by the Moments Method to Evaluate a Class of Numerical Integrals over an Infinite Interval, *Numerical Algorithms*, vol. 10, 155-165.
- [65] Morandi Cecchi M., Pirozzi E., Zavarise G. (1996) Numerical Evaluations of Special Integrals with Applications to Contact Problems, *Advanced Mathematical Tools in Metrology*, Ed. P. Ciarlini, M.G. Cox, F. Pavese, D. Richter, Series on Advances in Mathematics for Applied Sciences, vol. 40, 182-194.
- [66] NAG Fortran Library Routines . Mark15 . Distribuito dalla Numerical Algorithms Group, Oxford, U.K.
- [67] Nobile A.G., Ricciardi L.M. and Sacerdote L. (1985a) Exponential trends of Ornstein-Uhlenbeck first passage time densities. *J. Appl. Prob.* 22: 360–369.
- [68] Nobile A.G., Ricciardi L.M. and Sacerdote L. (1985b) Exponential trends of first-passage-time densities for a class of diffusion processes with steady-state distribution. *J. Appl. Prob.* 22: 611–618.
- [69] Ogorodnikov, V.A. and Prigarin, S.M. (1996) *Numerical Modelling od Random Processes and Fields. Algorithms and Applications*. VSP, Uthrecht, The Netherlands.
- [70] Pettitt A.N. and Stephens M.A. (1977) The Kolmogorov-Smirnov Goodness of Fit Statistic with Discrete and Grouped Data, *Technometrics*, vol. 19, no. 2, pp. 205-210.
- [71] Piessen R. (1987) *Modified Clenshaw-Curtis Integration and Applications to Numerical Computation of Integral Transform* , Numerical Integration, P. Keast and G.Fairweather (eds.), 35-51.
- [72] Ricciardi L.M. (1977) *Diffusion Processes and Related Topics in Biology*. Springer-Verlag, New York.
- [73] Ricciardi, L.M. and Sato, S. (1983) A note on first passage time for Gaussian processes and varying boundaries. *IEEE Trans. Inf. Theory* **29**, 454–457.

- [74] Ricciardi, L.M. and Sato, S. (1986) On the evaluation of first–passage–time densities for Gaussian processes. *Signal Processing* **11**, 339–357.
- [75] Ricciardi L.M., Di Crescenzo A., Giorno V. and Nobile A.G. (1999) An Outline of Theoretical and Algorithmic Approches to First Passage Time Problems with Applications to Biological Modeling. *Math. Japonica* 50: 247–322.
- [76] Ricciardi L.M. and Lánský P. (2002) Diffusion Models of neuron activity. In: Arbib MA (ed). *The Handbook of Brain Theory and Neural networks*. pp 343–348. The MIT Press, Cambridge.
- [77] Roberts, J.B. (1968) An approach to the first-passage problem in random vibration. *J. Sound Vib.* 8 No. 2, 301-328.
- [78] Ross, S.M. (2002) *Simulation*. Academic Press, San Diego.
- [79] Sacerdote, L. and Tomassetti, F. (1996) On the evaluations and approximations of first–passage–time probabilities. *Adv. Appl. Prob.* **28**, 270–284.
- [80] Shai I., Santo M. (1982) Heat transfer with contact resistance, *Int. J. of Heat and Mass Transfer*, 24-4:465.
- [81] Schindler M., Talkner P., Hänggi P. (2004) Firing times statistics for driven neuron models: analytic expressions versus numerics. *Phys Rev Lett* 93(4):048,102–1–048,102–4
- [82] Schindler M., Talkner P., Hänggi P. (2005) Escape rates in periodically driven Markov processes. *Physica A* 351:40–50
- [83] Schrefler B.A., Zavarise G. (1993) Constitutive laws for normal stiffness and thermal resistance on contact element, *Microcomputers in Civil Engineering*, 8:299.
- [84] Silverman B.W. (1986) *Density Estimation for Statistics and Data Analysis*, Chapman and Hall.
- [85] Snee R.D. and Pfeifer C.G. (1983) Histograms, *Encyclopedia of Statistical Sciences*, 3, J. Wiley and Sons, New York, pp. 635-640.
- [86] Stephens M.A., (1983) Kolmogorov-Smirnov statistics, *Encyclopedia of Statistical Sciences*, 4, Katz and Johnson, New York, pp. 393-396.
- [87] Stratonovich RL (1963) *Topics in Theory of Random Noise* Vol. 1. Gordon and Breach, New York.
- [88] Szegö G. (1939) *Orthogonal Polynomials* , American Mathematical Society.
- [89] Tong T. (1990) *The multivariate Normal Distribution*. Springer-Verlag, New York.
- [90] Tuckwell H.C. (1988a) *Introduction to Theoretical Neurobiology* Vol 1: Linear Cable Theory and Dendritic Structure. Cambridge University Press, Cambridge.

- [91] Tuckwell H.C. (1988b) *Introduction to Theoretical Neurobiology* Vol 2: Nonlinear and Stochastic Theories. Cambridge University Press, Cambridge.
- [92] Wegman E.J., (1982) Density Estimation, *Encyclopedia of Statistical Sciences*, 2, J.Wiley and Sons, New York, pp. 309-315.
- [93] Widder D.V. (1971) *An Introduction to Transform Theory*, Academic Press, New York.
- [94] Wolfram S. *Mathematica, A System for Doing Mathematics by Computer*, Second Edition, Addison-Wesley Publishing Company, Inc.
- [95] Wriggers P., Zavarise G. (1993) Thermomechanical contact - a rigorous but simple numerical approach, *Computers & Structures*, 46-1:47.
- [96] Yaglom A.M. (1987) *Correlation Theory of Stationary Related Random Functions* Vol.1: Basic Results. Springer-Verlag, New York.
- [97] Zavarise G. (1991) *Problemi termomeccanici di contatto - aspetti fisici e computazionali*, Ph.D. Thesis, Ist. di Scienza e Tecnica delle Costruzioni, Univ. of Padua, Italy.
- [98] Zavarise G., Wriggers P., Stein E., Schrefler B.A. (1992) A numerical model for thermomechanical contact based on microscopic interface laws, *Mech. and Res. Communications*, 19-3:173.
- [99] Zavarise G., Schrefler B.A. (1994) Numerical Analysis of Microscopic Elastic Contact Problems, *Proc. CMIS, Second Contact Mechanics Int. Symposium*, Marseille.